

令和2年度 修士学位論文

衝突に着目した理想気体中の粒子の短時間運動

名古屋大学 大学院工学研究科

物質科学専攻 ナノ解析物質設計学講座

レオロジー物理工学研究グループ

281922138 仲井文明

## 衝突に着目した理想気体中の粒子の短時間運動

増淵研究室 仲井文明

【背景と目的】 流体中に浮かぶマイクロ・ナノメートルスケールの微粒子は流体分子の衝突に駆動されてランダムに運動する。この運動はブラウン運動と呼ばれ、トレーサーと流体分子が多数回衝突する長い時間スケールにおいては、流体分子の自由度を粗視化した一般化ランジュバン方程式 [1] で記述できる。一方で、トレーサーと流体分子の衝突が多数回生じない短時間スケールにおいては、一般化ランジュバン方程式は使えず、個々の衝突を取り扱う必要がある。ボルツマン方程式は分子の衝突からトレーサーの運動を予測できる理論的枠組みの一つであるが、粒子の衝突が独立とみなせる希薄気体の場合でしか有効ではない [2]。ボルツマン方程式に流体の構造の相関を導入したエンスコッグ理論は準希薄な流体中のトレーサーの輸送までは再現するが、流体が濃厚な場合は流体分子同士の衝突が強く相関することにより有効ではなくなる [3]。トレーサーの運動を弾道的運動と流体分子との衝突の連続と捉えて確率過程の手法で濃厚流体中のトレーサーの運動を部分的に再現した理論 [4] はあるものの、理論内で扱われている衝突の統計は現象論的に導入されており分子論的根拠に欠ける。流体分子とトレーサーの衝突回数が多数回生じない短時間スケールにおける濃厚流体中のトレーサーの運動は、分光実験などの対象となる運動であるにも関わらず、上述のように十分な理解に至っていない。濃厚流体中のトレーサーの運動は、理想的なモデルでも調べられている。例えば、一次元の剛体球流体中のトレーサーの運動は、トレーサーの質量が流体分子と同じときのみ一次元の特性により解析的に求められている [5]。一方で、トレーサーの質量が流体分子と異なる場合においては、衝突の複雑な相関を取り扱う必要があるために十分に理解されていない。

上述のように濃厚流体中のトレーサーの短時間運動の難しさはトレーサーと流体分子の衝突が複雑に相関することである。そこで、本論文では流体分子同士の相互作用がない単純な系をまず理解する必要があると考え、理想気体中のトレーサーの短時間運動を3次元と1次元においてシミュレーションと理論で解析した。3次元の研究内容は論文 [6] で報告した。

【システムと手法】 理想気体中のトレーサーの運動は、温度  $T$ 、トレーサーの質量  $M$ ・サイズ  $\sigma$ 、理想気体粒子の質量  $m$ ・数密度  $\rho$  の内  $T$ 、 $\sigma$ 、 $m$  で無次元すると、 $M$  と  $\rho$  だけで特徴付けられる (理想気体分子のサイズは0である)。このようなシステムに対し、衝突を厳密に定義できるイベントドリブン型の剛体シミュレーションを用いてトレーサーの運動を解析した。合わせて、3次元においては1回の衝突の統計を、1次元においては1回の衝突の統計に加えてトレーサーの質量が理想気体粒子に比べて大きい場合と小さい場合の速度の時間相関関数も理論的に解析した。

【結果と考察】 3次元系に対してトレーサーの速度の時間相関関数  $\langle \mathbf{V}(0) \cdot \mathbf{V}(t) \rangle$  を調べた所、 $M$  が小さく  $\rho$  が大きい場合に短時間領域で負相関が生じることが分かった。このような挙動は周囲流体が相互作用しない系では報告例がない。この挙動を理解するために、速度の衝突回数に対する相関  $\langle \mathbf{V}_0 \cdot \mathbf{V}_n \rangle$  を考案しシミュレーションで解析したところ、一回の衝突で速度の負相関が生じることが分かった。この結果は気体分子論に基づく理論解析でも再現できた。さらに、速度の負相関はトレーサーが同一の理想気体粒子と複数回衝突することで生じる衝突の相関に起因することをシミュレーションで見出した [6]。

1次元系においては、時空間のダイアグラムから、トレーサーの質量が大きい場合はトレーサーと理想気体の衝突が独立になり、トレーサーの質量が小さい場合は同一の理想気体と繰り返し衝突することで衝突が強く相関する様子を観測した。この描像に基づいて、トレーサーの質量が大きい極限と小さい極限に対し確率過程の方法でトレーサーの速度の時間相関関数を解析し、シミュレーション結果を良好に再現できた。

【まとめ】 3次元と1次元における理想気体中のトレーサーの短時間運動を衝突に基づいて解析した。周囲流体が相互作用しないにも関わらず、トレーサーの質量と理想気体の密度によっては衝突が相関することが分かった。さらに、衝突の相関は同一の理想気体粒子と衝突することで生じることを見出した。1次元系においては、トレーサーの質量が大きい極限と小さい極限に対してトレーサーの速度の時間相関関数を解析的に求めることができた。

[1]K. Kawasaki, J. Phys. A: Math. Nucl. Gen. 6 1289 (1973). [2]S. Chapman and T. G. Cowling, The mathematical theory of non-uniform gases (1990). [3]B. J. Alder, D. M. Gass, and T. E. Wainwright, J. Chem. Phys. 53, 3813 (1970). [4]K. Lindenberg, R. I. Cukier, J. Chem. Phys. 67, 568 (1977). [5]L. Lebowitz and J. K. Percus, Phys. Rev. 155, 122, (1967). [6]F. Nakai, Y. Masubuchi and T. Uneyama, Phys. Rev. E. 102, 032104, (2020).

## **Abstract**

The particle immersed in a fluid (hereafter called as a “tracer”) shows Brownian motion due to the collisions of surrounding fluid molecules. The Brownian motion is often written by the Langevin equation, which is the coarse grained description and has the limited applicability. When we focus on the short time scale where the number of collision between the tracer and fluid molecules is not sufficiently large, the Langevin description is not valid. In such a time scale, we have to consider the individual collisions. In this work, we investigated the short time dynamics of the tracer in ideal gas by using the simulations and theory from the view point of the collisions. Some parts of the contents in this thesis have been published[1].

# Contents

<b>1</b>	<b>Introduction</b>	<b>3</b>
1.1	Diffusion of particles in fluid . . . . .	3
1.2	Langevin equation . . . . .	3
1.3	Kinetic theory of gases . . . . .	5
1.4	Stochastic process of the molecular dynamics . . . . .	6
1.5	Purpose and constitution . . . . .	6
<b>2</b>	<b>Method of simulation</b>	<b>8</b>
2.1	Simulation setting . . . . .	8
2.2	Validity of simulation . . . . .	10
2.2.1	Conservation law of classical mechanics . . . . .	10
2.2.2	Check of basic equilibrium property . . . . .	11
2.2.3	Estimation of time where system size affects . . . . .	14
2.3	Analysis methods . . . . .	15
<b>3</b>	<b>Short time dynamics of tracer in 3 dimensional ideal gas</b>	<b>17</b>
3.1	Introduction . . . . .	17
3.2	Results of the simulations . . . . .	18
3.3	Discussions . . . . .	23
3.3.1	Single collision . . . . .	23
3.3.2	Correlation of collisions . . . . .	24
3.3.3	Comparison with other simulations . . . . .	27
<b>4</b>	<b>Statistics of single collision in arbitrary dimension</b>	<b>29</b>
4.1	Introduction . . . . .	29
4.2	Theoretical analysis . . . . .	30
4.2.1	Single collision statistics . . . . .	30
4.2.2	Free time analysis . . . . .	32
4.2.3	Velocity correlation analysis . . . . .	34
4.3	Discussions . . . . .	35
4.3.1	Test of the theoretical results . . . . .	35

4.3.2	Transformation to the equilibrium probability . . . . .	36
4.3.3	Velocity correlation before and after single collision $\gamma_1$ .	38
4.3.4	Relation to other system . . . . .	39
<b>5</b>	<b>Short time dynamics of tracer in 1 dimensional gas</b>	<b>41</b>
5.1	Introduction . . . . .	41
5.2	Results of simulations . . . . .	42
5.3	Theoretical analysis . . . . .	44
5.3.1	Case for heavy tracer . . . . .	44
5.3.2	Case for light tracer . . . . .	47
5.4	Discussion . . . . .	51
5.4.1	Comparison theory with simulation results . . . . .	51
5.4.2	Expandability of our theory . . . . .	53
<b>6</b>	<b>Conclusions</b>	<b>54</b>

# Chapter 1

## Introduction

### 1.1 Diffusion of particles in fluid

The micro or nano meter sized particle immersed in Newtonian fluid (hereafter called as a “tracer”) shows the diffusive motion in the long time scale where the number collisions between the tracer and fluid molecules is sufficiently large[2]. In such a time scale, the displacement of the tracer  $\Delta\mathbf{r}$  and the time  $t$  have the linear relation as

$$\langle \Delta\mathbf{r}(t)^2 \rangle = 6Dt \quad (1.1)$$

where the  $\langle \dots \rangle$  is the equilibrium statistical average and  $D$  is the diffusion coefficient. The  $D$  is related to the fluid viscosity as

$$D = \frac{k_B T}{6\pi\eta\sigma} \quad (1.2)$$

where  $k_B$  is the Boltzmann constant,  $T$  is the temperature,  $\eta$  is the viscosity and  $\sigma$  is the size of the tracer. This relation is called the Stokes Einstein relation [3]. From this relation, we can understand that the dynamics of the particle and fluid property has the strong relation. This relation is simple and widely used in the physics, chemistry and engineering etc.

However, the Stokes-Einstein relation can be used only for the diffusive dynamics. If we see the ballistic motion of the tracer, the displacement of the tracer is proportional to the square of the time [4, 5, 6] and the Stokes-Einstein relation does not describe such a behavior.

### 1.2 Langevin equation

If we see the dynamics of the tracer including the ballistic motion the Langevin equation is useful. In this section, we introduce the brief property and the

limit of applicability of this equation.

The dynamics of the tracer and all the fluid molecules are completely determined by the initial positions and velocities of the tracer and all the fluid molecules via the Hamiltonian if the dynamics obeys the classical mechanics (if we consider the quantum effects, the dynamics is not completely determined because of the uncertainty principle between a position and a momentum). However, the analysis of all the degrees of freedom of the tracer and all the fluid molecules are generally difficult. In the situation where we are interested only in a partial degree of freedom, coarse graining methods are often useful. If we only see the dynamics of the tracer, the generalized Langevin equation (GLE) for the coarse-grain for the degrees of freedom of the fluid molecules is widely used [7, 8, 9].

$$M \frac{d^2 \mathbf{R}}{dt^2} = - \int_{-\infty}^t K(t-t') \frac{d\mathbf{R}(t')}{dt'} dt' + \mathbf{W}(t) \quad (1.3)$$

where  $M$  is the mass of the tracer,  $\mathbf{R}$  is the tracer position,  $\Gamma$  is the friction coefficient kernel considering the relaxation of the fluid and  $\mathbf{W}$  is the Gaussian noise. This Gaussian noise is justified by the central limit theorem when the number of the collisions between the tracer and fluid molecules is sufficiently large.

Meanwhile, when we focus on the short time scale where the fluid molecules does not collide with the tracer many times, the Gaussian noise approximation can not be justified. If the GLE works, the distribution of the displacement is Gaussian because the GLE is a linear equation and the noise is Gaussian. In contrast to this, the noise is non-Gaussian if the displacement is non-Gaussian. Thus, we can check the validity of the Gaussian approximation by analyzing the Gaussianity of the displacement. Rahman studied the dynamics of the Lennard-Jones fluid by the simulation and showed that the distribution of the displacement of the constituent particles is non-Gaussian in the short time scale[10]. Yamaguchi and Kimura studied the dynamics of the tracer in the dilute hard sphere gas by the Monte Carlo method and showed that the displacement of the tracer is non-Gaussian in the short time scale[11]. In contrast, Montgomery showed that the Langevin description can be justified even for the short time dynamics of the tracer in a limited case[12]. Namely, for the case where the tracer mass is sufficiently large and the gas is dilute, the Boltzmann equation can be expanded in terms of the mass ratio and the Fokker-Plank equation corresponding to the Langevin equation can be derived. Therefore, we do not blindly use the GLE for the dynamics of the tracer in the short time scale except for the limited case. In the short time scale, we have to consider the individual collisions between the tracer and the fluid molecules.

### 1.3 Kinetic theory of gases

If we consider the dynamics of the tracer from the collision picture, the kinetic theory[13, 14, 15] is useful. The kinetic theory is one of the most developed area in the statistical physics. This theory provides the several frameworks to analyze the diffusion constant, viscosity, thermal conductivity, etc.

Although the gas kinetic theory is powerful, this has the limitation of the applicability. The gas kinetic theory treats the phase space distribution function of the particles. To understand the dynamics of a particle (or a tracer) in the fluid, we have to obtain the one-body distribution function from the Liouville equation of the  $N$ -body distribution function by integrating all degrees of freedom other than the particle of interest. This integration can be done formally, but since the results are not closed only in the one-body distribution, we can not proceed to the specific calculations. In other words, we need  $(n + 1)$ -body distribution to get the  $n$ -body distribution. This is called the BBGKY (Bogoljubov-Born-Green-Kirkwood-Yvon) hierarchy[16, 17, 18]. To overcome the difficulty of the calculation due to the BBGKY hierarchy, the density expansion methods are employed[16]. This methods can reduce the 2-body distribution function to the functional of the two 1-body distribution functions in a low density limit, then this is the derivation of the Boltzmann equation (Boltzmann derived this equation by a phenomenological consideration[19]). In an operation of the reduction of the 2-body distribution function, since the static and dynamics correlations are usually eliminated, the Boltzmann equation can be justified only for the dilute fluid.

Enskog extended the Boltzmann equation to deal with non dilute fluid by incorporating the static correlation[15]. His approach succeeded for the moderately dense fluids with packing fraction less than 30% to describe the transport coefficient such as the diffusion constant or viscosity. However, for higher density cases, Enskog theory fails because dynamic correlation of the collisions between the fluid particles which is not considered in the theory significantly affects the dynamics of the particles [20].

Thus, the kinetic theory provides the useful ways to analyze the dynamics of tracer or fluid particles. However, such a theory does not work for the dense system in which the dynamic correlation is dominant.

## 1.4 Stochastic process of the molecular dynamics

Not only the kinetic theory but also the stochastic process has been utilized for the description of the dynamics of the tracer in fluids. Lindenberg and Cukier [21] analyzed the dynamics of the hard sphere tracer in low, intermediate and high density fluids by using the stochastic point process. They incorporated the complex correlations due to the particle interactions into the distribution of the free time between the collisions by the phenomenological considerations and reproduced the characteristic behaviors of the velocity autocorrelation function of the tracer for the low, intermediate and high density fluids. However, the time interval distributions that they introduced are not valid. Actually, Taloni et al. [22] showed that the distribution of free time is almost exponential by using the hard core simulations, even if the fluid density is high.

Burshtein and Krongauz [23] analyzed the velocity autocorrelation function of the tracer in dense hard sphere fluids in the short time scale and proposed the several phenomenological theories to describe the negative velocity correlation typically seen in high density fluids. Although their theories can reproduce the characteristic behavior of the velocity autocorrelation function, the various assumptions for the collision statistics in the theories are not validated.

Actually, the stochastic process methods is useful for the description of the hard sphere dynamics, the collision statistics employed in the theory should be carefully chosen.

## 1.5 Purpose and constitution

As we explained above, the short time dynamics of the tracer in a dense fluids is not fully understood. The difficulty of the dynamics is due to the dynamic correlation caused by the particles interactions. To tackle this problem, we consider that the dynamics of the tracer in a relatively simple system should be understood. In this study, we investigate the short time dynamics of the tracer in the ideal gas composed of the point masses.

In chapter 2, we explain the methods of the simulation and check the validity of our system for the mechanics and statistical mechanics. In chapter 3, we analyze the dynamics of the tracer in ideal gas in 3 dimensions by using the simulations. In this chapter, we show the dynamics of the tracer can exhibit non-trivial behavior even in the ideal gas system and such a behavior is caused by the correlated collisions. In chapter 4, we analyze the

statistics of a single collision between the tracer and an ideal gas particle by the theory to describe the results related to the single collision in the chapter 3. In chapter 4, based on the pictures obtained in the chapters above, we analyze the dynamics of the tracer in ideal gas in 1 dimension by the theory.

# Chapter 2

## Method of simulation

In this work, we analyze the dynamics of the tracer focusing on the collisions. The method solving the equation of motion[24, 25] can not strictly detect the collisions between the particles. Thus, we employ the hard core simulation methods which is event driven type one developed by Alder[26].

### 2.1 Simulation setting

We introduce a tracer particle of size  $\sigma$  and mass  $M$  and  $N$  ideal gas particles of size 0 and mass  $m$  into the simulation box with the periodic boundary conditions in  $d$  dimensions. The side length of the simulation box  $L$  was chosen by the number density  $\rho$  so that  $L$  and  $\rho$  satisfy the relation  $L^d = \frac{N}{\rho} + \frac{\pi^{d/2}}{\Gamma(\frac{d}{2}+1)} \left(\frac{\sigma}{2}\right)^d$ , where the second term is the volume of the tracer in  $d$  dimension. Then, we define the volume of the simulation box  $L^d$  as  $\mathcal{V}$ . The initial positions of the tracer and gas particles are uniformly distributed without overlap between the tracer and gas particles. The initial velocities of the tracer and gas particles obeys the Maxwell-Boltzmann distribution. We subtracted the constant vector from the velocities of tracer and gas particles to realize that the momentum of the system becomes  $\mathbf{0}$  and multiplied the constant to the all velocities to realize the kinetic energy of the system become  $(N+1)dk_B T$ , where  $k_B$  is the Boltzmann constant and  $T$  is the temperature. In this system, the parameters which characterize the system can be reduced only to  $M$  and  $\rho$  by choosing  $m$ ,  $\sigma$  and  $k_B T$  as units in the thermodynamic limit ( $L \rightarrow \infty$  and  $N \rightarrow \infty$  for fixed  $\rho$ ). In the simulation, since the analysis is performed in the finite yet sufficiently large system in which the system size does not affect the results, the parameters in the simulation is practically  $M$  and  $\rho$ . The system size effect is discussed in the following section.

In our system, the mean free path of the ideal gas particles exceed the

size of the simulation box. In this case, the tracer and the gas particle in the mirror image sometimes collide earlier than those in the simulation box. Due to such a type of the event, the calculation of the dynamics fails if we use the conventional hard core algorithm[26]. To solve this issue, we modified the algorithm as below.

1. Calculate the minimum time when the gas particle in the mirror image possibly collides  $t'_{min}$ . That is, we analyze the max relative speed between the tracer and ideal gas particle  $V_{max}$  and calculate the minimum time as  $t'_{min} = \frac{L-\sigma}{2V_{max}}$ .
2. Find the gas particles which approaches to tracer by using the relation below.

$$(\mathbf{R} - \mathbf{r}_i) \cdot (\mathbf{V} - \mathbf{v}_i) < 0 \quad (2.1)$$

where  $\mathbf{R}$  and  $\mathbf{r}_i$  are the positions of the tracer and  $i$ -th gas particle and  $\mathbf{V}$  and  $\mathbf{v}_i$  are the velocities of the tracer and  $i$ -th gas particle. If the condition (2.1) is satisfied, the  $i$ -th particle possibly collides with the tracer.

3. For the gas particle which satisfies the condition (2.1), we test whether the particle collides with the tracer by the condition below

$$\sigma^2 > r_{ti}^2 - \left( \mathbf{r}_{ti} \cdot \frac{\mathbf{v}_{ti}}{v_{ti}} \right)^2 \quad (2.2)$$

where  $\mathbf{r}_{ti}$  and  $\mathbf{v}_{ti}$  are the relative position and the velocity between the tracer and  $i$ -th gas particle defined as  $\mathbf{r}_{ti} = \mathbf{r}_i - \mathbf{R}$ ,  $\mathbf{v}_{ti} = \mathbf{v}_i - \mathbf{V}$ . Then, we define the right hand side of the equation (2.2) as  $b_{ti}^2$ .

4. For the gas particle which satisfies the condition (2.2), we calculate the time when the tracer and  $i$ -th gas particle collides  $t_i$  by the following equation

$$t_i = -\frac{1}{v_{ti}} \left[ \frac{\mathbf{r}_{ti} \cdot \mathbf{v}_{ti}}{v_{ti}} + (\sigma^2 - b_{ti}^2)^{\frac{1}{2}} \right] \quad (2.3)$$

and find the gas particle that collides with the tracer in the shortest time  $t_i$ .

5. If  $t'_i$  is smaller than  $t_i$ , evolve the position of all particles for the period of  $t'_i$  and back to the step 2, otherwise go to the next step.

6. Evolve the positions of all particles for the period of  $t_{min}$ .
7. Evolve the velocity for the tracer and colliding gas particle by the following collision rule based on the hard core interaction as

$$\mathbf{V}' = \mathbf{V} + \frac{2m}{m+M} (\mathbf{v}_i - \mathbf{V}) \cdot \hat{\mathbf{r}} \hat{\mathbf{r}} \quad (2.4)$$

$$\mathbf{v}_i = \mathbf{v} - \frac{2M}{m+M} (\mathbf{v}_i - \mathbf{V}) \cdot \hat{\mathbf{r}} \hat{\mathbf{r}} \quad (2.5)$$

where  $\mathbf{V}$  and  $\mathbf{V}'$  are the velocities of tracer before and after the collision,  $\mathbf{v}$  and  $\mathbf{v}'$  are the velocities of gas particle before and after the collision and  $\hat{\mathbf{r}}$  is the unit vector from the center of tracer to the gas particle on the collision.

8. Go back to the step 1 and repeat.

We use the data after 1 million collisions occur so that the history of the initial setting of the simulation does not affect the results. From the simulation setting, we calculated the dynamics of the tracer in the ideal gas.

## 2.2 Validity of simulation

In this section, we checked the conservation law related to the classical mechanics and the basic property related to the equilibrium statistical mechanics for our simulation in the following subsections.

### 2.2.1 Conservation law of classical mechanics

In the hard core and event driven type simulation scheme employed in this work, the velocities of the tracer and gas particles are changed by the collision conserving the momentum and the kinetic energy. Since the time evolution of the system is the successive ballistic motion and the velocity changes between the tracer and gas particles, the momentum and kinetic energy of the system are not changed for the time evolution. In our system, we set the initial momentum of the system  $\mathbf{p}_{sum}(0)$  defined by  $\mathbf{p}_{sum}(0) = \mathbf{P}(0) + \sum_i \mathbf{p}_i(0)$  as  $\mathbf{0}$  and the initial averaged kinetic energy per particle  $E_{ave}(0)$  defined by  $E_{ave}(0) = \frac{1}{N+1} (M\mathbf{V}^2(0) + \sum_i m\mathbf{v}_i^2(0))$  as 1. These values have to keep the initial value for the time development. To check the conservation laws, we plot the time evolution of  $E_{ave}(0)$  and  $\mathbf{p}_{sum}$  in the 3 dimensions in Figure 2.1. From Figure 2.1, we found that the  $E_{ave}(0)$  decreases and  $\mathbf{p}_{sum}$  fluctuate for the time development, although the variations of quantity are

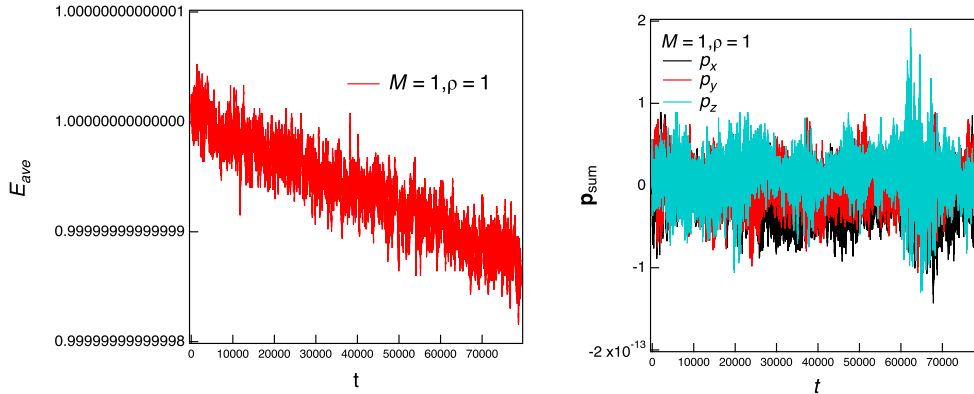


Figure 2.1: Time development of the averaged kinetic energy per particle  $\bar{E}_k$  and momentum of the system  $\mathbf{p}_{sum}$  in 3 dimensions.

rather small compared with the results shown in following chapters. These changes would be due to the numerical errors and inevitable in the numerical simulation. Thus, we can say that our simulation satisfies the conservation law of mechanics in the range of the numerical errors. Also since the changes of  $E_{ave}(0)$  and  $\mathbf{p}_{sum}$  are rather small, these would not affect the results shown in the following chapters.

## 2.2.2 Check of basic equilibrium property

In this subsection, we check the velocity distribution of the tracer and the structure of the gas particles around the tracer. In the equilibrium state, the velocity distributions of tracer and gas particles obey the Maxwell Boltzmann distribution as follows,

$$P_{MB}(M, \mathbf{V}) = \mathcal{N} \exp\left(-\frac{M\mathbf{V}^2}{2k_B T}\right) \quad (2.6)$$

$$P_{MB}(m_i, \mathbf{v}_i) = \mathcal{N} \exp\left(-\frac{m_i \mathbf{v}_i^2}{2k_B T}\right) \quad (2.7)$$

where  $\mathbf{V}$  is the velocity of the tracer and  $\mathbf{v}_i$  is the velocity of  $i$ -th gas particle. From the distribution of the tracer described by equation (2.6), we obtain the distribution of the speed of the tracer  $|\mathbf{V}| = \sqrt{V_x^2 + V_y^2 + V_z^2}$  in 3 dimensional system as

$$P_{MB}(M, |\mathbf{V}|) = 4\pi |\mathbf{V}|^2 \left(\frac{M}{2\pi k_B T}\right)^{\frac{3}{2}} \exp\left(-\frac{M|\mathbf{V}|^2}{2k_B T}\right) \quad (2.8)$$

We compare the speed distribution of the tracer from the simulation with the equation (2.8) in figure 2.2. From this figure, the tracer speed in our system

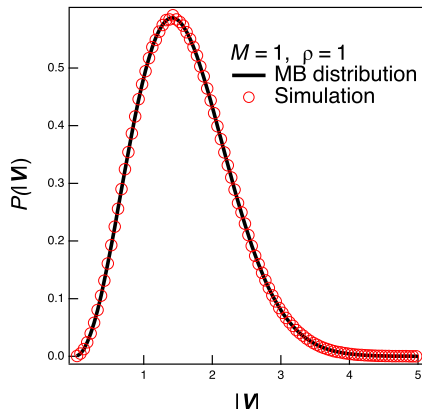


Figure 2.2: The velocity distribution of the tracer with the Maxwell Boltzmann distribution (MB distribution) in 3 dimensional system.

satisfies the Maxwell Boltzmann distribution.

We also analyzed the radial distribution function around the tracer(RDF). In general, analytical calculation of RDF for fluids is rather difficult. To calculate the RDF, the various approximations have been employed[27]. Meanwhile, in a few cases, exact expression of RDF can be obtained such as ideal gas or one-dimensional system cases[28]. Also in our system, the RDF can be obtained analytically because of the non-interacting nature of gas particles.

To calculate the RDF, we first analyze the partition function of the system  $Z_N$ . The Hamiltonian of our system  $\mathcal{H}$  is

$$\mathcal{H}(\mathbf{R}, \mathbf{V}, \{\mathbf{r}_i\}, \{\mathbf{v}_i\}) = \frac{\mathbf{P}^2}{2M} + \sum_{i=1}^N \frac{\mathbf{p}_i^2}{2m} + \sum_{i=1}^N U(|\mathbf{R}_t - \mathbf{r}_i|) \quad (2.9)$$

where  $\{\mathbf{r}_i\} = \mathbf{r}_1, \mathbf{r}_2 \cdots \mathbf{r}_N$ ,  $\{\mathbf{p}_i\} = \mathbf{p}_1, \mathbf{p}_2 \cdots \mathbf{p}_N$ ,  $\mathbf{P}$  and  $\mathbf{p}_i$  are the momentum of tracer and i-th ideal gas particle,  $U$  is the hard core interaction between tracer and gas particles defined as

$$U(r) = \begin{cases} \infty & (r \leq \frac{\sigma}{2}) \\ 0 & (r > \frac{\sigma}{2}) \end{cases} \quad (2.10)$$

From the Hamiltonian, we can calculate the partition function as follows

$$Z_n = \int d\mathbf{r}_t d\mathbf{r}_i d\mathbf{v}_t d\mathbf{v}_i e^{-\beta\mathcal{H}} \quad (2.11)$$

Since the interaction potential depends only on the distance between tracer and fluid particle, we can reduce the partition function as follows.

$$Z_{N+1} = \left(\frac{2\pi k_B T}{M}\right)^{d/2} \left(\frac{2\pi k_B T}{m}\right)^{Nd/2} \mathcal{V} \left(\mathcal{V} - \frac{\pi^{d/2}}{\Gamma(\frac{d}{2} + 1)}\right)^N \quad (2.12)$$

$$= \left(\frac{2\pi k_B T}{M}\right)^{d/2} \left(\frac{2\pi k_B T}{m}\right)^{Nd/2} Q_{N+1} \quad (2.13)$$

where  $Q_{N+1}$  is the configuration integral. The partition function(2.12) is the same as the ideal gas case, although the tracer has the interaction between the fluid particles. From this partition function, the thermodynamic property is the same with the ideal gas if the system size is sufficiently large.

The 2-body density distribution  $\rho^{(2)}(\mathbf{R}, \mathbf{R} + \mathbf{r}_j)$  of the tracer and gas particle  $j$  is

$$\rho^{(2)}(\mathbf{R}, \mathbf{r}_j) = \langle \delta(\mathbf{R} - \mathbf{R}') \delta(\mathbf{r}_j - \mathbf{r}'_j) \rangle \quad (2.14)$$

$$= \frac{1}{Q_{N+1}} \int \delta(\mathbf{R} - \mathbf{R}') \delta(\mathbf{r}_j - \mathbf{r}'_j) \times \exp\left(-\beta \sum_{i=1}^N U(\mathbf{R}' - \mathbf{r}'_i)\right) d\mathbf{r}'_t \{d\mathbf{r}'_i\} \quad (2.15)$$

$$= \frac{1}{\mathcal{V} \left(\mathcal{V} - \frac{\pi^{d/2}}{\Gamma(\frac{d}{2} + 1)}\right)} \exp[-\beta U(|\mathbf{R} - \mathbf{r}_j|)] \quad (2.16)$$

$$= \frac{1}{\mathcal{V} \left(\mathcal{V} - \frac{\pi^{d/2}}{\Gamma(\frac{d}{2} + 1)}\right)} \exp[-\beta U(r_j)] \quad (2.17)$$

$$= \rho^{(2)}(r_j) \quad (2.18)$$

where  $r_j$  is the relative distance between the tracer and  $j$ -th gas particle as  $r_j = |\mathbf{R} - \mathbf{r}_j|$ . From this, we can obtain pair density  $\rho^{(2)}$  between the tracer and ideal gas particles as

$$\rho^{(2)}(r) = \sum_{i=1}^N \rho^{(2)}(r_j) = \frac{\rho}{\mathcal{V}} \exp[-\beta U(r)] \quad (2.19)$$

where  $r$  is the distance from the tracer. The radial distribution function can be obtained by integration of  $\rho^{(2)}$  by  $\mathbf{R}$ . Consequently, we have

$$\int \rho^{(2)}(\mathbf{R}, \mathbf{r}) d\mathbf{R} = \rho \exp(-\beta U(r)) = \rho g(r) \quad (2.20)$$

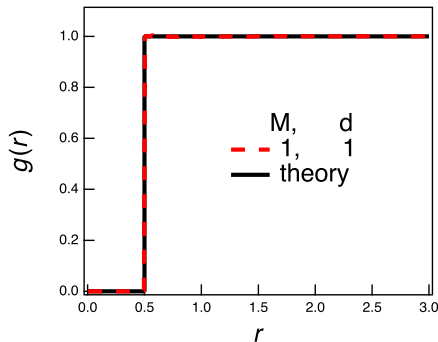


Figure 2.3: Radial distribution function around the tracer for  $M = 1$  and  $\rho = 1$  in 3 dimensions.

Thus, we could get  $g(r)$  as  $\exp(-\beta U(r))$ . We compare this analytical expression with the simulation results in 3 dimensions in Figure 2.3. In this figure, we can see the almost complete agreement between the analytical expression and the simulation result. For other parameters and dimensions, the RDF satisfies the equilibrium property in a similar way.

From the analysis of the velocity distribution and RDF shown above, our simulation satisfies the basic equilibrium properties. Therefore, we can confirm our simulations are performed in the equilibrium state.

### 2.2.3 Estimation of time where system size affects

In many cases, molecular simulations are performed in the periodic boundary conditions and these conditions cause the undesirable artifacts such as the nonphysical sound propagation etc. for the long time dynamics of particles[29]. In our system, because the gas particles do not interact each other, the sound propagation does not occur. However, the artificial correlation may be induced between the collisions if the tracer collides with the same gas particle flies beyond the periodic boundaries. Below, we estimate the characteristic time for such a event.

The number density of the tracer particle  $\rho_t$  is  $\rho_t \sim 1/L^D$ , the relative mean speed of the tracer and gas particle  $\bar{v}_{it}$  is about  $\bar{v}_{it} \sim \left(\frac{k_B T m M}{m+M}\right)^{1/2}$  and the cross section of the collision between the tracer and gas particle  $S$  is  $S \sim \sigma^{D-1}$ . From these value, we can roughly estimate the time scale of re-collisions of the tracer and the gas particle due to the periodic boundary condition  $\tau_{peri}$  as  $\tau_{peri} \sim (\rho_t \bar{v}_{it} \sigma^{D-1})^{-1}$ . The free time of the tracer  $\tau_t$  is about  $\tau_t \sim \rho \bar{v}_{ti} \sigma^{D-1}$  and this is about  $N^{-1} \tau_{peri}$ . This means that the re-collision

event due to the periodic boundary condition can occur in the long time scale where the number of collisions is comparable to the number of gas particles. Therefore, the undesired re-collision events rarely occur in the short time scale which is focused in this work if the number of particles is sufficiently high.

## 2.3 Analysis methods

The dynamics of the tracer is completely determined by the successive velocities and time intervals between the collisions. However, we can not find the characteristic behavior of tracer dynamics by simply looking the raw data because these data always fluctuate. Therefore, we need to calculate the some sort of averaged value.

The basic idea characterizing the fluctuating quantity is the time correlation function methods[29] as follows,

$$C(t) = \langle A(0)B(t) \rangle \quad (2.21)$$

where  $A$  and  $B$  are the arbitrary dynamic variables and  $\langle \dots \rangle$  indicates the average for the time or ensemble. In the ergodic and equilibrium state, the time and the ensemble averages are the same, thus we employ the time average for calculating the various correlation functions. In general, the correlation of  $A(0)$  and  $B(t)$  decreases as  $t$  increases, and it will be decoupled as below,

$$C(t) = \langle A(0) \rangle \langle B^*(t) \rangle = \langle A(0) \rangle \langle B^*(0) \rangle \quad (2.22)$$

where we use the stationary condition in equilibrium. From equation (2.22),  $C(t)$  approaches to 0 if  $A$  and  $B$  fluctuate around 0.

The most typical time correlation function characterizing the dynamics of the tracer is the normalized velocity autocorrelation function (VAC) defined as

$$\frac{\langle \mathbf{V}(0) \cdot \mathbf{V}(t) \rangle}{\langle \mathbf{V}^2(0) \rangle} \quad (2.23)$$

This VAC is 1 at the initial time and approaches to 0 at the long time limit. Since the VAC is directly related to the diffusion of the tracer, it is an important quantity[29, 14, 15]. Therefore, we analyze the VAC to characterize the dynamics of the tracer in the ideal gas.

The Other correlation function appeared in this work is the non-Gaussian parameter (NGP) defined as

$$\text{NGP} = \frac{3\langle\Delta\mathbf{R}^4(t)\rangle}{5\langle\Delta\mathbf{R}^2(t)\rangle^2} - 1 \quad (2.24)$$

where  $\Delta\mathbf{R}(t)$  is the displacement of the tracer given as  $\mathbf{R}(t) - \mathbf{R}(0)$ . The NGP can detect the non-Gaussianity of  $\Delta\mathbf{R}(t)$ . The non 0 value of NGP means the non-Gaussianity nature of  $\Delta\mathbf{R}(t)$ . Rahman used NGP and showed that the dynamics of the constituent molecules of the argon liquid can not be written by the Langevin equation [10]. Also, the NGP is widely used to detect the dynamic heterogeneity of the glassy liquids[30] or the polymer solutions[31] although the relation between the Gaussianity and heterogeneity is not fully clear. In this work, we use the NGP to compare our ideal gas system to other complex systems and Langevin description.

# Chapter 3

## Short time dynamics of tracer in 3 dimensional ideal gas

### 3.1 Introduction

When we focus on the short time dynamics of the tracer in a fluid, Langevin description can not be used [10, 11], and we have to consider the individual collisions of fluid molecules. If the fluid is dilute or has an intermediate density, the individual collisions are not strongly correlated each other and the dynamics of the tracer can be described by the Enskog theory which incorporate the contribution of the fluid structure [14, 15, 32]. In contrast, for the dense fluid case, the collisions are strongly correlated, and this leads to the slow relaxation of the tracer motion. In such a case, the dynamics of the tracer have not been fully understood, despite many simulation works [32].

The dynamics of the tracer is strongly related to the static structure of the fluid. The mode-coupling theory can predict the dynamics of the tracer (or constituent particles) in some dense systems by incorporating the static correlations[33]. Götze tested the mode-coupling theory for the super-cooled liquids and showed that it quantitatively predicts the results of the simulations and experiments[34]. Thus, the mode-coupling theory is the one of the useful approaches for the tracer dynamics in the dense fluids. However, the mode-coupling theory can not predict the dynamics of the tracer in the structureless fluids because the structural information required for the theory is missing. Frenkel and Maguire[35, 36] analyzed the dynamics of the fluid composed of the infinitely thin hard rods by using the simulations. This system does not have any structures, thus the static equilibrium property is the same as the ideal gas. In this system, they showed that the dynam-

ics of the rods can be predicted by the Enskog theory when the rods are dilute. However, the Enskog theory fails for high density case. Such a behavior purely originates from the correlated collisions of rods and can not be predicted by the mode-coupling theory. In addition to the important works by Frenkel and Maguire mentioned above, various structureless fluids which have the dynamic correlations have been analyzed by the simulation[37, 38], theory[39, 40] and experiment[41]. However, the dynamics of the constituent particles have not been fully understood for high density cases, although the low and middle density cases are well understood.

As we mentioned above, the difficulty of the dynamics of many body-systems arises from the dynamic correlations. If we consider the short time dynamics of the tracer in the fluid, we have to consider the correlated collisions caused by the tracer-fluid and fluid-fluid interactions. To understand such a complicated problem, it would be informative to consider the system which does not have the correlated collisions caused by the fluid-fluid interactions. Thus, we analyze the dynamics of the tracer in the ideal gas composed of the point masses in this work. There is a similar work considering the dynamics of the tracer in the fluid in which the fluid particles does not interact each other by Zwanzig[9]. He considered the tracer tied with many linear oscillators as the heat bath, and he solved the tracer dynamics analytically. This model is instructive for many-body problems, but it does not give any insights for the correlated collisions of the tracer and fluid particles.

In this chapter, we investigate the dynamics of the tracer in the ideal gas by using the hard sphere simulations as shown in chapter 2. The construction of the chapter is as follows. First, we analyze the velocity autocorrelation functions and non-Gaussianity parameter of the tracer particle by changing the tracer mass  $M$  and number density of the ideal gas  $\rho$ . Although the gas particles do not have the interaction each other, the non-trivial dynamics of the tracer is observed. Second, we analyze the dynamics of the tracer by focusing on the successive collisions between the tracer and gas particles and identify the origin of the nontrivial dynamics of the tracer.

## 3.2 Results of the simulations

We show the velocity autocorrelation functions (VAC) of the tracer with various  $M$  and  $\rho = 1$  in Figure 3.1, together with the theoretical prediction by so-called Enskog theory[13].

$$\langle \mathbf{V}(t) \cdot \mathbf{V}(0) \rangle = \frac{3k_B T}{M} \exp\left(-\frac{4m}{3(m+M)}t\right) \quad (3.1)$$

The calculation methods of VAC is shown in section 2.3. The vertical and horizontal axis are normalized by the kinetic energy  $\langle \mathbf{V}^2 \rangle = 3k_B T/M$  and the mean free time  $\bar{\tau}$ . From figure 3.1(a), the VAC of tracer decays rapidly as

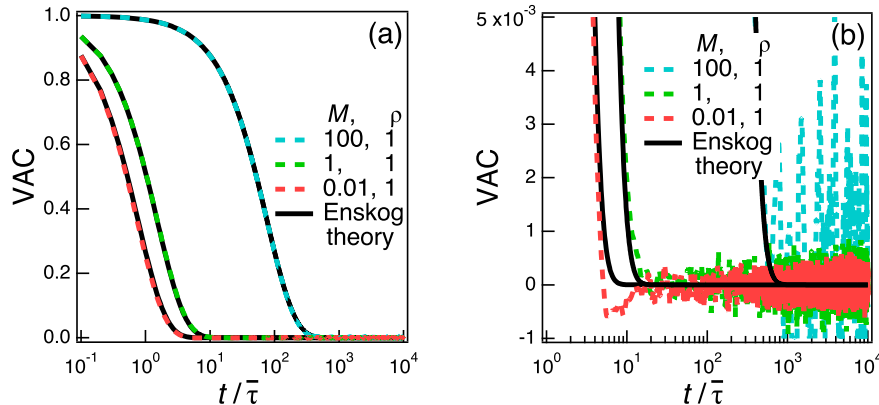


Figure 3.1: (a) Velocity autocorrelation function (VAC) of the tracer changing  $M$  for fixed number density  $\rho = 1$ . (b) Enlarged view of figure 3.1(a).

the mass of the tracer decreases, and the VAC decays to zero at the time scale where a single collision occurs for the low mass case  $M \ll 1$ . This behavior is trivial because the velocity of the light tracer can be changed easily by a single collision, and this leads to the rapid decay of the velocity correlation of the tracer. Also, the Enskog theory can reproduce the VAC of tracer for  $M = 1$  and  $100$ . This means that the VAC of tracer is exponential function and this suggests that the dynamic correlation can be safely ignored. For the low mass case  $M = 0.01$ , although the Enskog theory almost reproduces the VAC of the tracer, we can see the minor deviation from the theory in Figure 3.1(b). This suggests that a dynamic correlation occurs even if the fluid particles do not interact each other.

The non-Gaussian parameter defined in equation(2.24) of the tracer with various  $M$  and fixed  $\rho$  at 1 is shown in figure 3.2. We observe the clear peaks of NGPs for  $M = 0.01, 1$  in the short time scale. Yamaguchi and Kimura [11] analyzed the NGP of the tracer in the hard sphere fluid composed of the identical particles by using the Monte Carlo simulations and reported the peak of the NGP of the tracer occur in the short time scale. Our results of NGP agrees qualitatively with those by Yamaguchi and Kimura. Besides, we observe that the peak of the NGP decreases as the mass of the tracer increases. This behavior means that the displacement of the tracer approaches to the Gaussian in the high mass case. For the dynamics of the tracer at

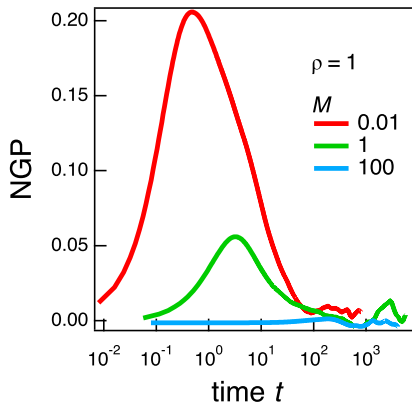


Figure 3.2: Non Gaussian parameter of the tracer changing  $M$  for fixed number density  $\rho = 1$

the short time scale, we have to consider the collision dynamics and can not use the Langevin description. However, when the tracer mass is sufficiently large, the Langevin equation can be theoretically derived from the Boltzmann equation into the expansion of the mass ratio [12]. Our simulation results support this theory and the Langevin equation can be used for the dynamics of the heavy tracer.

We show the VAC with various  $\rho$  and fixed mass  $M = 1$  in Figure 3.3 with the Enskog theory. From Figure 3.3(a), the curves of VAC are roughly

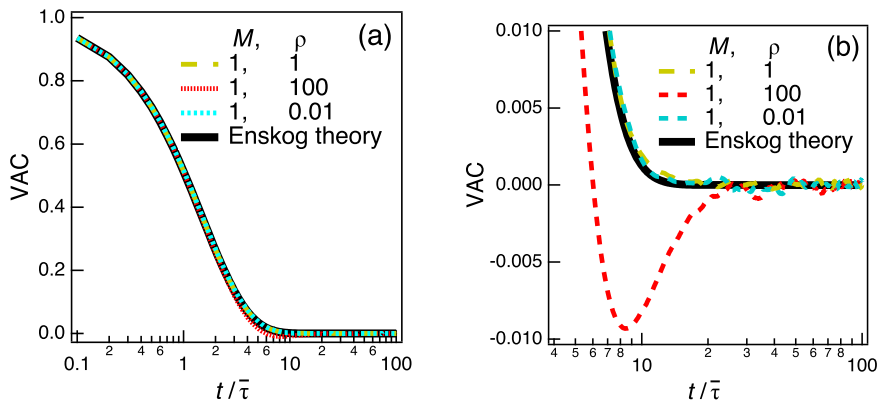


Figure 3.3: (a)VAC of tracer changing  $\rho$  for fixed mass  $M = 1$ . (b)Enlarged view of figure 3.3(a).

the same and the Enskog theory can reproduce these behaviors. However, for the high density case ( $\rho = 100$ ), we observed the minor negative velocity correlation in the short time scale and this VAC deviates from the Enskog theory in Figure 3.3(b). In the Enskog theory, since the dynamic correlations of collisions are not considered, the deviation from the Enskog theory implies the dynamics correlation can occur even if the fluid particles do not interact with each other. Although the negative correlation and deviation from the Enskog theory of the VAC of the hard sphere have been reported [42], these are not fully understood yet.

We show the NGP of the tracer with the various number density  $\rho$  and fixed mass  $M = 1$  in Figure 3.4. From Figure 3.3, we observe the peaks of NGP in the short time scale for all densities. This means that the displacement of the tracer is non Gaussian even when the mass of the tracer is the same with the gas particles for all number densities. Also, we can find that the peak of NGP increases when the number density is high ( $\rho = 100$ ). In general, the NGP can show large peaks in various systems such as the glass[30] or polymer solutions[31] and the origin of the large peaks of the NGP is considered to be a dynamic heterogeneity of the fluid around the particle. However, in our system, the fluid does not have the dynamic heterogeneity because the fluid does not interact with each other. Thus, the origin of the increase of the peak of NGP at high densities observed in our system would be different from those for the glass or polymer solutions.

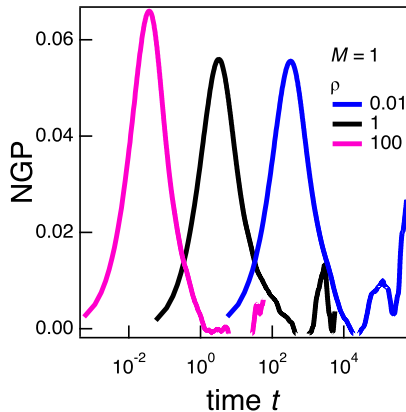


Figure 3.4: NGP of tracer for various  $\rho$  at fixed mass  $M = 1$

From the results of the VAC and NGP for the various  $M$  and  $\rho$ , we found that the behavior of the tracer is qualitatively changed by these parameters. When the mass of the tracer is high, the behavior of the tracer can be repro-

duced by the Enskog theory and the Langevin equation. However, when the mass of the tracer is small, the VAC shows a negative peak and NGP shows positive peak, and such behaviors can not be reproduced by the Enskog theory or the Langevin equation. In the low density cases, the dynamics of the tracer is consistent with the Enskog theory. However, in the high density cases ( $\rho \gg 1$ ), the VAC shows the negative peak and NGP shows positive peak. The origin of such behavior is not the dynamic heterogeneity because of the ideal gas nature of our system. Thus, we found that the dynamics of the tracer in ideal gas is not trivial when the mass of the tracer is small  $M \leq 1$  and number density is high  $\rho \geq 1$ . In the following analysis, we focus on such a parameter region.

We show the VAC and NGP in the region of  $M \leq 1$  and  $\rho \geq 1$  in Figure 3.5 with the Enskog theory. From this figure, we find the strong negative peak of VAC for  $M = 0.01, \rho = 100$ , and such a behavior deviates from the Enskog theory. The peak of the NGP is enhanced for the  $M = 0.01$  and  $\rho = 100$  case. Thus, we confirm that the dynamics of the tracer in the region of the low mass and high number density is non-trivial.

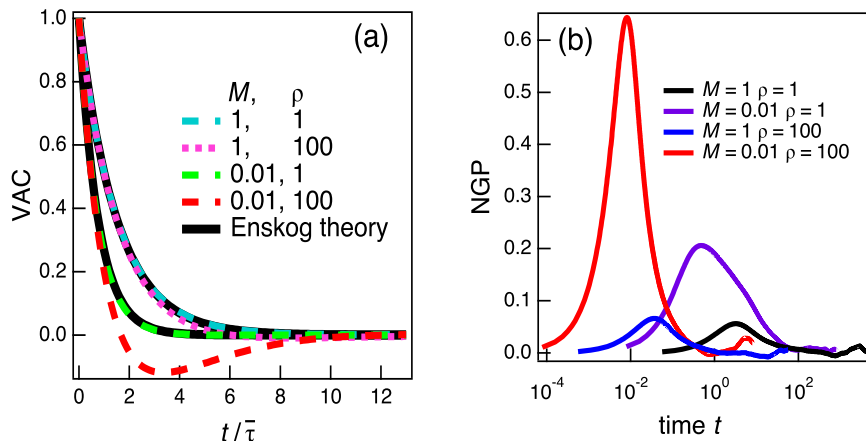


Figure 3.5: (a) VAC for various  $M$  and  $\rho$  in the ranges  $M \leq 1$  and  $\rho \geq 1$ . (b) NGP for the same ranges.

## 3.3 Discussions

### 3.3.1 Single collision

The dynamics of the tracer in our system is the ballistic motion and the instantly velocity change by the collisions. Thus, it would be reasonable to focus on the collision dynamics between the tracer and gas particles.

We have found the negative VAC of the tracer occurs when the mass of the tracer is low  $M \leq 1$  in figures 3.3 and 3.5(a). Below, we consider the naive hypothesis for the negative correlations. When the tracer mass is small, the speed of the tracer is high compared with the gas particles due to the Maxwell Boltzmann distribution shown in equation (2.6). In this case, the probability that the tracer has the frontal collisions with the gas particles increases. Besides, the tracer velocity can be easily changed by the single collision with a gas particle due to the hard sphere interaction (eq (2.4)) In this case, the back reflection of the tracer may occur by the single collision. To check this hypothesis, we calculated the inner product of the velocities before and after the single collision  $\gamma_1$  as

$$\gamma_1 = \frac{\sum \mathbf{V}_i \cdot \mathbf{V}_{i+1}}{\sum \mathbf{V}_i^2} \quad (3.2)$$

We plot this  $\gamma_1$  for various  $M$  and  $\rho$  from the simulation in Figure 3.6(a). This figure shows that the  $\gamma_1$  does not depends on  $\rho$ . Also,  $\gamma_1$  approaches to 1 for large  $M$ , and 0 for small  $M$ . The behavior of  $\gamma_1$  for large  $M$  is consistent with our naive intuition because the velocity of the heavy tracer is almost not changed by the single collision with a gas. The behavior of  $\gamma_1$  for small  $M$  means that the back reflection does not occur by the single collision. Thus, the our hypothesis above is not acceptable.

Burshtein and Krongauz[23] considered the theoretical model for the dynamics of the tracer in the hard sphere fluid. They calculated the VAC of the tracer by considering the collision process and showed that there is 2 necessary conditions causing the negative VAC if the successive collisions are independent; (1) the velocity correlation before and after a single collision is negatively correlated and (2) the distribution of the free time between a collision deviates from the exponential distribution. This theory is constructed for the tracer in the hard sphere fluid. However, the theory can be applied for our ideal gas system because the theory does not consider the interaction between the fluid particles explicitly. In our system, the first condition for the negative VAC is not satisfied as shown above. Then, we consider the necessary condition (2). We plot the distribution of the free time of the tracer between the collisions for various  $M$  and  $\rho$  in Figure 3.6(b), with the

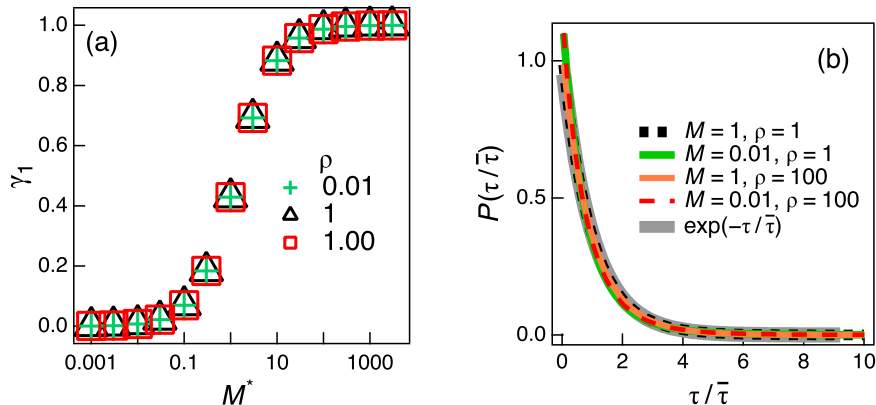


Figure 3.6: (a)  $\gamma_1$  for various  $M$  and  $\rho$ . (b) Distribution of the free time of tracer between collision scaled by mean free time.  $\bar{\tau}$

exponential function. This figure shows that the distribution of the free time is almost exponential for all parameters. Thus, the second condition for the negative VAC is not satisfied neither.

These discussions of the velocity correlation before and after a single collision and distribution of the free time suggests that the individual collisions are not independent even if the ideal gas particles do not interact each other. Therefore, we consider the correlated collisions in the following section. The theoretical analysis and further discussions of the statistics of the single collision are performed in chapter 4.1.

### 3.3.2 Correlation of collisions

The VAC of the tracer deviates from Enskog theory when  $M$  is low and  $\rho$  is high in Figure 3.5(a). The Enskog theory considers only the static correlation such as the structure of the fluids, and it does not consider the dynamic correlation. Thus, the deviation of VAC from the Enskog theory means that the dynamic correlation exists even if the fluid is an ideal gas. Also in the discussion in section 3.3.1, we arrived at the conclusion that the collisions can be correlated for the case where  $M < 1$  and  $\rho > 1$ . In this section, we analyze the correlation of collisions.

Taloni et al investigated the dynamics of the hard disk in 2 dimensions by introducing the correlation functions for the statistical average on collisions and showed that the correlations averaged by collisions has the similar behavior of the correlations averaged by time[22]. However, they analyzed only the equal mass system in 2D, so their results would not be directly applicable

to our system. In the following analysis, we use the quantity introduced by Taloni et al.

We have analyzed the correlation of the velocities before and after single collision by introducing  $\gamma_1$ . We generalize this quantity to analyze the correlation of velocities before and after  $n$  successive collisions as follows.

$$\gamma_n = \frac{\langle \mathbf{V}_n \cdot \mathbf{V}_0 \rangle_{coll}}{\langle \mathbf{V}_0^2 \rangle_{coll}} \quad (3.3)$$

where  $\langle \dots \rangle_{coll}$  means the statistical average over collisions. To the author's best knowledge, this quantity is first introduced by Taloni et al. This quantity can be obtained in our simulation as follows

$$\gamma_n = \frac{\sum_{i=1}^N \mathbf{V}_{i+n} \cdot \mathbf{V}_i}{\sum_{i=1}^N \mathbf{V}_i^2}. \quad (3.4)$$

Although  $\gamma_n$  is similar to the VAC, the VAC is the average over the time while  $\gamma_n$  is the average over the collision. VAC is affected by the several multiple collisions, and we can not distinguish the contributions of different numbers of collisions in the VAC in principle. However  $\gamma_n$  can distinguish the contribution of different numbers of collisions. We show  $\gamma_n$  for various

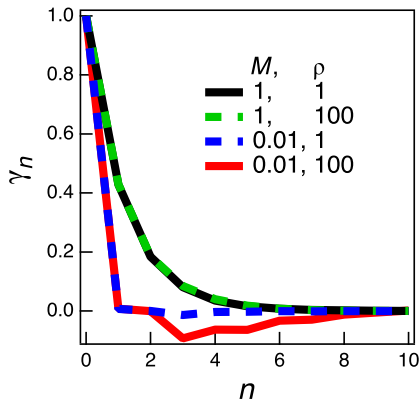


Figure 3.7:  $\gamma_n$  for various  $M$  and  $\rho$  in the ranges of  $M \leq 1$  and  $\rho \geq 1$ .

$M$  and  $\rho$  in the figure 3.7. We observe that  $\gamma_n$  is the positive for  $M = 1$ . In contrast, for  $M = 0.01$  and  $\rho = 100$ ,  $\gamma_n$  becomes negative in  $n \geq 3$  while  $\gamma_1$  and  $\gamma_2$  are positive. This results suggest that the successive collisions are correlated when  $M$  is low and  $\rho$  is high, and negative velocity correlation is caused by 3 or more collisions. Taloni et al obtained the similar negative value of  $\gamma_n$  for the fluid composed of the identical hard disks in 2D when the

density of the fluid is high. However, they did not discuss the origin of the negative correlation of  $\gamma_n$ .

We discuss the origin of negative  $\gamma_n$  which occurs after 3 collisions. For high density cases where the mean distance between the gas particles is smaller than the size of the tracer  $\sigma$ , the gas particles surrounding the tracer would effectively form the cage for the tracer. Such a phenomenological picture is often used to explain the negative VAC in some dense systems such as the hard sphere fluid[43], Lennard-Jones fluid[44], or granular fluid[45]. However, the cage model is rather phenomenological and does not tell us the details of the collision dynamics. Also, the cage model does not explain the reason why  $\gamma_n$  becomes negative for  $n \geq 3$ . Thus, we do not employ the cage picture to study the dynamics in our system.

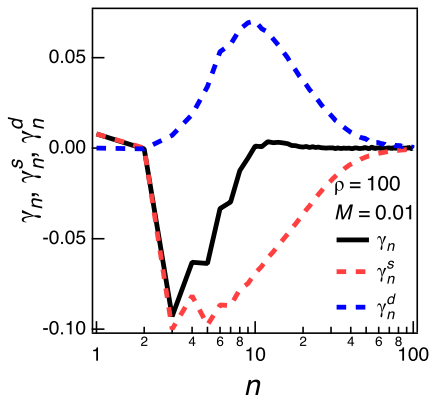


Figure 3.8:  $\gamma_n^s$ ,  $\gamma_n^d$  and  $\gamma_n$  for  $M = 0.01$  and  $\rho = 100$ .

Here, we consider the origin for the correlated collisions. The fluid particles do not interact with each other, and this leads to the uniform distribution of the position as shown in fig 2.3. Thus, when all the gas particles successively colliding the tracer are different, the dynamics of the tracer would be Markovian. In such a case, the distribution of the free time is almost exponential function and negative VAC does not occur as discussed in section 3.3.1. Therefore, we naively think that the correlated collision is caused by the collisions with the same gas particles. To confirm this hypothesis, we analyze  $\gamma_n$  in detail. We decompose  $\gamma_n$  into 2 parts; self  $\gamma_n^s$  and distinct parts  $\gamma_n^d$ . The former is the contribution in the case where the first collision and n-th collision are caused by the same particle. The latter is the contribution

of collisions by different particles. The explicit expressions of  $\gamma_n^s$  and  $\gamma_n^d$  is

$$\gamma_n = \gamma_n^s + \gamma_n^d \quad (3.5)$$

$$\gamma_n^s = \frac{\sum_{i=1}^N \mathbf{V}_{i+n} \mathbf{V}_i \delta_{K_{i+1} K_{i+n}}}{\sum_{i=1}^N \mathbf{V}_i^2} \quad (3.6)$$

$$\gamma_n^d = \frac{\sum_{i=1}^N \mathbf{V}_{i+n} \mathbf{V}_i (1 - \delta_{K_{i+1} K_{i+n}})}{\sum_{i=1}^N \mathbf{V}_i^2} \quad (3.7)$$

where  $K_i$  is the label of the particle  $i$  and  $\delta_{K_i K_{i+n}}$  is the Kronecker delta. The contributions of  $\gamma_n^s$  and  $\gamma_n^d$  are shown in Figure 3.8. From this figure,  $\gamma_n^d$  is 0 for  $n = 1$ . This is obvious from the definition of  $\gamma_n^d$  (eq (3.7)). Also,  $\gamma_n^s$  is 0 for  $n = 2$ . This is trivial from the collision rule (eq (2.4)), namely the tracer leaves away from a gas particle after a collision, so the tracer can not collide with the gas particle of the first collision in the second collision. The most important feature in the figure 3.8 is the negative value of  $\gamma_n^s$  for  $n \geq 3$ . This behavior indicates that the negative value of  $\gamma_n$  is contributed only by  $\gamma_n^s$ . Namely, we can say that the collision with the same gas particles is the origin of the negative  $\gamma_n^s$ . From the discussions above, we can understand why  $\gamma_n$  shows negative value for  $n \geq 3$ . The correlated collisions can occur only by the collisions with the same gas particles in our system. To collide the same gas particles, 2 collisions are not sufficient and 3 or more collisions are required.

### 3.3.3 Comparison with other simulations

Our system shows complex behavior even if the fluid is composed of point masses which do not interact each other. In this subsection, we compare such behavior with other works.

Mizuta et al investigated the dynamics of the fullerene particles in the Lennard-Jones (LJ) fluid and Weeks-Chandler-Andersen (WCA) fluid with various fullerenes with different size [46]. They showed that the dynamics of the fullerenes in both fluids can be described by the Enskog theory only in the very short time scale. In our result of Figure 3.5(a), the Enskog theory can describe the dynamics of the tracer in the very short time scale where only a single collision occurs, although the deviation is observed after the very short time scale for small  $M$  and high  $\rho$  case. These results imply that the correlated collisions do not affect the dynamics of the tracer in the very short time scale regardless of the existence of the interactions between the fluid particles.

Frenkel and Maguire investigated the dynamics of the fluid composed of the infinitely thin hard rods by using the event driven type simulations.

They showed that the dynamics of the hard rods can be described by the Enskog theory for low density case where the collisions are uncorrelated. In contrast, the dynamics of the rods deviate from the Enskog theory for high density case because of the dynamic correlation of the rods. In such a high density regime, Frenkel and Maguire suggested that dynamics of the rods has the analogy with the stiff polymer and the phenomenological scaling of the diffusion constant for the stiff polymers constructed by Doi and Edwards[47] can describe the dynamics of the rods in the long time diffusive regime. Hofling et al investigated the dynamics of a infinitely thin hard needle in the fixed obstacles in 2 dimensions and showed that the diffusion coefficient of the needle has the same scaling relation with the stiff polymers[37]. Since our system does not treat the rod, we can not expect the analogy to the polymeric fluids. However, the dynamics in the ideal gas in the long time regime may be described by the simple phenomenological scaling theory like the idealized rods models. For the short time scale dynamics, in contrast, we would have to consider the complex collision dynamics.

# Chapter 4

## Statistics of single collision in arbitrary dimension

### 4.1 Introduction

In the previous chapter, we analyzed the dynamics of the tracer in an ideal gas in 3 dimensions and found that the VAC of the tracer shows the non-trivial behavior for low  $M$  and high  $\rho$  case. To understand such behavior, we analyzed the individual collisions and found that the correlated collisions can be caused after 3 or more correlated collisions. For single collision case, the statistics of collision such as the correlation of the velocity before and after single collision  $\gamma_1$  and distribution of the free time  $P(\tau)$  is not affected by the correlated collisions as discussed in subsection 3.3.1. Even in such a case, the non-intuitive behavior was observed for  $\gamma_1$  for the light tracer case. In this subsection, we consider the statistics of the single collision by the theory and analytically calculate  $\gamma_1$ . Before we proceed to the detailed analysis, we introduce works related to our work.

Herman and Alder analyzed the dynamics of the tracer in a hard sphere system and showed that the velocity autocorrelation function of the tracer has the negative peak in a short time scale when the tracer mass is smaller than the surrounding fluid particles[32]. They simply discussed that the negative peak originates from the small momentum of the tracer. However, our simulation result in figure 3.6(a) does not support their claim although our system can not be directly compared with their system simply.

The statistics of the single collision has been studied in many works. The distribution of the free path and time had been thought to be exponential by a rough estimation [48]. Alder developed the hard sphere simulation and showed the distribution of free path is roughly exponential for a widely range

of number densities including those for solids[49, 50]. However, in a recent work, the distribution of the free path and time are shown to be exactly the exponential even in the low density where the molecular chaos is expected [51, 22, 52]. Visco et. al. performed theoretical analysis by considering the transition rate from the pre-collision velocity to the post-collision velocity and showed that the non-exponential distribution of free path and time are due to the existence of the velocity distribution[52]. Strictly speaking, the conditional distribution that the tracer has a certain velocity is exponential, but the integration of the conditional probability over the velocity leads to a deviation from exponential. Although the theory by Visco et al. is precise, they performed calculation only for the case of the equal mass. Therefore, their theory can not be applied to our simulation results as it is.

In this chapter, we perform the theoretical analysis for the single collision statistics for arbitrary tracer masses. The derivation is different from the work by Visco et al. [52]. In our work, we first analyze the probability of collision occurring in  $t \sim t + dt$ ,  $\hat{\mathbf{r}} \sim \hat{\mathbf{r}} + d\hat{\mathbf{r}}$ ,  $\mathbf{v} \sim \mathbf{v} + d\mathbf{v}$  and  $\mathbf{V} \sim \mathbf{V} + d\mathbf{V}$ ,  $P(t, \hat{\mathbf{r}}, \mathbf{v}, \mathbf{V})$ , where  $t$  is the colliding time,  $\hat{\mathbf{r}}$  is the unit vector directed from center of tracer and it of colliding gas particle on collision,  $\mathbf{v}$  is the velocity of the colliding gas particle and  $\mathbf{V}$  is the velocity of tracer. This probability has the all information of the single collision statistics of the tracer. From  $P(t, \hat{\mathbf{r}}, \mathbf{v}, \mathbf{V})$ , we calculate the  $\gamma_1$  and  $P(t)$ . For the discussion of the  $\gamma_1$  and analysis of the one dimensional system in chapter 5, we perform the analysis of the single collision statistics in arbitrary dimensions.

## 4.2 Theoretical analysis

### 4.2.1 Single collision statistics

We analyze the probability of the first collision occurring in  $t \sim t + dt$ ,  $\hat{\mathbf{r}} \sim \hat{\mathbf{r}} + d\hat{\mathbf{r}}$ ,  $\mathbf{v} \sim \mathbf{v} + d\mathbf{v}$  and  $\mathbf{V} \sim \mathbf{V} + d\mathbf{V}$ ,  $P(t, \hat{\mathbf{r}}, \mathbf{v}, \mathbf{V})$ . This theory is essentially in the same manner with the work by Visco et. al[52].

First, we consider the probability that the tracer velocity  $\mathbf{V}$  is sampled after a collision,  $P_a(\mathbf{V})$ . This probability can be obtained by considering the collision frequency for the relative velocity of tracer and a gas particle.

$$P_a(\mathbf{V}) = \frac{\rho \left(\frac{\sigma}{2}\right)^{d-1} \int d\mathbf{v} \int d\hat{\mathbf{r}} (\mathbf{v} - \mathbf{V}) \cdot \hat{\mathbf{r}} P_{MB}(m, \mathbf{v}) P_{MB}(M, \mathbf{V})}{\rho \left(\frac{\sigma}{2}\right)^{d-1} \int d\mathbf{V} \int d\mathbf{v} \int d\hat{\mathbf{r}} (\mathbf{v} - \mathbf{V}) \cdot \hat{\mathbf{r}} P_{MB}(m, \mathbf{v}) P_{MB}(M, \mathbf{V})} \quad (4.1)$$

$$= \frac{F(\mathbf{V}) P_{MB}(\mathbf{V})}{\Lambda} \quad (4.2)$$

where  $F(\mathbf{V})$  is the collision frequency under the condition of the tracer having velocity  $\mathbf{V}$  and  $\Lambda$  is the collision frequency. They are defined as

$$\begin{aligned} F(\mathbf{V}) &= \rho \left(\frac{\sigma}{2}\right)^{d-1} \int d\mathbf{v} \int d\hat{\mathbf{r}} (\mathbf{v} - \mathbf{V}) \cdot \hat{\mathbf{r}} P_{MB}(m, \mathbf{v}) \\ \Lambda &= \int d\mathbf{V} F(\mathbf{V}) P_{MB}(M, \mathbf{V}) \end{aligned} \quad (4.3)$$

The analytical forms of  $F(\mathbf{V})$  in 1 and 3 dimensions are

$$F(\mathbf{V}) = \frac{\rho\pi \left(\frac{\sigma}{2}\right)^2}{\sqrt{\alpha}} \left[ \left( \sqrt{\alpha}V + \frac{1}{2\sqrt{\alpha}V} \right) \text{erf}(\sqrt{\alpha}V) + \frac{1}{\sqrt{\pi}} e^{-\alpha V^2} \right] \quad (\text{for } 3d) \quad (4.4)$$

$$F(\mathbf{V}) = \frac{\rho}{\sqrt{\alpha}} \left[ \sqrt{\alpha}V \text{erf}(\sqrt{\alpha}V) + \frac{e^{-\alpha V^2}}{\sqrt{\pi}} \right] \quad (\text{for } 1d) \quad (4.5)$$

where  $\alpha$  is defined as  $\alpha = \frac{m}{2k_B T}$ . Then, we calculate the probability of first collision occurring in  $t \sim t + dt$ ,  $\mathbf{v} \sim \mathbf{v} + d\mathbf{v}$ ,  $\hat{\mathbf{r}} \sim d\hat{\mathbf{r}} + d\hat{\mathbf{r}}$  under the condition that the tracer having velocity  $\mathbf{V}$ ,  $P(t, \hat{\mathbf{r}}, \mathbf{v}|\mathbf{V})$ . This probability is expressed as the product of 2 terms. One is the probability that the first collision occurs in  $t \sim dt$  and  $\hat{\mathbf{r}} \sim \hat{\mathbf{r}} + d\hat{\mathbf{r}}$ , ignoring the particle having velocity other than  $\mathbf{v}$ ,  $P'(t, \mathbf{v}|\mathbf{V})$ .

$$\begin{aligned} & P'(t, \hat{\mathbf{r}}, \mathbf{v}|\mathbf{V}) d\mathbf{v} dt d\hat{\mathbf{r}} \\ &= \rho \left(\frac{\sigma}{2}\right)^{d-1} (\mathbf{v} - \mathbf{V}) \cdot \hat{\mathbf{r}} P_{MB}(\mathbf{v}) d\mathbf{v} d\hat{\mathbf{r}} \\ & \quad \times \exp \left( -\rho \left(\frac{\sigma}{2}\right)^{d-1} (\mathbf{v} - \mathbf{V}) \cdot \hat{\mathbf{r}} P_{MB}(\mathbf{v}) d\mathbf{v} d\hat{\mathbf{r}} \right) dt \\ &= \rho \left(\frac{\sigma}{2}\right)^{d-1} (\mathbf{v} - \mathbf{V}) \cdot \hat{\mathbf{r}} P_{MB}(\mathbf{v}) d\mathbf{v} dt d\hat{\mathbf{r}} \end{aligned} \quad (4.6)$$

where we can regard the exponent in (4.6) as 0 because it is the infinitesimal value. Another is the probability that the any collisions do not occur in time  $0 \sim t$  for the gas particle having velocity other than  $\mathbf{v}$ ,  $P''(t|\mathbf{V})$ .

$$\begin{aligned} P''(t|\mathbf{V}) &= \left\{ 1 - \int d\mathbf{v}' \int d\hat{\mathbf{r}} \frac{\left(\frac{\sigma}{2}\right)^{d-1} (\mathbf{v}' - \mathbf{V}) \cdot \hat{\mathbf{r}} t}{\mathcal{V}} \right. \\ & \quad \left. \times P_{MB}(\mathbf{v}') (1 - \delta(\mathbf{v}' - \mathbf{v}) d\mathbf{v}) \right\}^{N(1 - P_{MB}(m, \mathbf{v}) d\mathbf{v})} \\ &= \left( 1 - \frac{F(\mathbf{V})t}{\rho\mathcal{V}} \right)^N \end{aligned} \quad (4.7)$$

where we have ignored the infinitesimal quantities. Then, we consider the thermodynamic limit ( $N \rightarrow \infty$ ) and obtain the following equation.

$$P''(t|\mathbf{V}) = \left(1 - \frac{F(\mathbf{V})t}{N}\right)^N = \exp(-F(\mathbf{V})t) \quad (4.8)$$

$P(t, \mathbf{v}|\mathbf{V})$  is the product of  $P'(t, \hat{\mathbf{r}}, \mathbf{v}|\mathbf{V})$  and  $P''(t|\mathbf{V})$ , we get

$$P(t, \hat{\mathbf{r}}, \mathbf{v}|\mathbf{V})d\mathbf{v}dtd\hat{\mathbf{r}} = \rho a^{d-1}(\mathbf{v} - \mathbf{V}) \cdot \hat{\mathbf{r}} P_{MB}(m, \mathbf{v}) \exp(-F(\mathbf{V})t)d\mathbf{v}dtd\hat{\mathbf{r}} \quad (4.9)$$

From this, we get  $P(t, \hat{\mathbf{r}}, \mathbf{v}, \mathbf{V})$  as

$$\begin{aligned} & P(t, \hat{\mathbf{r}}, \mathbf{v}, \mathbf{V})d\mathbf{v}dtd\hat{\mathbf{r}}d\mathbf{V} \\ &= \frac{F(\mathbf{V})P_{MB}(\mathbf{V})}{\Lambda} \rho a^{d-1}(\mathbf{v} - \mathbf{V}) \cdot \hat{\mathbf{r}} \\ & \quad \times P_{MB}(m, \mathbf{v}) \exp(-F(\mathbf{V})t)d\mathbf{v}dtd\hat{\mathbf{r}}d\mathbf{V} \end{aligned} \quad (4.10)$$

the expression (4.10) satisfies the condition of normalization as

$$\int dt \int d\mathbf{v} \int d\mathbf{V} \int d\hat{\mathbf{r}} P(t, \hat{\mathbf{r}}, \mathbf{v}, \mathbf{V}) = 1. \quad (4.11)$$

$P(t, \hat{\mathbf{r}}, \mathbf{v}, \mathbf{V})$  has the all information of the single collision statistics of the tracer.

If we select the coordinate so that the relative velocity  $\mathbf{v} - \mathbf{V}$  is parallel to  $\mathbf{e}_d$  with  $\mathbf{e}_i$  being the  $i$ -th Euclidean basis set vector ( $i = 1, 2, \dots, d$ ), we can reduce the equation (4.10) in the polar coordinate as

$$\begin{aligned} & P(t, \hat{\mathbf{r}}, \mathbf{v}, \mathbf{V})d\mathbf{v}dtd\hat{\mathbf{r}}d\mathbf{V} \\ &= \frac{F(\mathbf{V})P_{MB}(\mathbf{V})}{\Lambda} \rho a^{d-1} |\mathbf{v} - \mathbf{V}| \hat{r}_1 \cos \theta_1 \\ & \quad \times P_{MB}(m, \mathbf{v}) \exp(-F(\mathbf{V})t)d\mathbf{v}dtd\hat{\mathbf{r}}d\mathbf{V} \end{aligned} \quad (4.12)$$

where

$$\hat{r}_1 = \sin^{d-2} \theta_1 \sin^{d-3} \theta_2 \cdots \sin \theta_{d-2} d\theta_1 d\theta_2 \cdots d\theta_{d-1} \quad (4.13)$$

$$(0 \leq \theta_1 \leq \pi/2, 0 \leq \theta_2, \theta_3, \dots, \theta_{d-2} \leq \pi, 0 \leq \theta_{d-1} \leq 2\pi) \quad (4.14)$$

## 4.2.2 Free time analysis

In this subsection, we calculate the free time of the tracer between a collision  $P(\tau)$ . We can obtain  $P(t)$  from  $P(t, \hat{\mathbf{r}}, \mathbf{v}, \mathbf{V})$  (eq(4.10)) by integrating  $\mathbf{v}, \mathbf{V}$

and  $\hat{\mathbf{r}}$ . The integral of  $P(t, \hat{\mathbf{r}}, \mathbf{v}, \mathbf{V})$  over  $\mathbf{v}$  and  $\hat{\mathbf{r}}$  is

$$P(t, \mathbf{V}) = \int d\mathbf{v} \int d\hat{\mathbf{r}} P(t, \hat{\mathbf{r}}, \mathbf{v}, \mathbf{V}) \quad (4.15)$$

$$= \frac{F(\mathbf{V})^2 P_{MB}(M, \mathbf{V})}{\Sigma} \exp(-F(V)t) \quad (4.16)$$

This expression is equivalent to the result by Visco et al.[52] for  $M = m$ .

The integral of  $P(t, \mathbf{V})$  over  $\mathbf{V}$  is complex, thus we consider the low and high  $M$  limit. For the large  $M$  case, the tracer speed is small compared with the gas particles due to the nature of the Maxwell-Boltzmann distribution. Thus, in this case,  $F(\mathbf{V})$  can be reduced to

$$F(\mathbf{V}) = \begin{cases} 2\pi^{\frac{1}{2}}\alpha^{-\frac{1}{2}}\rho a^2 & (3d) \\ \pi^{-\frac{1}{2}}\alpha^{-\frac{1}{2}}\rho & (1d) \end{cases} \quad (4.17)$$

This equation shows that the collision frequency becomes independent of the  $M$  of the tracer for high  $M$  case. From the reduced forms of  $F(\mathbf{V})$  in the large  $M$  limit, we obtain the analytical form of the free time distributions in one dimension and three dimensions as

$$\begin{aligned} P(t)dt &= \int d\mathbf{V} P(t, \mathbf{V})dt \\ &= \begin{cases} s_{H3} \exp(-s_{H3}t)dt & (3d) \\ s_{H1} \exp(-s_{H1}t)dt & (1d) \end{cases} \end{aligned} \quad (4.18)$$

where  $s_{3H}$  is  $2\pi^{\frac{1}{2}}\rho a^2\alpha^{-\frac{1}{2}}$  and  $s_{1H}$  is  $\pi^{-\frac{1}{2}}\rho\alpha^{-\frac{1}{2}}$ . For the small  $M$  case, the tracer speed is much higher than those of the gas particles. In this case,  $F(\mathbf{V})$  can be reduced to

$$F(\mathbf{V}) = \rho\pi a^2|V| \quad (3d) \quad (4.19)$$

$$F(\mathbf{V}) = \rho|V| \quad (1d) \quad (4.20)$$

This relation indicates that the collision frequency becomes independent of the velocities of the gas particles. This is natural because the ideal gas behaves like fixed obstacles for the light tracer. From the reduced form of  $F(\mathbf{V})$  at the small  $M$  limit, we obtain the analytical forms of the free time

distribution in one dimension and three dimensions as

$$\begin{aligned}
& P(t)dt \\
&= \int d\mathbf{V} P(t, \mathbf{V})dt \\
&= \begin{cases} 2s_{L3} \left[ \pi^{\frac{1}{2}} \left( \frac{3}{4} + 3s_{L3}^2 t^2 + s_{L3}^4 t^4 \right) e^{s_{L3}^2 t^2} \operatorname{erfc}(s_{L3}t) - s_{L3}t \left( \frac{5}{2} + s_{L3}^2 t^2 \right) \right] & (3d) \\ 2s_{L1} \left[ \pi^{\frac{1}{2}} \left( \frac{1}{2} + s_{L1}^2 t^2 \right) e^{s_{L1}^2 t^2} \operatorname{erfc}(s_{L1}t) - s_{L1}t \right] & (1d) \end{cases} \\
& \hspace{15em} (4.21)
\end{aligned}$$

where  $s_{L3}$  is  $\frac{\rho\pi a^2}{2} \left( \frac{2k_B T}{M} \right)^{\frac{1}{2}}$  and  $s_{L1}$  is  $\frac{\rho}{2} \left( \frac{2k_B T}{M} \right)^{\frac{1}{2}}$ .

### 4.2.3 Velocity correlation analysis

From the expression (4.10), we can obtain the probability that the collision occurs in  $\mathbf{v} \sim \mathbf{v} + d\mathbf{v}$ ,  $\mathbf{V} \sim \mathbf{V} + d\mathbf{V}$  and  $\hat{\mathbf{r}} \sim \hat{\mathbf{r}} + d\hat{\mathbf{r}}$  by the integrating it over  $t$  as follows.

$$P(\hat{\mathbf{r}}, \mathbf{v}, \mathbf{V}) = \int dt P(t, \hat{\mathbf{r}}, \mathbf{v}, \mathbf{V}) \quad (4.22)$$

$$= \frac{\rho \left( \frac{\sigma}{2} \right)^{d-1} (\mathbf{v} - \mathbf{V}) \cdot \hat{\mathbf{r}} P_{MB}(m, \mathbf{v}) P_{MB}(M, \mathbf{V})}{\Lambda} \quad (4.23)$$

From this probability, we can calculate  $\gamma_1$  introduced in section 3.3.1 as follows.

$$\gamma_1 = \frac{\langle \mathbf{V} \cdot \mathbf{V}' \rangle_{coll}}{\langle \mathbf{V}^2 \rangle_{coll}} \quad (4.24)$$

Here,  $\langle \dots \rangle_{coll}$  denotes the statistical average over the collisions, namely,

$$\langle \dots \rangle_{coll} = \int d\hat{\mathbf{r}} \int d\mathbf{v} \int d\mathbf{V} (\dots) P(\hat{\mathbf{r}}, \mathbf{v}, \mathbf{V}) \quad (4.25)$$

If the velocities before and after a single collision are negatively correlated,  $\gamma_1$  shows negative value. The explicit form of  $\gamma_1$  is

$$\gamma_1 = \frac{\int d\hat{\mathbf{r}} \int d\mathbf{v} \int d\mathbf{V} (\mathbf{V} \cdot \mathbf{V}') P(\hat{\mathbf{r}}, \mathbf{v}, \mathbf{V})}{\int d\hat{\mathbf{r}} \int d\mathbf{v} \int d\mathbf{V} \mathbf{V}^2 P(\hat{\mathbf{r}}, \mathbf{v}, \mathbf{V})} \quad (4.26)$$

We can easily calculate integrals of the equation(4.26) by using the distributions for the velocity of the center of mass and the relative velocity, as

$$\begin{aligned}
\gamma_1 &= \frac{Md + m(d-3)}{Md + m(d+1)} = 1 - \frac{4m}{Md + m(d+1)} \\
&= 1 - \frac{4}{M^*d + (d+1)} \quad (4.27)
\end{aligned}$$

where  $M^*$  is the dimensionless tracer mass. From this expression,  $\gamma_1$  monotonically increases with  $M^*$  and asymptotically reaches to 1 for  $M \gg 1$  in all dimensions. However,  $\gamma_1$  depends on  $d$  strongly when  $M \ll 1$ . Further discussions are shown in the following section.

## 4.3 Discussions

### 4.3.1 Test of the theoretical results

In this subsection, we compare the theoretical results with the simulation results. Direct evaluation of  $P(t, \hat{\mathbf{r}}, \mathbf{v}, \mathbf{V})$  from the simulation is difficult because  $P(t, \hat{\mathbf{r}}, \mathbf{v}, \mathbf{V})$  has the  $3d(= 1 + d - 1 + d + d)$  variables, and it leads to the lack of the statistical samples. Thus, we indirectly test the theoretical results by comparing integrated forms of the free time distribution ( equation (4.18) and (4.21) ) and  $\gamma_1$  ( equation (4.26) ).

We compare the theoretical results of the free time distributions at the high (equation (4.18)) and the small (equation (4.21)) mass limits with the simulation results for dilute ( $\rho = 0.01$ ) and 3 dimensional case in Figure 4.1. In Figure 4.1, we scaled the horizontal and vertical axis by  $s_{H3}$  and  $s_{L3}$ . From Figure 4.1, the expression (4.18) and (4.21) agree with the simulation results at the high and low mass limit.

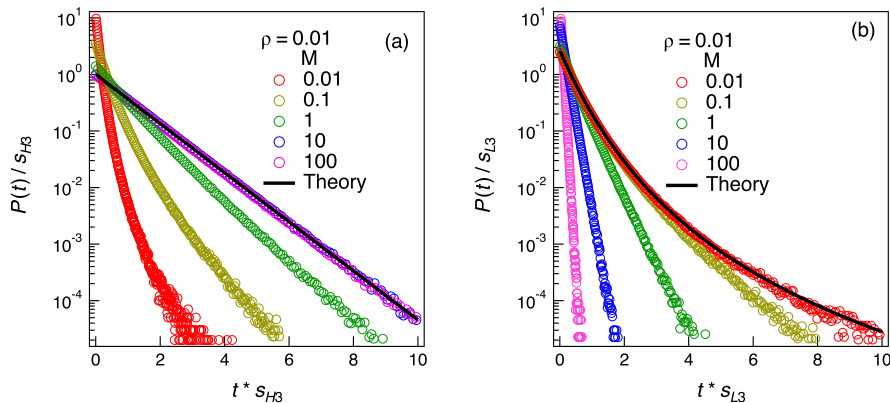


Figure 4.1: Free time distributions of the theoretical results for large mass case (a) (eq. (4.18)) and small mass case (b) (eq (4.21)) in  $\rho = 0.01$ , together with the simulation results. Figures(a) and (b) are scaled by  $s_{H3}$  and  $s_{L3}$

When the ideal gas is dense, the collisions of tracer and ideal gas particles are correlated as shown in subsection 3.3.2. In such a case, the theory of single

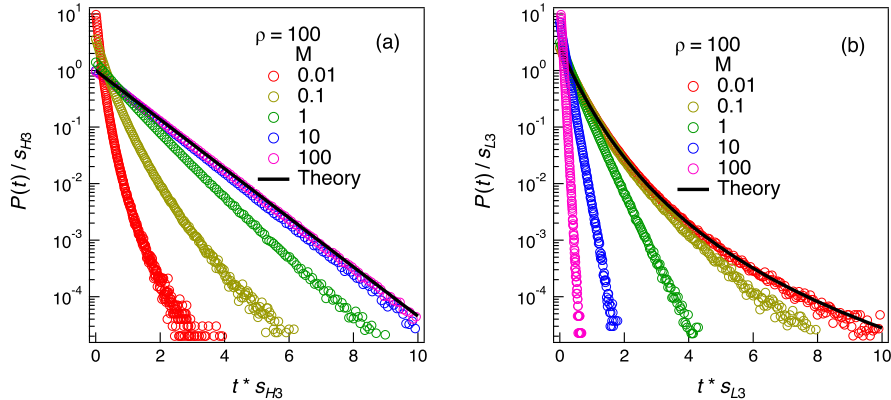


Figure 4.2: Free time distributions of the theoretical results for large mass case (a) (eq. (4.18)) and small mass case (b) (eq (4.21)) in  $\rho = 100$ , together with the simulation results. Figures(a) and (b) are scaled by  $s_{H3}$  and  $s_{L3}$ .

collision derived in section 4.2 would not be simply justified because the theory assumes the Markovian process. Thus, we need to test the theoretical results for high density case. We show the theoretical results of the free time distribution at the high mass (equation (4.18)) and low mass (eq. (4.21)) limits with the simulation results in figure 4.2. The horizontal and vertical axis is scaled by  $s_{H3}$  and  $s_{L3}$ . From Figure 4.2, the theoretical results agree well with the simulation results at the high and low mass limits even if the ideal gas is dense.

Here, we test the theoretical results of  $\gamma_1$  (equation (4.27)) by comparing them with the simulation results. We show the  $M$  dependencies of  $\gamma$  for 1, 2, 3, 4 and 10 dimensions from the theoretical results with the simulation results for 1, 2, 3 and 4 dimensions in Figure 4.3. From the fig 4.3, the theory agrees well with the simulation results.

From the comparison of the theory and simulation results above, we conclude that the theory works for our ideal gas systems even if the fluid is dense.

### 4.3.2 Transformation to the equilibrium probability

The probability of the single collision (equation (4.9)) is the probability sampled from the state immediately after a collision. Thus, this probability is slightly different from the probability in the equilibrium state. To get the probability in equilibrium state, the probability should be sampled from the arbitrary time, and such a probability can be obtained by the method of

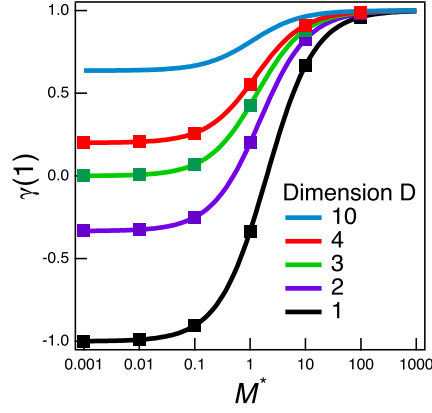


Figure 4.3:  $M$  dependencies of  $\gamma$  in various dimensions from the theoretical results (eq.(4.27)), together with the simulation results

renewal process as follows.

We consider the situation where the tracer has the successive collisions with the gas particles at  $t_-$  and  $t$ . The diagram of such a event is shown in Figure 4.4.

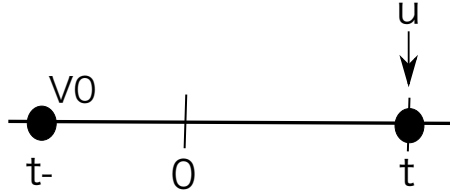


Figure 4.4: Diagram of single collision.

The probability corresponds to this diagram is

$$\begin{aligned}
& P(t - t_-, \hat{\mathbf{r}}, \mathbf{u}, \mathbf{V}_0) d\mathbf{u} dt_- dt d\hat{\mathbf{r}} d\mathbf{V}_0 \\
&= \Lambda \frac{F(\mathbf{V}_0) P_{MB}(\mathbf{V}_0)}{\Lambda} \rho a^{D-1} (\mathbf{u} - \mathbf{V}_0) \cdot \hat{\mathbf{r}} \\
&\quad \times P_{MB}(m, \mathbf{u}) \exp(-F(\mathbf{V}_0)(t - t_-)) d\mathbf{u} dt_- dt d\hat{\mathbf{r}} d\mathbf{V}_0 \quad (4.28)
\end{aligned}$$

where we have multiplied the probability where the collision occurs at time  $t_-$ . Then, we integrate the time  $t_-$  from  $-\infty$  to 0 and obtain the single

collision probability sampled from the equilibrium state as

$$\begin{aligned}
P_{eq}(t, \hat{\mathbf{r}}, \mathbf{u}, \mathbf{V}_0) &= \int_{-\infty}^0 P(t - t_-, \hat{\mathbf{r}}, \mathbf{u}, \mathbf{V}_0) dt_- \\
&= \rho a^{D-1} (\mathbf{u} - \mathbf{V}_0) \cdot \hat{\mathbf{r}} P_{MB}(m, \mathbf{u}) P_{MB}(M, \mathbf{V}_0) \exp(-F(\mathbf{V}_0)t)
\end{aligned} \tag{4.29}$$

Thus, the single collision probabilities sampled from the state immediately after collision and the state in equilibrium are slightly different.

### 4.3.3 Velocity correlation before and after single collision $\gamma_1$

From Figure 4.3, the  $\gamma_1$  monotonically increases and approaches to 1 at the heavy tracer limit ( $M^* \gg 1$ ) in arbitrary dimensions. This behavior is trivial because the velocity of the heavy tracer is almost unchanged only by the single collision with a gas particle. This intuitive description can be justified by the rough scaling argument for the equation(2.4), namely  $|\mathbf{v}| \propto m^{-1/2}$  and  $|\mathbf{V}| \propto M^{-1/2}$  from the Maxwell-Boltzmann distributions, and reduce to the relation (2.4) to  $\mathbf{V}' \simeq \mathbf{V}$ . Then, we can obtain the  $\gamma_1$  for  $M \gg 1$  as  $\gamma_1 \simeq 1$ .

Also, From Figure 4.3, we can see the strong  $d$  dependencies of  $\gamma$  for a light tracer ( $M^* \ll 1$ ). Only in 1 or 2 dimensions,  $\gamma_1$  becomes the negative, whereas  $\gamma_1$  are positive in three or higher dimensions. To understand the origin of the dimension dependencies of  $\gamma_1$ , we consider the limit of the small mass  $M \ll 1$ . In this case, equation (2.4) reduces to

$$\mathbf{V}' \simeq \mathbf{V} - 2\mathbf{V} \cdot \hat{\mathbf{r}} \hat{\mathbf{r}} \tag{4.30}$$

Then, the inner product of  $\mathbf{V}$  and  $\mathbf{V}'$  becomes

$$\mathbf{V} \cdot \mathbf{V}' \simeq V^2(1 - 2 \cos \theta_1) \tag{4.31}$$

This equation shows that the part of the inner product of the velocity in (4.27) switches the sign at  $\theta_1 = \pi/4$  and is independent of the dimensions. This implies that the term of the probability in equation(4.26) depends on the dimensions. The equation (4.31) of the equation (4.27) to

$$\gamma_1 \simeq \frac{\int d\hat{\mathbf{r}} \int d\mathbf{v} \int d\mathbf{V} V^2 (1 - 2 \cos \theta_1) P(\hat{\mathbf{r}}, \mathbf{v}, \mathbf{V})}{\int d\hat{\mathbf{r}} \int d\mathbf{v} \int d\mathbf{V} V^2 P(\hat{\mathbf{r}}, \mathbf{v}, \mathbf{V})} \tag{4.32}$$

We can integrate the degrees of freedom other than  $\theta_1$  and obtain

$$\gamma_1 \simeq \int d\theta_1 (1 - 2 \cos^2 \theta_1) (d - 1) \cos \theta_1 \sin^{d-2} \theta_1. \tag{4.33}$$

From this, we can say that the dimension dependent of  $\gamma_1$  for  $M^* \ll 1$  is due to the distribution of the direction vector on a collision.

From the calculation above, we obtain the reduced forms of the inner product of the velocities before and after single collision  $\mathbf{V} \cdot \mathbf{V}'$  as  $\beta(\theta_1) = 1 - 2 \cos \theta_1$  and the probability occurring such collision  $P(\mathbf{r}, \mathbf{v}, \mathbf{V})$  as  $P(\theta_1) = (d - 1) \cos \theta_1 \sin^{d-2} \theta_1$  in the small mass limit ( $M \ll 1$ ). We can obtain the physical picture of the single collision in small mass limit precisely by visualizing them. We plot  $\beta(\theta_1)$  and  $P(\theta_1)$  for 1, 2, 3, 4 and 10 dimensions in Figure 4.5. From Figure 4.5(a),  $\beta(\theta_1)$  does not depend on the dimensions and monotonically increases with  $\theta_1$  and reaches to 1 at  $\theta_1 = \frac{\pi}{2}$ . The sign of  $\beta(\theta_1)$  changes at  $\theta_1 = \frac{\pi}{4}$ . This is intuitive behavior because the collision at high angle is just like the grazing collision and the velocity is almost unchanged by such a collision. From the figure 4.5(b), we observe that the distribution shifts towards the high angle by the dimension of the system increases. This indicates that the probability of the grazing collision increases with the increase of the dimensions. This is the reason why the  $\gamma_1$  increases with the increase of the dimension in the small mass limit. In 3 dimensions, the contributions of the grazing collision and back reflection to  $\gamma_1$  are the same and this leads to  $\gamma_1 = 0$  in the small mass limit.

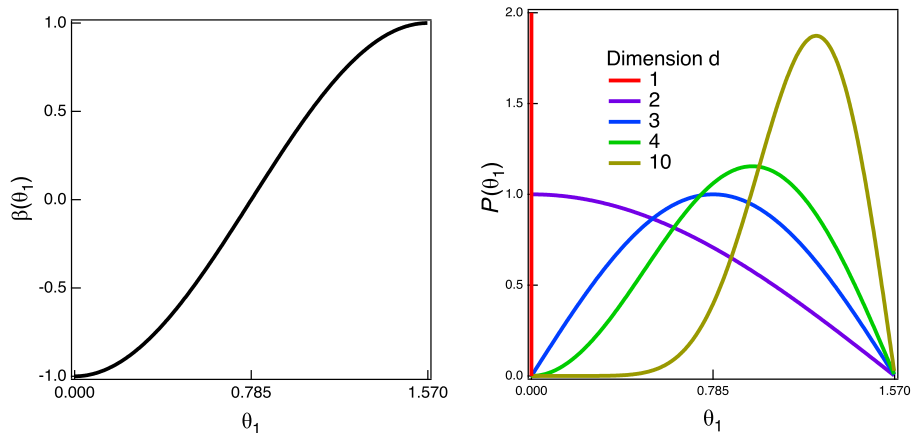


Figure 4.5:  $\beta(\theta_1)$  and  $P(\theta_1)$

#### 4.3.4 Relation to other system

In this subsection, we mention the relation of the analysis of the single collision above to other systems. Herman and Alder showed that the VAC of the light tracer in hard sphere fluids shows the negative peak in 3 dimension

and explained the origin of such a behavior is simply due to the small momentum of the tracer[32]. However, in our analysis of  $\gamma_1$  in subsection 4.3.3, we showed that the negative correlation can not be occurred by the single collision in 3 dimensional system. Although our analysis did not consider the structure of the fluid, our analysis suggests that the negative correlation of the tracer velocity in 3 dimensional system is caused by the correlated collisions.

In our theory, we did not consider the static structure of the gas. This is justified only in our simulation because of the non-interacting nature of the ideal gas. Actually, the RDF does not have any structure as shown in Figure 2.3. However, in the general systems where the fluid particles interact with each other and static structure exists, we have to consider the complicated structure for the single collision statistics. Actually, Burshtein and Krongauz studied the negative velocity correlation of the hard sphere fluid from the viewpoint of the collisions and pointed out that the fluid structure affects the distribution of the direction vector between the tracer and a gas particle on a collision[23]. Thus, further theoretical analyses involving the static structure is required to construct the theory for the system having the interaction between the fluid particles.

We derived the single collision statistics of the hard core interaction systems. This theory would be generalized to some system in which the 2-body collision is well defined. For instance, the single collision statistics for the systems composed of the short-ranged potential such as the WCA potential would be able to constructed. However, if the system is composed of the particles having long-ranged potential, we can not construct the single collision statistics because we can not define the collision well in such a system.

# Chapter 5

## Short time dynamics of tracer in 1 dimensional gas

### 5.1 Introduction

In Chapter 3.1, we found that the dynamics of the tracer shows the complex behavior even if the fluid is an ideal gas. Such dynamics would be difficult to express analytically. One of the difficulties is the geometry of the correlated collisions in 3 dimensions. If the system is in 1 dimension, the geometry is rather simple than the higher dimensional systems because the angle does not exist in 1 dimension. Thus, the dynamics of the tracer in the 1 dimensional system is relatively easy compared with higher dimensional systems.

The 1 dimensional system has been studied by many researchers in statistical mechanics because of its simplicity and the analytic results of the 1 dimensional system are informative for systems in higher dimensions. The one dimensional Ising model would be the most famous example in the statistical mechanics. Also in the field of the classical fluid, the one dimensional systems have been extensively investigated. For instance, the structure of the one dimensional fluid composed of the identical hard rods have been exactly solved[28].

For the dynamics of the one dimensional system, the analytical expressions have been obtained in the limited cases. The dynamics of a one dimensional fluid composed of the point particles have been analytically solved only for the case where the mass of all the fluid particles are equal and the system is infinite by Jepsen[53], Lebowitz and Percus [54, 55]. Also for the periodic boundary case, the dynamics is solvable[56]. In the equal mass case, the velocity of particles is simply exchanged by a collision with a neighboring particles, and the theory utilizes this properly. In contrast, when the masses

of the particles are not equal, the velocity is not simply exchanged by a collision. In such a case, the analytical expression of the dynamics have not been analytically obtained.

The dynamics of the tracer having the different mass from those of the fluid particles in one dimensional system is qualitatively different from the equal mass case. Roy et al showed that the function of the decay of the VAC is changed from  $t^{-3}$  to  $-\ln^2 t$ . Marro and Masolover reported that the power of the VAC decay changes by varying the mass ratio from 1, although their functional form is different from the results by Roy et al. Anyway, such changes of the VAC decay by mass implies that the dynamics of the equal mass case is special.

In this chapter, we focus on the short time dynamics of the tracer in the 1 dimensional ideal gas. In the 1 dimensional system, whether the fluid particles interact with each other does not affect the dynamics of the tracer. This is because the velocities of fluid particles simply exchange by a collision with the neighboring particle and the tracer does not feel such an event. Therefore, we consider the situation where the fluid particles do not interact with each other for simplicity. Such a system would be compared with the 3 dimensional ideal gas system analyzed in the chapter 3.1.

Before the detail analysis, we briefly introduce the 1 dimensional system here. In a 1 dimensional hard sphere system, the volumes of the tracer and gas do not affect the dynamics of the tracer although affects the structure strongly. Therefore, we treat the all particles as the point masses. In such a reason, the characteristic length scale of the system is only the mean distance  $\bar{L}$  between the particles in an infinite system. Therefore, this system is characterized only by mass of the tracer  $M$  in dimensionless units in mean distance  $\bar{L}$ , kinetic energy  $k_B T$  and mass of the gas  $m$ .

## 5.2 Results of simulations

We map the time evolution of the position of the tracer and ideal gas particles to the space-time plain in Figure 5.1 for the same, heavy and light tracer cases. The black curve and points are the trajectory and collision times of the tracer. The red and other color curves are the trajectories of the gas particles. To distinguish each curves of the gas particles, some curves are high lighted. From Figure 5.1(a), we can see that the velocities of tracer are fully exchanged by the collision with gas particles only for  $M^* = 1$ . Such a behavior makes the dynamics of the tracer simple, and this enables to the analytical solution for the dynamics [53, 54, 55]. In contrast, for the heavy tracer case ( $M^* = 100$ ), the tracer moves slowly compared with surrounding

gas particles and tracer velocity is almost unchanged in a single collision. In this case, the event that the tracer collides with the same gas particle hardly occurs and collisions would be almost independent. For the light tracer case  $M = 0.01$ , the behavior is rather different from the heavy tracer case. In this case, the tracer moves faster than the surrounding gas particles and the tracer velocity is easily changed by a single collision with a gas particle. We can observe the back reflections by the single collision and such behavior can be reproduced by the theoretical analysis in chapter 4.1. The most characteristic behavior in Figure 5.1(c) is the repeated collisions with the same gas particle. The tracer reciprocates between the two closest gas particles several times. In such a case, we can say that the collisions are strongly correlated.

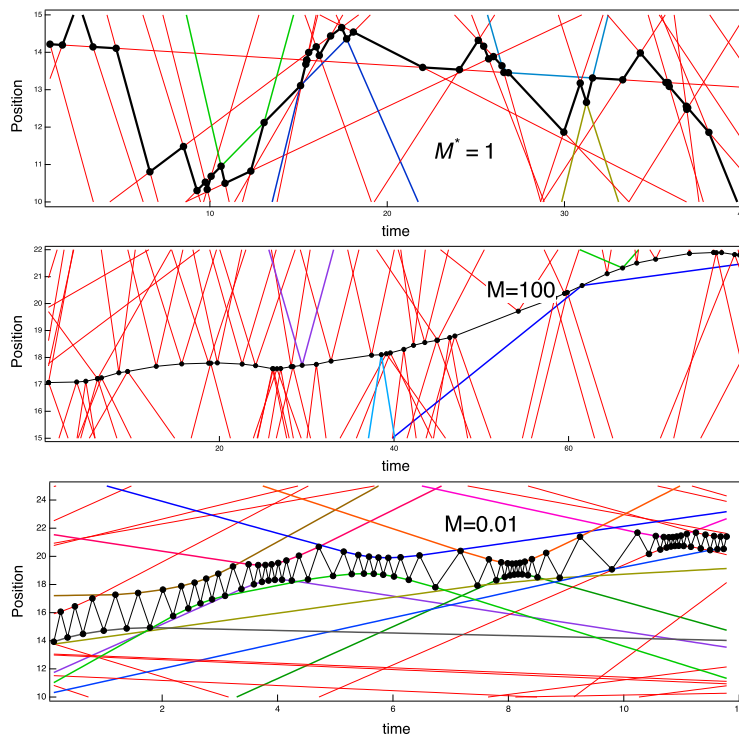


Figure 5.1: The space-time diagram of the tracer and surrounding gas particles for  $M = 1$ ,  $M = 100$  and  $M = 0.01$  case.

To characterize the dynamics of the tracer in 1 dimension, we analyze the VAC of tracer for various masses and plotted the simulation results in Figure 5.2. In figure 5.2, we observe that the decay rates of the VAC decreases as the mass of the tracer increases. This is trivial because the collision rate is low and the velocity change by collision is small in the heavy tracer case,

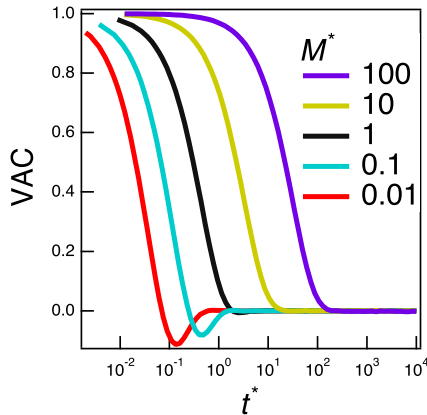


Figure 5.2: VAC of tracer in 1dimension for various  $M$ .

and this directly leads to the slow decay of the VAC. The most important feature in Figure 5.2 is the shape of the VAC. For the heavy tracer case ( $M > 1$ ), the VAC shows monotonic decay and such a behavior is consistent with the picture of the independent collision as shown in Figure 5.1. In contrast, for the light tracer case  $M < 1$ , the VAC shows a negative peak in the short time scale and the negative peak increases as  $M$  decreases. Such a behavior implies that the collisions are correlated and this is consistent with the picture in Figure 5.1(c)

## 5.3 Theoretical analysis

In section 5.2, we analyzed the dynamics of the tracer and found that the dynamics is qualitatively changed by the tracer mass. For the heavy tracer case, the collisions are independent and VAC shows the simple decay. In contrast, for the light tracer case, the collisions are strongly correlated and VAC shows a negative peak in the short time scale. In this section, we theoretically analyze the VAC in the heavy and light limits.

### 5.3.1 Case for heavy tracer

When the tracer mass is large, the collisions are not correlated as shown in Figure 5.1. In such a case, the dynamics is governed only by the statistics of the single collision. In this subsection, we show the VAC of the heavy tracer from the statistics of the single collision by applying the theoretical methods of Lindenberg[21] introduced in section 1.4.

The dynamics of the tracer is composed of the ballistic free motions and velocity changes by the collision with the gas particles. We describe such dynamics as the diagram shown in Figure 5.3. This diagram describes the dynamics with  $n$ -collisions. The tracer velocity  $V_0$  is sampled from the state just after a collision at  $t = t_-$  and the collision with the gas particle having velocity  $u_i$  at time  $t_i$  occurs. The collision times satisfy  $t_- < 0 < t_1 < t_2 < \dots < t_{n-2} < t_{n-1} < t_n < t < t_+$ . We can describe the probability density

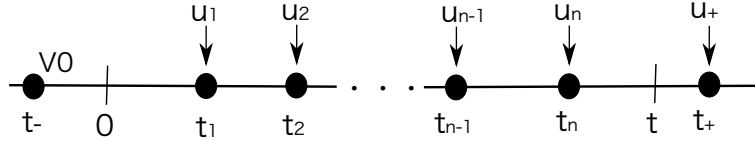


Figure 5.3: Diagram of the dynamics of tracer for  $n$ -th collisions.

corresponding to the diagram with  $n$ -collisions as

$$P(u_+, t_+, u_n, t_n, u_{n-1}, t_{n-1}, \dots, u_2, t_2, u_1, t_1, V_0, t_-) \quad (5.1)$$

The collisions are statistically independent for the heavy tracer case and this safely leads to the Markovian approximation:

$$P(u_+, t_+ | V_n) P(u_n, t_n | V_{n-1}) \dots P(u_2, t_2 | V_1) P(u_1, t_1 | V_0) P_a(V_0) \quad (5.2)$$

where  $P_a(V_0)$  is the probability of the tracer velocity  $V$  sampled from the state just after a collision and is given by equation (4.2).  $P(u, t | V)$  is the conditional probability that the tracer collides with the gas particle having velocity  $u$  on time  $t$  under the condition where the tracer has velocity  $V$  and is given by equation (4.9). The explicit expressions for  $P_a(V_0)$  and  $P(u, t | V)$  are

$$P_a(V) = \frac{F(V) P_{MB}(V)}{\Lambda} \quad (5.3)$$

$$P(u, t | V) = \rho |u - V| P_{MB}(u) \exp(-F(V)t) \quad (5.4)$$

where  $\Lambda$  is the average collision frequency.  $F(V)$  is one under conditional collision frequency for the tracer with velocity  $V$ .

The VAC can be expanded into the number of collisions:

$$\frac{\langle V(0)V(t) \rangle}{\langle V(0)^2 \rangle} = \frac{M}{k_B T} \sum_{n=0}^{\infty} \langle V(0)V(t) \rangle_n \quad (5.5)$$

where  $\langle V(0)V(t) \rangle_n$  is the VAC with n-collisions. The explicit expression of  $\langle V(0)V(t) \rangle_n$  is

$$\begin{aligned}
& \langle V(t)V(0) \rangle_n \\
&= \Lambda \int_t^\infty dt_+ \int_0^t dt_n \int_0^{t_n} dt_{n-1} \cdots \int_0^{t_3} dt_2 \int_0^{t_2} dt_1 \int_{-\infty}^0 dt_- \\
& \quad \int du_+ \int du_n \cdots \int du_2 \int du_1 \int dV_0(V_0V_n) \\
& \quad P(t_+ - t_n, u_+ | V_n) P(t_n - t_{n-1}, u_n | V_{n-1}) \cdots \\
& \quad P(t_3 - t_2, u_3 | V_2) P(t_2 - t_1, u_2 | V_1) P(t_1 - t_-, u_1 | V_0) P_a(V_0) \quad (5.6)
\end{aligned}$$

where  $V_n$  is the tracer velocity after the n-th collision. From the collision rule of equation (2.4),  $V_n$  is rewritten as

$$V_n = p^n V_0 + \sum_{i=1}^n p^{i-1} q u_i \quad (5.7)$$

where  $p = \frac{M-m}{M+m}$  and  $q = \frac{2m}{M+m}$ .

When the tracer mass is sufficiently large  $M^* \gg 1$ ,  $F(V)$  of equation (4.5) reduces to  $\frac{\rho}{\sqrt{\alpha\pi}}$ , and this gives simpler expression of  $P_a(V_0)$  and  $P(u, t|V)$  as follows.

$$P_a(V) = P_{MB}(V) \quad (5.8)$$

$$P(u, t|V) = \rho|u| P_{MB}(u) \exp\left(-\frac{\rho}{\sqrt{\alpha\pi}}t\right) \quad (5.9)$$

We substitute the reduced form of probability (equation (5.8) and (5.9)) into equation (5.6), to have

$$\begin{aligned}
& \langle V(t)V(0) \rangle_n \\
&= \Lambda \int_t^\infty dt_+ \int_0^t dt_n \int_0^{t_n} dt_{n-1} \cdots \int_0^{t_3} dt_2 \int_0^{t_2} dt_1 \int_{-\infty}^0 dt_- \\
& \quad \times \int du_+ \int du_n \cdots \int du_2 \int du_1 \int dV_0(V_0V_n) \\
& \quad \times \rho^{n+1} |u_+| |u_n| \cdots |u_2| |u_1| e^{-\frac{\rho}{\sqrt{\alpha\pi}}(t_+ - t_-)} \\
& \quad \times P(u_+) P(u_n) \cdots P(u_2) P(u_1) P_{MB}(V_0) \quad (5.10)
\end{aligned}$$

$$\begin{aligned}
&= \int_0^t dt_n \int_0^{t_n} dt_{n-1} \cdots \int_0^{t_3} dt_2 \int_0^{t_2} dt_1 \\
& \quad \times \int du_n \cdots \int du_2 \int du_1 \int dV_0(V_0V_n) \\
& \quad \times \rho^n |u_n| \cdots |u_2| |u_1| e^{-\frac{\rho}{\sqrt{\alpha\pi}}t} P(u_n) \cdots P(u_2) P(u_1) P_{MB}(V_0) \quad (5.11)
\end{aligned}$$

We can reduce the odd function term of  $u_i$  in  $V_n$ , then

$$\begin{aligned}
& \langle V(t)V(0) \rangle_n \\
&= p^n \int_0^t dt_n \int_0^{t_n} dt_{n-1} \cdots \int_0^{t_3} dt_2 \int_0^{t_2} dt_1 \\
&\quad \times \int du_n \cdots \int du_2 \int du_1 \int dV_0 V_0^2 \\
&\quad \times \rho^n |u_n| \cdots |u_2| |u_1| e^{-\frac{\rho}{\sqrt{\alpha\pi}}t} P(u_n) \cdots P(u_2) P(u_1) P_{MB}(V_0) \quad (5.12)
\end{aligned}$$

We can calculate all integrals as follows

$$\langle V(t)V(0) \rangle_n = \frac{k_B T}{M} \frac{1}{n!} \left( \frac{p\rho t}{\sqrt{\alpha\pi}} \right)^n e^{-\frac{\rho}{\sqrt{\alpha\pi}}t}$$

The VAC can be obtained by taking the sum of all term  $\langle V(t)V(0) \rangle_n$ , as

$$\langle V(t)V(0) \rangle = \sum_{n=0}^{\infty} \langle V(t)V(0) \rangle_n = \frac{k_B T}{M} e^{-\frac{2m}{M+m} \frac{\rho}{\sqrt{\alpha\pi}}t} = \frac{k_B T}{M} e^{-\frac{2}{M^*+1} \sqrt{\frac{2}{\pi}}t}$$

For the large mass limit  $M^* \rightarrow \infty$ , we can reduce the VAC as

$$\langle V(t)V(0) \rangle = \frac{k_B T}{M} e^{-\frac{2\sqrt{2}}{M^* \sqrt{\pi}}t} \quad (5.13)$$

### 5.3.2 Case for light tracer

In the short time scale, the tracer has the repeated collisions with the same gas particles as shown in Figure 5.1. In such a case, the neighboring gas particles to the tracer behave as fixed walls. The image of this model is shown in Figure 5.4 where  $t$  is the time,  $X$  and  $V$  is the initial position and

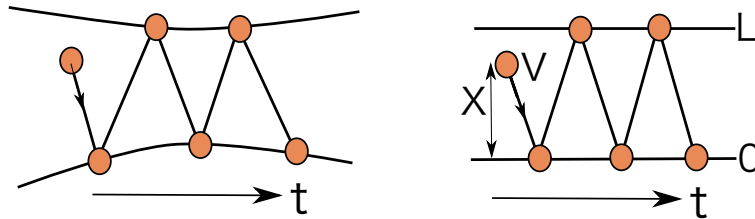


Figure 5.4: Theoretical model for dynamics of light tracer in short time scale.

velocity of the tracer sampled from the equilibrium distribution and  $L$  is the

distance between the fixed walls which mimic the neighboring gas particles to the tracer. Some distributions in this case are well defined by the equilibrium distributions. The position of the tracer is uniformly distributed in the walls and the velocity of the tracer is given by the Maxwell-Boltzmann distribution. The distribution of the distance between the neighboring particles is the exponential distribution, but the distribution of the distance between the walls is the Gamma distribution. This is because the tracer is confined between the walls, and the distance between the walls are the sum of the neighboring distances. The explicit expression of these distributions are

$$P(X) = \frac{1}{L} \quad (5.14)$$

$$P(V) = \left( \frac{m}{2\pi k_B T} \right)^{\frac{1}{2}} \exp \left( -\frac{MV^2}{2k_B T} \right) \quad (5.15)$$

$$P(L) = \frac{L}{\bar{L}^2} \exp \left( -\frac{L}{\bar{L}} \right) \quad (5.16)$$

where  $\bar{L}$  is the mean distance between the walls. Then, we assume the simple collision rule. The tracer velocity is changed by the collision with the wall. The tracer velocity is reversed if the walls are fixed. In such a situation, we can calculate the VAC under the condition where the initial tracer position, velocity and distance between the walls are  $X$ ,  $V$  and  $L$  as

$$\langle V(t)V(0) \rangle_{|X,V,L} = V^2 (-1)^{\lfloor \frac{Vt+X}{L} \rfloor} \quad (5.17)$$

where  $\lfloor \dots \rfloor$  is the floor function. We can obtain the VAC by taking the statistical averages for  $X$ ,  $V$  and  $L$ . This model would be justified when we consider the short time scale and the tracer mass is much smaller than the gas particle because the tracer speeds are smaller than that of tracer and they are almost unchanged by collisions with the tracer in such a case.

We take the average of (5.17) over  $X$ .

$$\langle V(t)V(0) \rangle_{|L,V} = \int \langle V(t)V(0) \rangle_{|X,L,V} P(X) dX \quad (5.18)$$

$$= \frac{1}{L} \int_0^L V^2 (-1)^{\lfloor \frac{Vt+X}{L} \rfloor} dX \quad (5.19)$$

$$= V^2 (-1)^{\lfloor \frac{Vt}{L} \rfloor} \left( 1 + 2 \left\lfloor \frac{Vt}{L} \right\rfloor - \frac{2Vt}{L} \right) \quad (5.20)$$

This is the even function of  $V$ , so we can change  $V$  by  $|V|$  as

$$\langle V(t)V(0) \rangle_{|L,V} = V^2 (-1)^{\lfloor \frac{|V|t}{L} \rfloor} \left( 1 + 2 \left\lfloor \frac{|V|t}{L} \right\rfloor - \frac{2|V|t}{L} \right) \quad (5.21)$$

Then, we take the average of (5.20) over  $L$ .

$$\langle V(t)V(0) \rangle_{|V} = \int \langle V(t)V(0) \rangle_{|L,V} P(L) dL \quad (5.22)$$

$$= \int_0^\infty V^2 (-1)^{\lfloor \frac{|V|t}{L} \rfloor} \left( 1 + 2 \left\lfloor \frac{|V|t}{L} \right\rfloor - \frac{2|V|t}{L} \right) \times \frac{L}{L^2} \exp\left(-\frac{L}{L}\right) dL \quad (5.23)$$

We introduce a variable transform from  $L$  to  $l = \frac{L}{L}$ ,

$$\langle V(t)V(0) \rangle_{|V} \quad (5.24)$$

$$= \int_0^\infty V^2 (-1)^{\lfloor \frac{|V|t}{lL} \rfloor} \left( 1 + 2 \left\lfloor \frac{|V|t}{lL} \right\rfloor - \frac{2|V|t}{lL} \right) l \exp(-l) dl \quad (5.25)$$

$$= \int_0^\infty V^2 (-1)^{\lfloor \frac{|\alpha|}{l} \rfloor} \left( 1 + 2 \left\lfloor \frac{|\alpha|}{l} \right\rfloor - \frac{2|\alpha|}{l} \right) l e^{-l} dl \quad (5.26)$$

where we defined  $\alpha = \frac{Vt}{L}$ . Then, we divide the integral over  $l$  into integrals over partial domains as,

$$\begin{aligned} & \langle V(t)V(0) \rangle_{|V} \\ &= V^2 \sum_{k=0}^{\infty} (-1)^k \int_{\frac{|\alpha|}{k+1}}^{\frac{|\alpha|}{k}} (l + 2kl - 2|\alpha|) e^{-l} dl \end{aligned} \quad (5.27)$$

$$= V^2 \sum_{k=0}^{\infty} (-1)^k (1 + 2k) \left( e^{-\frac{|\alpha|}{k+1}} - e^{-\frac{|\alpha|}{k}} \right) - (-1)^k |\alpha| \left( \frac{e^{-\frac{|\alpha|}{k+1}}}{k+1} + \frac{e^{-\frac{|\alpha|}{k}}}{k} \right) \quad (5.28)$$

$$= V^2 \sum_{k=0}^{\infty} (-1)^k (1 + 2k) \left( e^{-\frac{|\alpha|}{k+1}} - e^{-\frac{|\alpha|}{k}} \right) \quad (5.29)$$

Here, we consider the integral over  $V$ .

$$\langle V(t)V(0) \rangle \quad (5.30)$$

$$= \int \langle V(t)V(0) \rangle_V P(V) dV \quad (5.31)$$

$$= \int_{-\infty}^{\infty} V^2 \sum_{k=0}^{\infty} (-1)^k (1+2k) \left( e^{-\frac{|a|}{k+1}} - e^{-\frac{|a|}{k}} \right) \times \left( \frac{M}{2\pi k_B T} \right)^{\frac{1}{2}} \exp\left(-\frac{MV^2}{2k_B T}\right) dV \quad (5.32)$$

$$= 2 \left( \frac{a}{\pi} \right)^{\frac{1}{2}} \int_0^{\infty} V^2 \sum_{k=0}^{\infty} (-1)^k (1+2k) \times (e^{-b_{k+1}V} - e^{-b_k V}) \exp(-aV^2) dV \quad (5.33)$$

$$= \sum_{k=0}^{\infty} (-1)^k (1+2k) 2 \left( \frac{a}{\pi} \right)^{\frac{1}{2}} \times \int_0^{\infty} V^2 (e^{-b_{k+1}V} - e^{-b_k V}) \exp(-aV^2) dV \quad (5.34)$$

where  $a = \frac{M}{2k_B T}$  and  $b_k = \frac{t}{Lk}$ . We can proceed this calculation as

$$\begin{aligned} \langle V(t)V(0) \rangle &= \frac{1}{a} \sum_{k=0}^{\infty} (-1)^k (1+2k) \\ &\quad \left\{ \left[ \left( \frac{1}{2} + \frac{c^2}{(k+1)^2} \right) e^{\frac{c}{(k+1)^2}} \operatorname{erfc}(c_{k+1}) - \frac{c}{\sqrt{\pi}(k+1)} \right] \right. \\ &\quad \left. - \left[ \left( \frac{1}{2} + \frac{c^2}{k^2} \right) e^{\frac{c^2}{k^2}} \operatorname{erfc}(c_k) - \frac{c}{\sqrt{\pi}k} \right] \right\} \end{aligned} \quad (5.35)$$

where  $\frac{c}{k}$  is  $\frac{b_k}{2\sqrt{a}} = \frac{t}{L} \sqrt{\frac{k_B T}{2M} \frac{1}{k}}$ . We consider the normalization by the average kinetic energy  $k_B T$  as

$$\begin{aligned} \frac{\langle V(t)V(0) \rangle}{\langle V^2(0) \rangle} &= \sum_{k=0}^{\infty} (-1)^k (1+2k) \\ &\quad \left\{ \left[ \left( 1 + \frac{2c^2}{(k+1)^2} \right) e^{\frac{c^2}{(k+1)^2}} \operatorname{erfc}\left(\frac{c}{k+1}\right) - \frac{2c}{\sqrt{\pi}(k+1)} \right] \right. \\ &\quad \left. - \left[ \left( 1 + \frac{2c^2}{k^2} \right) e^{\frac{c^2}{k^2}} \operatorname{erfc}\left(\frac{c}{k}\right) - \frac{2c}{\sqrt{\pi}k} \right] \right\} \end{aligned} \quad (5.36)$$

Then, we divide the first term ( $k = 0$ ) in the summation as

$$\begin{aligned}
& \frac{\langle V(t)V(0) \rangle}{\langle V^2(0) \rangle} \\
&= (1 + 2c^2)e^{c^2} \operatorname{erfc}(c) - \frac{2c}{\sqrt{\pi}} \\
&+ \sum_{k=1}^{\infty} (-1)^k (1 + 2k) \\
&\quad \times \left[ \left( 1 + \frac{2c^2}{(k+1)^2} \right) e^{\frac{c^2}{(k+1)^2}} \operatorname{erfc} \left( \frac{c}{k+1} \right) - \left( 1 + \frac{2c^2}{k^2} \right) e^{\frac{c^2}{k^2}} \operatorname{erfc} \left( \frac{c}{k} \right) \right] \\
&- \sum_{k=1}^{\infty} (-1)^k (1 + 2k) \left( \frac{2c}{\sqrt{\pi}(k+1)} - \frac{2c}{\sqrt{\pi}k} \right) \tag{5.37} \\
&= (1 + 2c^2)e^{c^2} \operatorname{erfc}(c) - \frac{4c}{\sqrt{\pi}} + \sum_{k=1}^{\infty} (-1)^k (1 + 2k) \\
&\quad \times \left[ \left( 1 + \frac{2c^2}{(k+1)^2} \right) e^{\frac{c^2}{(k+1)^2}} \operatorname{erfc} \left( \frac{c}{k+1} \right) - \left( 1 + \frac{2c^2}{k^2} \right) e^{\frac{c^2}{k^2}} \operatorname{erfc} \left( \frac{c}{k} \right) \right] \\
&= e^{c^2} \operatorname{erfc}(c) - \frac{4c}{\sqrt{\pi}} + \sum_{k=1}^{\infty} (-1)^k (1 + 2k) \\
&\quad \times \left( e^{\frac{c^2}{(k+1)^2}} \operatorname{erfc} \left( \frac{c}{k+1} \right) - e^{\frac{c^2}{k^2}} \operatorname{erfc} \left( \frac{c}{k} \right) \right) \\
&\quad - 8c^2 \sum_{k=1}^{\infty} (-1)^k \frac{1}{k} e^{\frac{c^2}{k^2}} \operatorname{erfc} \left( \frac{c}{k} \right) \tag{5.38}
\end{aligned}$$

This is the analytical form of VAC at the low mass limit  $M \ll 1$

## 5.4 Discussion

### 5.4.1 Comparison theory with simulation results

We plot the analytical results (eq(5.13)) with the simulation results in Figure 5.5, with the time rescaled scaled time by  $M^{*-1}$ . In Figure 5.5, the theoretical results slightly deviates from the simulation results in the large mass cases. This deviation would be due to the approximation for collision statistics of equation (5.9). To reproduce the VAC in the high mass case precisely, we should carefully consider the approximations for the mass ratio expansion.

We plot the analytical expression (eq(5.38)) with the simulation results in Figure 5.6 with the time scaled the time by  $M^{*-\frac{1}{2}}$ . We find that the theory

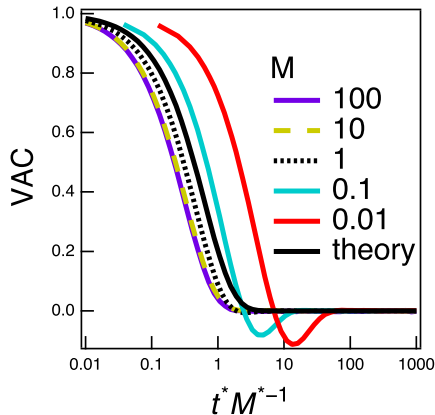


Figure 5.5: VAC of theoretical results for large  $M$  case (eq. (5.13)), together with simulation results for various  $M$ . Horizontal axis is scaled by  $M^{*-1}$ .

successfully reproduces the short time behavior of the simulation results at the low mass case. In Figure 5.4, our theoretical model does not have any fitting parameters and the value appeared in the theory can be completely determined from the simulation setting. Therefore, we can say that our model successfully incorporates the effect of correlated collisions as we observed in Figure 5.1(c) although this model is slightly phenomenological.

From the theoretical analysis above, we find the difference of the factor used for the rescaling of the time between the high mass and low mass cases. The time scale of the relaxation of VAC of the tracer would be roughly determined by the collision frequency(4.5) and collision rule(2.4). When the mass of the tracer is sufficiently large, the characteristic time of the VAC is scaled by  $M^{*-1}$ . In this case, the velocity of the tracer is small compared with the ideal gas, and this make the collision frequency to be the constant as can be seen in equation (4.5). Thus, the dominant factor affecting the relaxation time is the collision rule (2.4). This is the reason why the time should be scaled by  $M^{*-1}$  in the high mass case. For the sufficiently low mass case, the tracer velocity is sufficiently high compared with that of the gas particle and reversed by the single collision. In this case, the velocity of the ideal gas particle is almost unchanged by the velocity change of the tracer. In this case, the collision frequency is the dominant factor for the relaxation time of the VAC. Thus, the factor  $M^{-\frac{1}{2}}$  appears in the VAC in the small mass case.

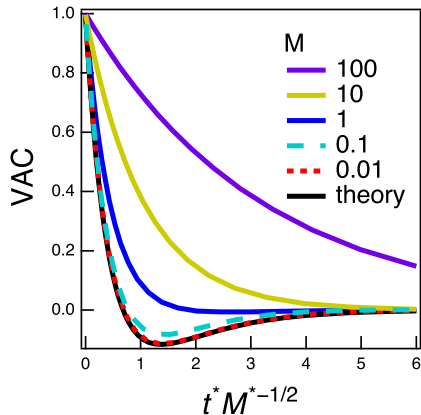


Figure 5.6: VAC of theoretical results of VAC for low  $M$  case (eq.(5.38)), together with the simulation results of various  $M$ . Horizontal axis is scaled by  $M^{*-1/2}$ .

## 5.4.2 Expandability of our theory

The theoretical model describing the VAC of the light tracer shown in subsection 5.3.2 can not describe the cases for the arbitrary masses and dimensions. In this subsection, we consider the relation of the theory to such cases.

In our model, we regard the gas particles neighboring the tracer as two fixed walls. This model can be described by the renewal theory formalism by employing the appropriate statistics of the correlated collisions in light tracer limit. If the tracer mass is not sufficiently small compared with the gas particles, the fixed wall picture is not valid. In this case, we have to consider the statistics of the correlated collisions for such a tracer mass in the renewal theory to reproduce the tracer dynamics.

In the model, we use the properties of the one dimensional system. Thus, our model would not be directly expanded to the high dimensional cases. In such cases, we have to consider the complex geometry of the correlated collisions that does not exist in one dimensional system. Nevertheless, we believe that our model is instructive for high dimensional systems because the model can incorporate the correlated collisions successfully.

# Chapter 6

## Conclusions

In this work, we studied the short time dynamics of the tracer in the ideal gas by using the simulations and theories. Here, we show the summary of the results and conclusions.

### **Chapter3: Short time dynamics of tracer in 3 dimensional ideal gas**

In this chapter, we performed the hard sphere simulations for the short time dynamics of the tracer in the ideal gas. When the mass of the tracer is high or the number density is low, the velocity autocorrelation function (VAC) shows the exponential decay and such a behavior can be reproduced by the Enskog theory. However, when the mass of the tracer is small and the number density is high, the VAC shows negative value and the Enskog theory fails to reproduce such a behavior. In such a case, the collisions are strongly correlated even though the fluid molecules do not interact each other. To understand the origin of the correlated collisions in the ideal gas, we focused on the individual collisions and introduced velocity autocorrelation according to the number of collision events,  $\gamma_n$ . From the detail analysis of  $\gamma_n$ , the correlated collisions are caused by the collisions with the same gas particles.

### **Chapter4: Statistic of single collision in arbitrary dimension**

In this chapter, we theoretically analyzed the single collision statistics of the tracer to reproduce the simulation results in chapter 3. We obtained the analytical expression of the single collision statistics for arbitrary tracer masses

in arbitrary dimensions. From the statistics, we deductively calculated the free time distribution and the velocity correlation of single collision,  $\gamma_1$  in 3 dimension. We confirmed that the theory completely agree with the simulation results. Although our theoretical calculation can be justified only for the non-interacting ideal gas systems, it would be instructive for the systems in which the fluid particles interact with each other.

## **Chapter5: Short time dynamics of tracer in 1 dimensional gas**

From the pictures of the correlated collisions obtained in chapter 3, we theoretically analyzed the VAC of the tracer in 1 dimensional systems in the short time scale. For the heavy tracer cases, the collisions are independent of each other and the VAC can be analyzed by the renewal theory formalism. However, our calculation has the slight deviation from the simulation results, and this deviation is due to the approximation of the collision statistics employed in our calculation. For the light tracer cases, the correlated collisions are caused by the collisions with the same gas particles. In such a case, we can construct the phenomenological model incorporating the correlated collisions. This model successfully reproduce the VAC from the simulation for  $M \ll 1$  cases. In these models, all the variables appeared in the models can be determined by the system settings. Namely, there are no fitting parameters.

# Acknowledgments

名古屋大学工学研究科物質科学専攻の増淵研究室にて学部4年から博士前期課程の3年間研究しました。今後も同研究室で博士後期課程の学生として研究に取り組みますのでどうぞ宜しくお願い致します。以下、先生方及び学生の皆さんへの謝辞を記します。

増淵先生には、私が思うままに研究をさせて貰えたことに感謝したいです。研究のアイデアを相談したり、取り組んでみたい研究対象を相談したりすると、いつもやってみようとお応援して頂きました。また、学会に関しても興味がある学会に全て参加させて頂けて、多くの知識を得ることができました。自由に考えて自由に学べる雰囲気のおかげで楽しく研究に取り組むことができました。

畝山先生には私の研究に関して最も議論して頂きました。本修士論文の3章は、先生のご指導の下、論文として投稿した内容です。また、研究の方法論についても色々教えて頂きました。印象深いのが「分からないもので分からないものを測定しても何も分からない」という言葉です。今考えてみると、本修士論文の非常に単純なシステムはこの言葉の影響を強く受けているような気がします。結果として、単純化したことで多くの面白い現象を理解することができました。さらに、単純化するという視点を持って他の研究を見ることができるようになったと思います。

長谷川先生には副査として修士論文を見て頂き、細かい解析を丁寧に実施したことを評価して頂きました。また、本修士論文3章で出てくるノンガウシアンパラメータの物理的な解釈に関する質問を頂いたことで、ノンガウシアンパラメータの意義に関して深く議論することができました。

土肥先生、木田先生には学会や修士論文発表会のプレゼンテーションに関して多くのアドバイスを頂きました。研究分野が異なるお二人のアドバイスはとても有益で、他分野の研究者にも伝わるプレゼンテーションを構成できました。また、博士後期課程や海外での研究生活のお話を聞いて、ますます将来研究者としてやっていきたいと思いました。

M1の福永君とM2の広井君には、本研究に関する議論を何度もして頂きました。特に5章の一次元系の理論計算は、私だけの力でなく彼らの援助に負ったところが多いです。

福永君、B4の大石君及び榎本（圭）君と「連続体の力学（佐野理）」及

び「The theory of simple liquids (Hansen et al)」を自主的に輪講していました。彼らとの輪講のおかげで流体力学や液体の物理について基本的な事項を学ぶことができました。

博士後期課程のLixin、M2の木津君、休学中の斎藤君、M1の河合君、榎本(雄)君、B4の安井君、白石君、北村君のおかげで楽しく研究生活に取り組めました。

# Bibliography

- [1] Fumiaki Nakai, Yuichi Masubuchi, and Takashi Uneyama. *Physical Review E*, 102(3), 2020.
- [2] Robert Brown. *The Philosophical Magazine*, 4(21):161–173, 1828.
- [3] A. Einstein. *Annalen der Physik*, 322(8):549–560, 1905.
- [4] Simon Kheifets, Akarsh Simha, Kevin Melin, Tongcang Li, and Mark G. Raizen. *Science*, 343(6178):1493–1496, 2014.
- [5] Tongcang Li, Simon Kheifets, David Medellin, and Mark G. Raizen. *Science*, 328(5986):1673–1675, 2010.
- [6] Rongxin Huang, Isaac Chavez, Katja M. Taute, Branimir Lukić, Sylvia Jeney, Mark G. Raizen, and Ernst Ludwig Florin. *Nature Physics*, 7(7):576–580, 2011.
- [7] Kyozi Kawasaki. *Journal of Physics A: General Physics*, 6(9):1289–1295, 1973.
- [8] J Albers, J M Deutch, and Irwin Oppenheim. *Journal of Chemical Physics*, 54:114102, 1971.
- [9] Robert Zwanzig. *Journal of Statistical Physics*, 9(3):215–220, 1973.
- [10] A Rahman. *Physical Review*, 136(2A), 1964.
- [11] T Yamaguchi and Y Kimura. *Journal of Chemical Physics*, 114(7):3029–3034, 2001.
- [12] David Montgomery. *Physics of Fluids*, 14(10):2088–2090, 1971.
- [13] Sydney Chapman, Thomas George Cowling, and David Burnett. *The mathematical theory of non-uniform gases: an account of the kinetic theory of viscosity, thermal conduction and diffusion in gases*. Cambridge university press, 1990.

- [14] JR Dorfman and H Van Beijeren. The kinetic theory of gases. *Statistical Mechanics, Part B: Time-Dependent Processes*, 1977.
- [15] Pierre Resibois and Marcel De Leener. Classical kinetic theory of fluids. 1977.
- [16] Nikolaj Nikolaevič Bogoljubov. *Problems of a dynamical theory in statistical physics*. North-Holland Pub. Co., 1962.
- [17] Max Born and Herbert S Green. *A general kinetic theory of liquids*. CUP Archive, 1949.
- [18] John G. Kirkwood. *The Journal of Chemical Physics*, 14(3):180–201, 1946.
- [19] Ludwig Boltzmann. *Lectures on gas theory*. Courier Corporation, 2012.
- [20] B. J. Alder, D. M. Gass, and T. E. Wainwright. *The Journal of Chemical Physics*, 53(10):3813–3826, 1970.
- [21] Katja Lindenberg and Robert I. Cukier. *The Journal of Chemical Physics*, 67(2):568–578, 1977.
- [22] Alessandro Taloni, Yasmine Meroz, and Adriÿan Huerta. *Physical Review E - Statistical, Nonlinear, and Soft Matter Physics*, 92(2):022131, 2015.
- [23] A. I. Burshtein and M. V. Krongauz. *The Journal of Chemical Physics*, 102(7):2881–2887, 1995.
- [24] Michael P. Allen and Dominic J. Tildesley. *Computer simulation of liquids*. Oxford university press, 2017.
- [25] Daan Frenkel and Berend Smit. *Understanding molecular simulation: from algorithms to applications. Vol. 1*. Elsevier, 2001.
- [26] B. J. Alder and T. E. Wainwright. *The Journal of Chemical Physics*, 31(2):459–466, 1959.
- [27] Jerome K. Percus and George J. Yevick. *Physical Review*, 110(1):1–13, 1958.
- [28] Zevi W. Salsburg, Robert W. Zwanzig, and John G. Kirkwood. *The Journal of Chemical Physics*, 21(6):1098–1107, 1953.

- [29] Jean-Pierre Hansen and Ian Randal McDonald. *Theory of simple liquids: with applications to soft matter*. Academic Press, 2013.
- [30] Walter Kob, Claudio Donati, Steven J. Plimpton, Peter H. Poole, and Sharon C. Glotzer. *Physical Review Letters*, 79(15):2827–2830, 1997.
- [31] Chundong Xue, Xu Zheng, Kaikai Chen, Yu Tian, and Guoqing Hu. *Journal of Physical Chemistry Letters*, 7(3):514–519, 2016.
- [32] P. T. Herman and B. J. Alder. *The Journal of Chemical Physics*, 56(2):987–991, 1972.
- [33] U Bengtzelius, W Götze, and A Sjolander. Technical report, 1984.
- [34] Wolfgang Götze. Technical report, 1999.
- [35] Daan Frenkel and John F. Maguire. *Physical Review Letters*, 47(15):1025–1028, 1981.
- [36] D. Frenkel and J. F. Maguire. *Molecular Physics*, 49(3):503–541, 1983.
- [37] Felix Höfling, Tobias Munk, Erwin Frey, and Thomas Franosch. *Physical Review E*, 77(6):060904, 2008.
- [38] Willem Van Ketel, Chinmay Das, and Daan Frenkel. *Physical Review Letters*, 94(13):135703, 2005.
- [39] Matthias Otto, Timo Aspelmeier, and Annette Zippelius. *Journal of Chemical Physics*, 124(15):154907, 2006.
- [40] R. Schilling and G. Szamel. *Europhysics Letters*, 61(2):207–213, 2003.
- [41] Dror Kasimov, Tamir Admon, and Yael Roichman. *Physical Review E*, 93(5):050602, 2016.
- [42] B. J. Alder and T. E. Wainwright. *Physical Review Letters*, 18(23):988–990, 1967.
- [43] B. Doliwa and A. Heuer. *Physical Review Letters*, 80(22):4915–4918, 1998.
- [44] Claudio Donati, Sharon C. Glotzer, Peter H. Poole, Walter Kob, and Steven J. Plimpton. *Physical Review E - Statistical Physics, Plasmas, Fluids, and Related Interdisciplinary Topics*, 60(3):3107–3119, 1999.

- [45] Andrea Fiege, Timo Aspelmeier, and Annette Zippelius. *Physical Review Letters*, 102(9):098001, 2009.
- [46] Keisuke Mizuta, Yoshiki Ishii, Kang Kim, and Nobuyuki Matubayasi. *Soft Matter*, 15(21):4380–4390, 2019.
- [47] M. Doi and S. F. Edwards. *Journal of the Chemical Society, Faraday Transactions 2: Molecular and Chemical Physics*, 74(0):560–570, 1978.
- [48] James Jeans. *The dynamical theory of gases*. University Press, 1921.
- [49] B J Alder and T Einwohner. 1965.
- [50] T Einwohner and B J Alder. *I. General Method The Journal of Chemical Physics*, 49(4):3813, 1968.
- [51] L. Lue. *Journal of Chemical Physics*, 122(4):044513, 2005.
- [52] Paolo Visco, Frédéric Van Wijland, and Emmanuel Trizac. *Physical Review E*, 77(4):041117, 2008.
- [53] D. W. Jepsen. *Journal of Mathematical Physics*, 6(3):405–413, 1965.
- [54] J. L. Lebowitz and J. K. Percus. *Physical Review*, 155(1):122–138, 1967.
- [55] J. L. Lebowitz, J. K. Percus, and J. Sykes. *Physical Review*, 171(1):224–235, 1968.
- [56] Anjan Roy, Onuttom Narayan, Abhishek Dhar, and Sanjib Sabhapandit. *Journal of Statistical Physics*, 150(5):851–866, 2013.

# Nomenclature

We showed the parameters used in this work in the table below.

Parameter	Meaning
$t$	time
$\sigma$	tracer size
$M$	mass of tracer
$M^*$	dimensionless mass of tracer
$m$	mass of ideal gas particle
$\rho$	number density of ideal gas
$\rho^*$	dimensionless number density of ideal gas
$d$	dimension
$L$	side length of simulation box
$\mathcal{V}$	volume of simulation box
$N$	number of ideal gas particle
$\mathbf{R}$	position of tracer
$\mathbf{V}$	velocity of tracer
$\mathbf{r}_i$	position of i-th ideal gas particle
$\mathbf{v}_i$	velocity of i-th ideal gas particle
$\hat{\mathbf{r}}$	unit vector between centers of tracer and gas particle
$k_B$	Boltzmann constant
$T$	temperature
$D$	diffusion coefficient
$\eta$	fluid viscosity
$K$	friction coefficient kernel
$\mathbf{W}$	Gaussian noise
$\bar{\tau}$	mean free time between collisions
$\bar{L}$	mean distance between neighboring particles in 1 dimension

(名古屋大学) ○仲井文明, 山本哲也, 畷山多加志, 増渕雄一

E-Mail to Name: nakai.fumiaki@b.mbox-nagoya-u.ac.jp

キーワード: (粉体, 粒度偏析, ブラジルナッツ現象, 離散要素法)

【はじめに】 粉体は身近であるにも関わらず、その物理は非常に複雑であり、いまだに未解明の問題が多い。例えば、大きさや密度が異なる2種の粉体の混合は、工学的に重要であるが、一般に非常に難しいことが知られている。特に、大きさが異なる粒子を容器に入れ加振すると、大きい粒子が表面に析出する(ブラジルナッツ現象)。ブラジルナッツ現象の機構として「対流により大きい粒子が表面に運ばれるため[1]」「大きい粒子の下方に小さい粒子が入り込むため[2]」などと言った説があるが、現象が十分に解明されているとは言い難い。そこで、本研究では離散要素法(DEM)[3]を用いてブラジルナッツ現象を調べ、その機構を考察した。

【方法】 本研究ではDEMを用いて、小さな粒子中(半径4mm)に大きな粒子(半径16mm)を1個置いた系のシミュレーションを行った。粒子を重力下で円柱状容器(半径48mm)に高さ約200mm程度まで詰め、大きな粒子は底面の中心に置いた状態を初期状態とした。底面を振動数10Hz、振幅7.4mmの正弦波で動かすことで加振を行った。大きい粒子の真密度は $2.5\text{g/cm}^3$ とし、小さい粒子の真密度は $2.5, 7.5, 10\text{g/cm}^3$ と変化させた。大きい粒子の位置の時間変化を調べた。得られたシミュレーション結果から大きな粒子の底面からの距離を求め、振動10周期(1s)の平均位置を求めた。

【結果】 今回試したパラメータ範囲では、すべての場合において大きい粒子は底面から徐々に上に動いていき表面に析出した。Fig. 1 に小さい粒子の真密度が異なる系における大きい粒子の位置の時間変化を示す。大きい粒子の上昇速度は一定ではなく、表面に近づくにつれて速度が上がる様子が確認できる。また、小さい粒子の密度が大きい方が、大きい粒子の上昇速度が小さくなっていることが分かる。既存のシミュレーションでは、大きい粒子の上昇速度が上がるという報告[1]と変わらないという報告[2]があるが、本研究の結果は[1]を支持するものである。

【考察】 既存の報告によると、大きい粒子の上昇にともなう上昇速度の増加は対流によるものとされる。すなわち、高さによって周囲の小さな粒子の流れが異なるために上昇速度が変わると説明されている[1]。

しかし、小さな粒子がどのような流動場を形成しているかはあまり明らかではない。例えば、本研究では小さな粒子の真密度によらず大きな粒子の上昇速度の関数形は非常に類似している。このことから、対流を考える従来のモデルの代わりに小さい粒子の密度の影響をより直接的に取り込んでモデル化ができないかと考えた。すなわち、大きい粒子のダイナミクスは、小さい粒子による圧力の影響を受けると考えた。そこで、非常

に粗い近似として大きい粒子に働く力とそれによる仕事に注目する。大きい粒子は、加振時の最高速度 $A\omega$ に相当する運動エネルギー $m(A\omega)^2/2$ を得ると考える( $m$ は大きい粒子の質量)。このエネルギーのうちの一部が粒子位置の上昇にともなう位置エネルギー変化 $mg\Delta z$ になり( $\Delta z$ は上昇幅)、残りは散逸するものとする。このとき、散逸は大きい粒子の上部にある小さい粒子を持ち上げるための仕事 $W$ に相当するものと仮定した。このとき、小さな粒子の密度が小さいほど仕事 $W$ が小さいので上昇幅は大きくなることになる。

以上の仮定に基づいて粒子の位置変化を計算したものをFig. 1中に破線で示す。DEMシミュレーション結果とモデルの予測にはずれがあるが、このモデルはフィッティングパラメータを含まないことを考えれば、シミュレーション結果をある程度妥当に記述できていると考えられる。シミュレーション結果とモデルの予測とのずれは系統的であり、これは対流の効果を考えてないためではないかと考えられる。

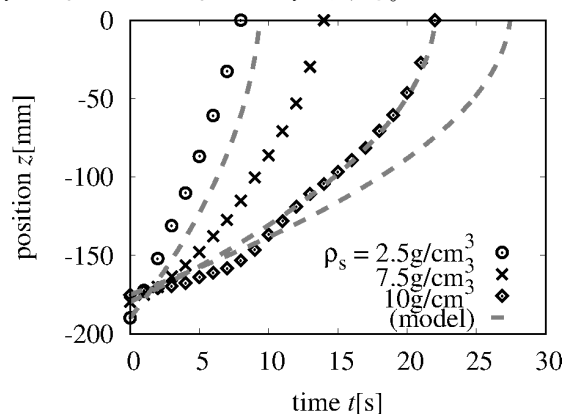


Fig. 1: The time-evolution of the position of the large particle from the bottom of the cylinder. The densities of the small particles are 2.5, 7.5, and  $10\text{g/cm}^3$ . Symbols represent the DEM simulation data and dashed curves are model predictions.

【結論】 DEMを用いて、小さな粒子の真密度を変化させてブラジルナッツ現象のシミュレーションを行った。大きい粒子の上昇は小さな粒子の密度に大きな影響を受けることがわかった。小さな粒子の密度の影響を説明するため簡単なモデルを考えた。

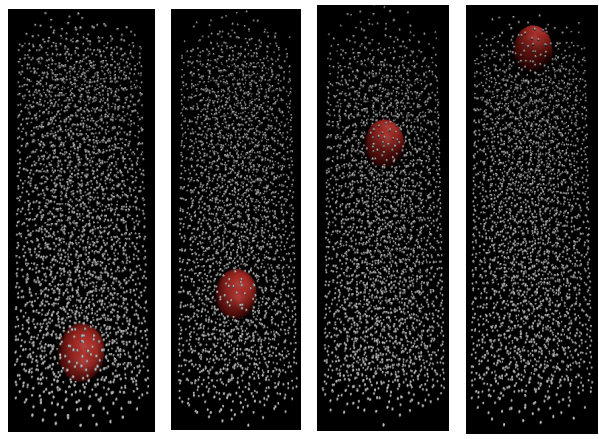
#### 【引用文献】

- [1] J. B. Knight, H. M. Jaeger, and S. R. Nagel, *Physical Review Letters* **70**, 3728 (1993).
- [2] R. Jullien, P. Meakin, and A. Pavlovitch, *Physical Review Letters* **69**, 640 (1992).
- [3] P. A. Cundall and O. D. L. Strack, *Geotechnique* **29**, 47 (1979).

# 粉体粒子の圧力分布に注目した ブラジルナッツ現象のダイナミクスの解析

○仲井文明, 山本哲也, 畝山多加志, 増淵雄一 (名古屋大学)

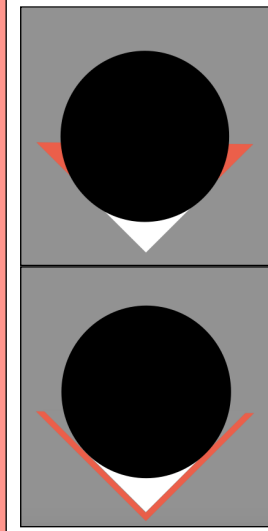
## ブラジルナッツ現象



加振すると大きい粒子は登る

## 1 背景

Jullienのモデル<sup>[1]</sup>



- ・大粒子の下に小粒子が入り込む
- ・赤部の体積が一致
- ・幾何的なモデル
- ・大粒子の上昇速度一定
- ・粒子の質量は無影響

本当に正しいだろうか？

## 2 概要

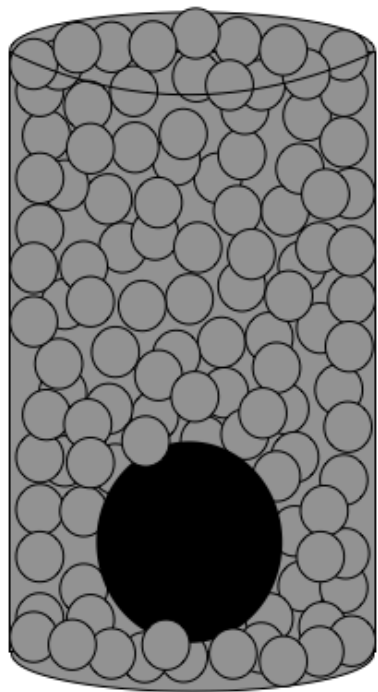
DEMシミュレーション<sup>[2]</sup>を製作  
大粒子のダイナミクスを解析

小粒子の密度が大きいほど  
大粒子はゆっくり上昇

圧力に注目したモデルを構築  
シミュレーション結果と比較

## 3 シミュレーション

初期状態



円柱容器

高さ h	200 mm
半径 L	48 mm
振幅 A	15.5 mm
角速度 ω	62.8 rad / s

小粒子

半径 r	4 mm
密度 ρ	1.25, 2.5, 5.0 7.5, 10.0 g/cm <sup>3</sup>

大粒子

半径 R	16 mm
密度 ρ <sub>0</sub>	2.5 g / cm <sup>3</sup>

小粒子の密度を変え  
大粒子の変位を解析

## 4 圧力モデル (理論)

仮定

大粒子が1加振で得る運動エネルギー  $E_k = \frac{1}{2}M(A\omega)^2$

||

大粒子の位置エネルギー  $\Delta U = Mg\Delta Z$

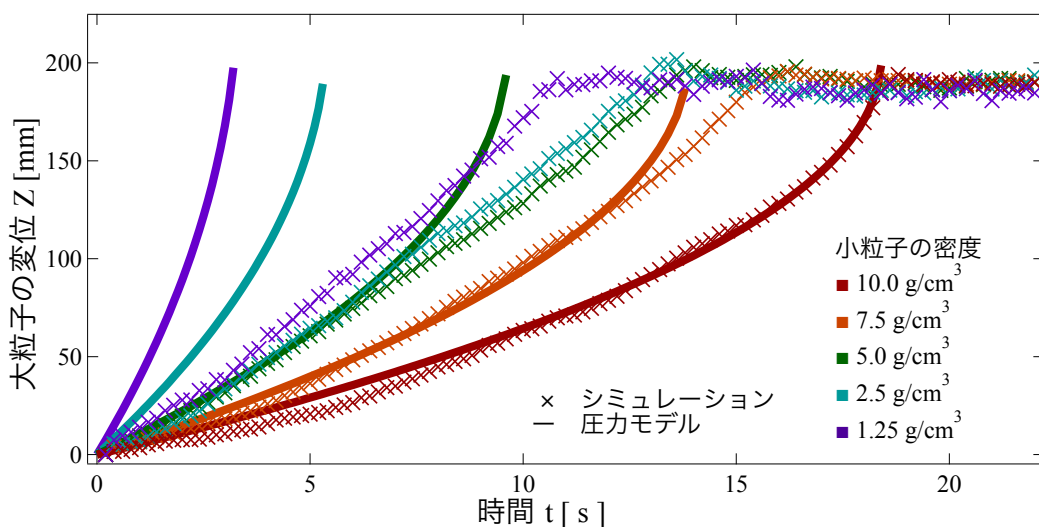
+

圧力に対する仕事  $W = \rho g \pi R^2 (h - Z) \Delta Z$

大粒子の変位の発展式

$$Z_{n+1} = Z_n + \frac{A^2 \omega^2}{g} \frac{1}{2 + \frac{3\rho(h-Z)}{2\rho_0 R}}$$

## 5 結果



シミュレーション

大粒子は加速的に上昇

小粒子の密度が大きい程、大粒子の上昇速度は低下

圧力モデル

「加速的な上昇」と「密度の影響」を再現

密度が大きいと、シミュレーション結果と一致

## 6 考察

Jullienのモデル

「加速的な上昇」と「密度の影響」を説明できない

加速的な上昇の原因

対流の影響<sup>[3]</sup>

もしくは

大粒子上方の小粒子による圧力の影響

圧力モデル

密度が小さいほど

シミュレーション結果からズれる

逆ブラジルナッツ現象を示唆

# Small particles drive vibration of large particle

Fumiaki Nakai, Takashi Uneyama and Yuichi Masubuchi

Department of applied physics Engineering, Nagoya University, Nagoya 464-8603, Japan  
Nakai.fumiaki@b.mbox@nagoya-u.ac.jp

## 1. Introduction:

A colloidal particle placed in a solvent moves randomly. This motion is driven by collisions of many solvent molecules. Such a random motion is called as the Brownian motion, and phenomenologically, it can be described by the Langevin equation. However, the use of the Langevin equation is not always justified. In this study, we found an unexpected vibrational motion of a large particle immersed in a liquid. We analyze the short-time scale motion of a large particle by simulations and theoretical model.

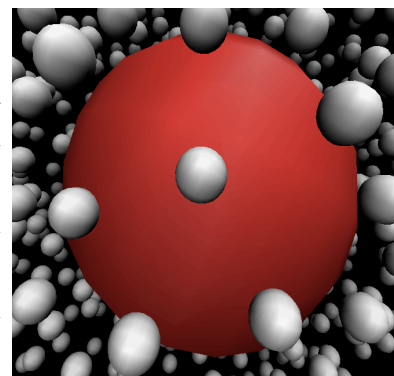


Fig.1 Snapshot of simulation.  
The tracer and the small particles.

## 2. Simulation:

We use molecular dynamics simulation to analyze the motion of a tracer particle. We put the tracer particle and many small particles in the simulation box with the periodic boundary condition. We use dimensionless units by setting the small particle diameter  $\sigma$ , mass  $m$  and the Lennard-Jones(LJ) potential energy  $\epsilon$  as unity. We set thermal energy  $k_B T$  as 1. The interaction between small particles is the LJ potential, whereas the interaction between the tracer and the small particles is the shifted LJ potential, these particles only show repulsive interactions. To control the temperature, we employ the Langevin thermostat for small particles. The tracer particle is not directly coupled to the Langevin thermostat. We applied the numerical integration scheme recently developed for the Langevin equation<sup>1</sup> for the small particles and the standard velocity Verlet scheme for the tracer particle. We varied the diameter  $R$  and mass  $M$  of tracer particle to see their effects.

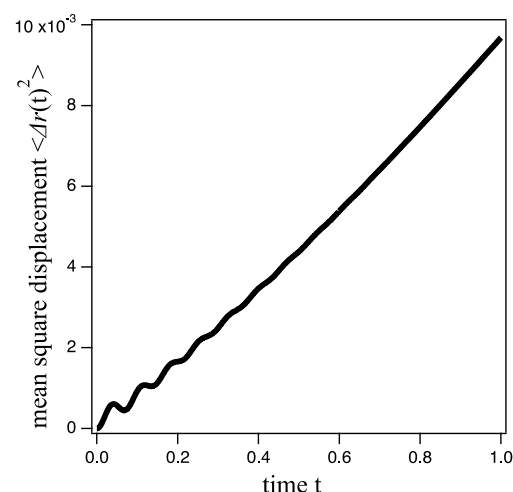


Fig.2 The mean square displacement of the tracer particle  $\langle \Delta r(t)^2 \rangle$

## 3. Results:

Fig.1 is a snapshot of the simulation for the tracer particle diameter with the  $R=5$  and  $M=1$ . Fig.2 shows the mean square displacement (MSD) of the tracer particle. At the short-time scale ( $t < 0.5$ ), we observed a clear oscillation in the MSD. Fig.3 shows the correlation of the velocity of the tracer particle. At this time scale, the small particles move ballistically. Thus the velocity of the large particle is changed by series of collisions of small particles. The oscillation may be driven if the velocities of a large particle before and after a collision event has a negative correlation. The detailed simulation data and theoretical analysis will be presented on site.

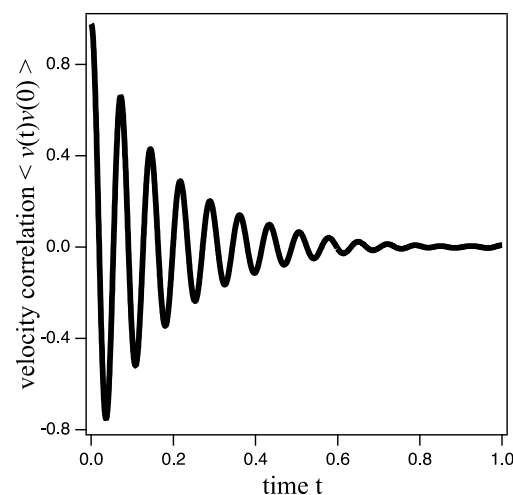


Fig.3 The velocity correlation of the tracer particle  $\langle v(t)v(0) \rangle$

## References:

(1) N. Grønbech-Jensen, and O. Farago, *Mol. Phys.* 111, 983, 2013.

# Small particles drive vibration of large particle

○Fumiaki Nakai, Takashi Uneyama and Yuichi Masubuchi (Nagoya Univ.)

## 0 Free Brownian motion

Langevin equation<sup>[1]</sup>

$$m\dot{v} = -\eta v + W(t)$$

Mean Square Displacement (MSD)

$$\langle \Delta r^2 \rangle = \frac{2kT}{\eta} \left[ t + \frac{m}{\eta} \exp\left(-\frac{\eta}{m}t\right) - 1 \right]$$

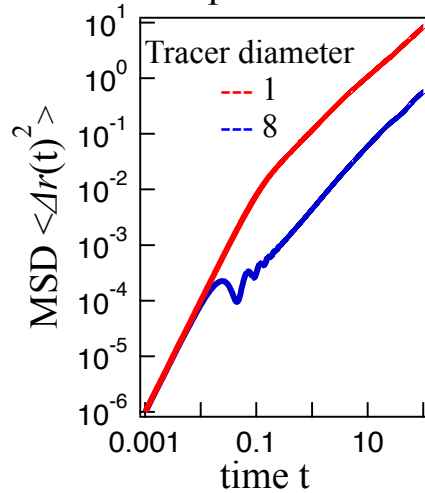
Consider two limits

$$\langle \Delta r^2 \rangle \rightarrow \frac{2kT}{\eta} t \quad (\tau_m > 0)$$

$$\langle \Delta r^2 \rangle \rightarrow \frac{kT}{m} t^2 \quad (\tau_m < 0)$$

## 1 Background

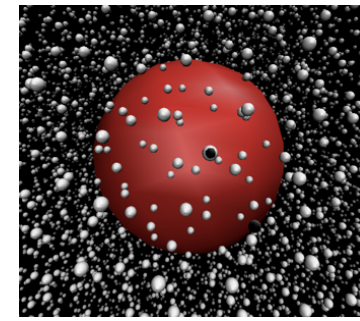
We found unexpected MSD vibration



Vibration occurs when tracer is large

What works for tracer ?

## 2 Simulation



Tracer mass  $M$ , size  $R$

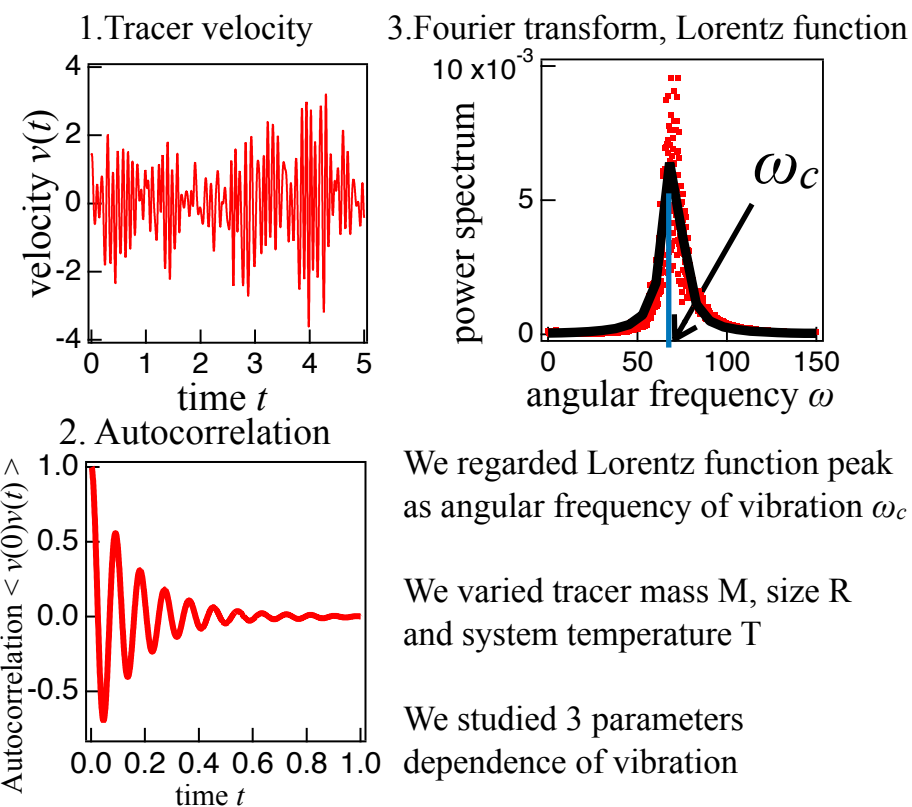
Small particles temp.  $T$

Single tracer and small particles are in simulation box

Langevin thermostat worked for small particles only

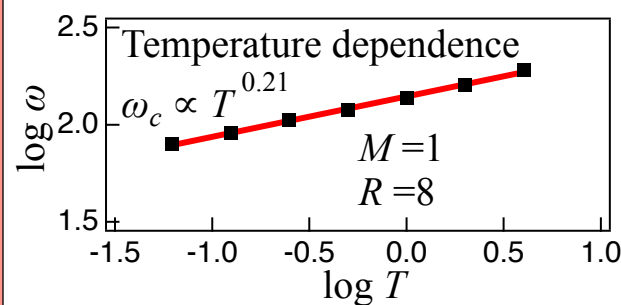
Lenard-Jones interaction is considered between particles

## 3 Analysis

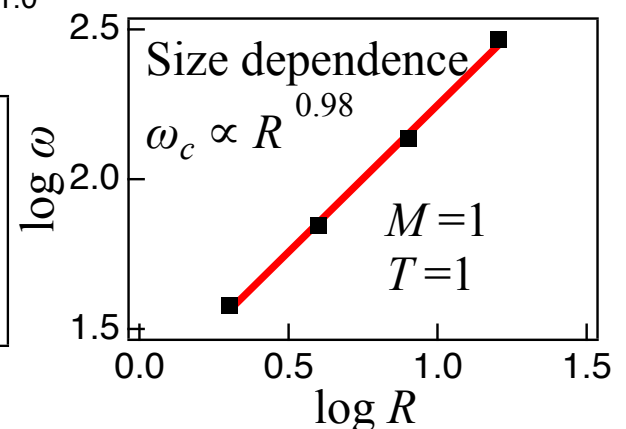
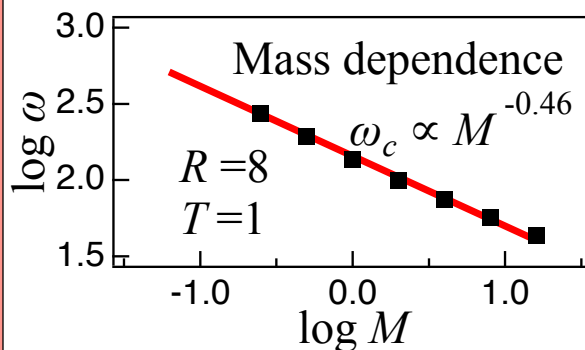


## 4 Result

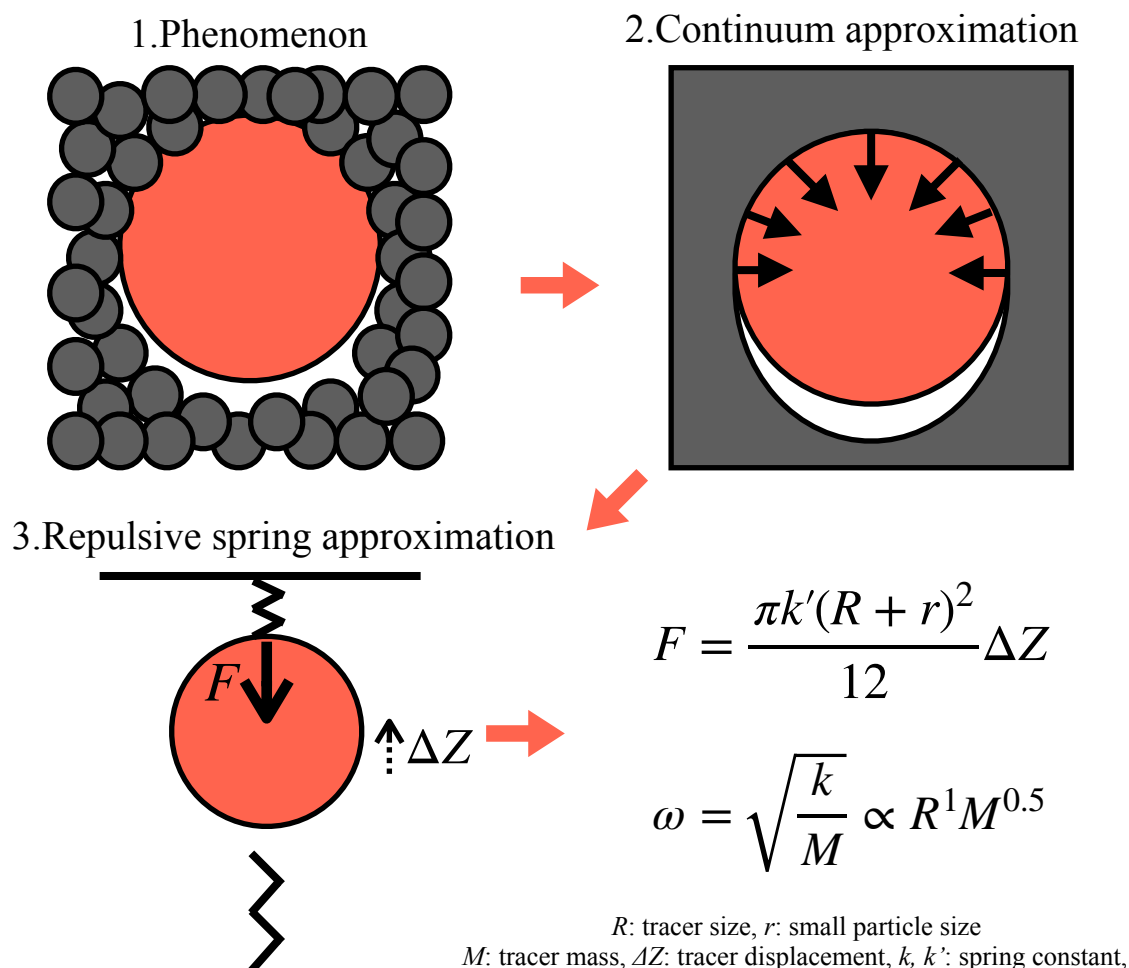
3 parameters dependence of angular frequency  $\omega_c$



$$\omega_c \propto R^1 M^{-0.5} T^{0.2} ?$$



## 5 Theoretical model



## 6 Summary

We found unexpected tracer vibration that disobey Langevin dynamics

For tracer vibration, We found angular frequency  $\omega_c$  is proportional to  $R^1 M^{0.5} T^{0.2}$

We constructed theoretical model that explain  $\omega_c$  for  $R$  and  $M$

We may find mechanism of  $T$  dependence of  $\omega_c$  by considering small particles distribution

# 流体中の大粒子の特異な振動機構：密度による機構の変化

(名大院工) ○仲井 文明, 畝山多加志, 増渕 雄一

## Mechanism of Unusual Vibration of Large Particle in Fluid

F. Nakai, T. Uneyama, and Y. Masubuchi  
Graduate School of Engineering, Nagoya University

### ABSTRACT

By the molecular simulations, we study the colloid dynamics in a short time scale in which the number of collisions between the colloid particle and the fluid particles is not sufficiently large. We found the mean square displacement (MSD) exhibits oscillations at the short time scale region. We studied the dependence of the various parameters on the oscillation frequency. The oscillation mechanism can be categorized to the three different regions depending on the fluid density. We propose the three models for these regions.

### 1. 緒言

工学的に、流体の物性を理解するのは重要である。流体の物性と、流体中の粒子（以降トレーサーとする）のダイナミクスは密接に関係している。例えば、流体中のトレーサーの拡散係数は粘度と関係している（Einstein の関係 [1]）。また、近年ではトレーサーの平均自乗変位（MSD）と緩和弾性率を関係付ける理論も提案されている [2]。これらは主に、長時間スケールのダイナミクスを考慮しており、流体粒子との十分多くの回数の衝突が生じ、統計的に平均できるとして正当化される。一方で、流体粒子との衝突回数が十分ではない短時間領域のダイナミクスに関しての知見は少ない。

同種の粒子から構成される流体中での粒子のダイナミクスに関しては報告がある。Lahman らは、分子シミュレーションで、液体アルゴンのダイナミクスを解析した [3]。速度のパワースペクトルが、Langevin 方程式から導かれる Lorentzian にならないことが報告されているが、ダイナミクスの機構は未解明である。

本研究では、短時間領域のトレーサーのダイナミクスを理解するため、シミュレーションと理論解析

を行った。

### 2. シミュレーション方法

微小な粒子およそ 10000 個で構成する流体中に、トレーサーを 1 個導入した。シミュレーションボックスには周期境界条件を課した。流体粒子のみに熱浴を課した。流体粒子間の相互作用にレナードジョーンズ (LJ) ポテンシャルを課した。流体粒子とトレーサーの相互作用には、トレーサーのサイズを反映し発散位置をシフトした LJ ポテンシャルを課した。いずれも、斥力のみはたらくようにカットオフ長  $r_c$  を定めた。LJ のエネルギー  $\epsilon$ 、流体粒子のサイズ  $\sigma$ 、質量  $m$  で無次元化した。トレーサーのサイズ  $R$ 、質量  $M$ 、温度  $k_B T$ 、流体粒子の数密度  $\rho$  を無次元パラメータとした。平衡化が完了した後、種々のパラメータに対する、トレーサーのダイナミクスを調べた。パラメータの範囲は、 $R = 4 \sim 16$ ,  $M = 0.03125 \sim 1$ ,  $T = 0.125 \sim 8$ ,  $\rho = 0.05 \sim 1.2$  とした。

### 3. シミュレーション結果

流体粒子に比べて、 $R$  が大きく  $M$  が小さいとき、短時間領域でトレーサーの MSD が振動を起こすことを発見した。Fig.1 に示した。同時間領域でノンガウシアンパラメータが 0 からシフトすることから、ガウシアンノイズを仮定した一般化ランジュバン方程式による解析を適用できないことが分かった。

MSD の振動をより詳細に調べるため、トレーサーの速度の自己相関関数 (VACF) を調べた。 $R = 8$ ,  $M = 0.0625$  として、 $\rho$  を変化させた際の VACF を Fig.2 に示す。 $\rho$  が小さいと 0 に単調減少し、 $\rho$  が大きいと MSD と類似した振動を起こすことが分かった。この振動の角周波数  $\omega_c$  に対する各種パラメータの依存性を調べたところ、

$\omega_c \propto R^\alpha M^{-\beta} T^\gamma$  のようなべき指数依存性を示した。べき指数  $\alpha, \beta, \gamma$  を  $\rho$  を変えて求めた。結果を Fig.3 に示す。  $T$  依存性に関しては、流体の相転移の影響を受け  $T$  依存性が急に変わる温度が存在したので、その前後で分けて解析した。  $\omega_c$  に対する  $R, M, T$  の依存性は、  $\rho$  が小さいとき  $\omega_c \propto R^2 M^{-0.5} T^{0.5}$ 、  $\rho$  が大きいとき  $\omega_c \propto R^1 M^{-0.5} T^{0 \sim 0.2}$  となることが分かった。

#### 4. 理論解析

以上のシミュレーション結果から、流体密度  $\rho$  によってトレーサーのダイナミクスの機構は3つに分けられるものと考えられる。それぞれの密度領域に対して、トレーサーが十分軽い ( $M \ll m$ ) として理論解析を行った。

流体密度  $\rho$  が低いとき、トレーサーの運動は、静止している流体粒子に対する、ランダムな衝突としてモデル化できる。剛体散乱を仮定し散乱角  $\theta$  を解析したところ、  $\langle \cos \theta \rangle = 0$  となることが分かった。これは、VACF が指数関数型で0に単調減少することに対応し、シミュレーション結果と一致する。

流体密度  $\rho$  が中程度のとき、トレーサーは流体粒子により構成される擬似的なケージの中で運動すると考えられる。  $\omega_c$  の依存性は、  $\omega_c \propto R^2 M^{-0.5} T^{0.5}$  となり、シミュレーション結果と一致する。

流体密度  $\rho$  が高いとき、トレーサーは流体粒子により構成されるポテンシャル中を運動すると考えられる。そこで、周囲流体が調和ポテンシャルを形成するとみなした。  $\omega_c$  の依存性は、  $\omega_c \propto R^1 M^{-0.5} T^0$  となり、シミュレーション結果と一致する。

#### 5. 結論

シミュレーションによって流体粒子中のトレーサーの運動を調べた。流体中の大きく軽いトレーサーは、振動を起こすことを発見した。流体の密度によって、大きく軽いトレーサーのダイナミクスは3つの機構に分類されることが分かった。

#### 参考文献

- [1] A. Einstein. *Annalen Der Physik*, 17(8):549–560, 1905.
- [2] T. G. Mason. *Rheologica Acta*, 39(4):371–378, 2000.
- [3] A. Rahman. *Physical Review*, 136(2A), 1964.

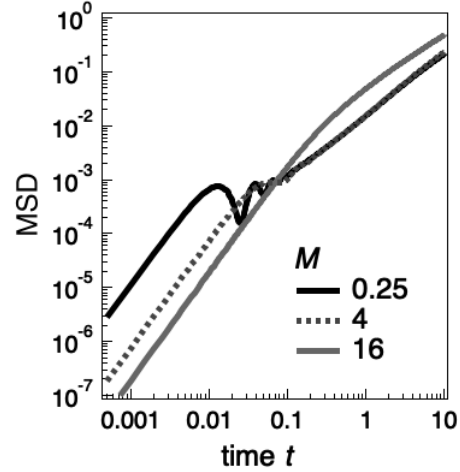


Fig.1 Mean square displacement for  $M = 0.25, 4$  and  $16$ . The tracer size and the fluid density are  $R = 8$  and  $\rho = 0.8$

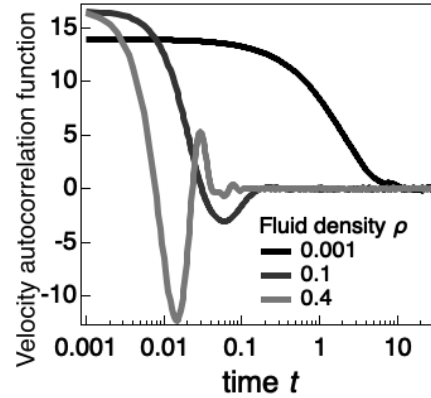


Fig.2 Velocity autocorrelation functions for  $\rho = 0.001, 0.1$  and  $0.4$ . The tracer size and mass are  $R = 8$  and  $M = 0.0625$ .

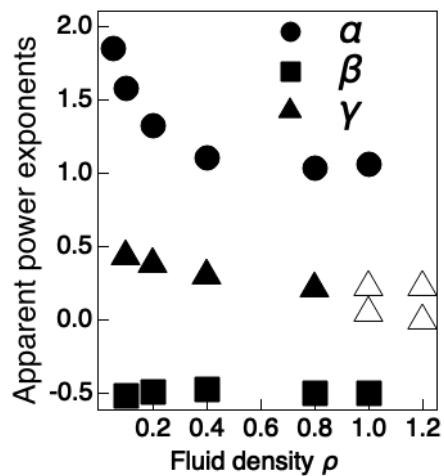


Fig.3 Apparent power-law exponents of the characteristic angular frequency for the velocity autocorrelation function.

# 流体中の大粒子の特異な振動機構：密度による機構の変化

○仲井文明, 畝山多加志, 増淵雄一(名大院工)

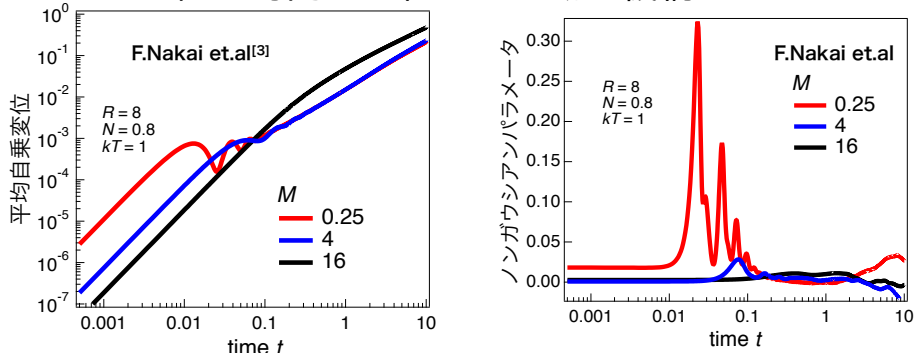
## 1. 背景

流体中のトレーサーの運動の記述に一般化ランジュバン方程式(GLE)<sup>[1]</sup>が使われる

$$m \frac{d\mathbf{r}^2}{dt^2} = - \int_0^\infty -\zeta(t)\mathbf{v}(t-t')dt' + \mathbf{W}(t) \quad \left\{ \begin{array}{l} \zeta: \text{メモリアーネル} \\ \mathbf{W}: \text{ガウシアンノイズ} \end{array} \right.$$

しかし、極短時間の運動に関してガウシアンノイズを仮定したGLEは有効ではない<sup>[2]</sup>

極短時間での粒子の運動の機構は？

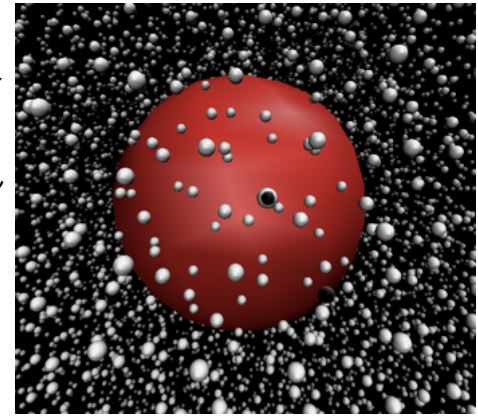


軽いトレーサーのMSDは短時間領域で振動する  
この振動はなに？

## 2. シミュレーション方法

短時間領域のトレーサーのダイナミクスを調べた

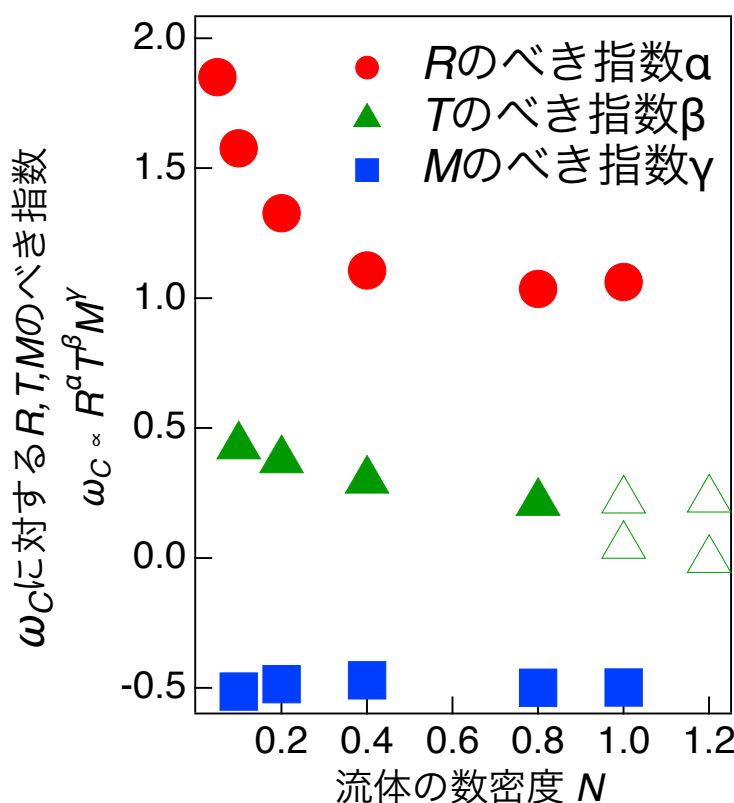
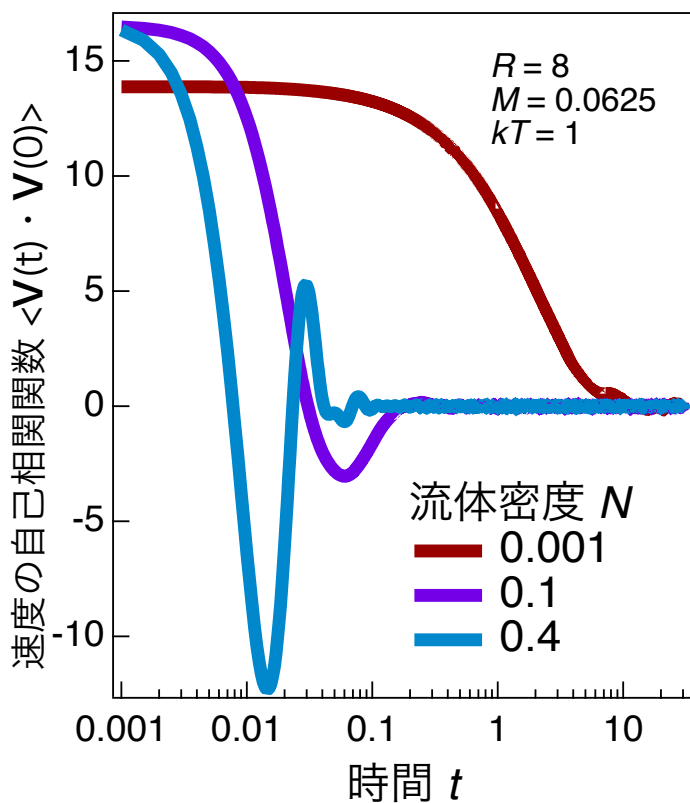
- ・トレーサー1個と多数の流体粒子を導入
- ・ボックスには周期境界を課した
- ・相互作用は斥力のみ働くLJポテンシャル
- ・LJ単位系で無次元化
- ・流体粒子だけにランジュバン熱浴
- ・平衡化完了後のデータを取得



速度の自己相関関数  $\langle V(t) \cdot V(0) \rangle$   
及び、角周波数  $\omega_c$  に注目した

トレーサーのサイズ  $R$ 、系の温度  $T$   
質量  $M$ 、流体粒子の数密度  $N$  を変えた

## 3. 結果：速度の自己相関関数（左図）と、 $\omega_c$ に対する $R, T, M$ のべき指数（右図）



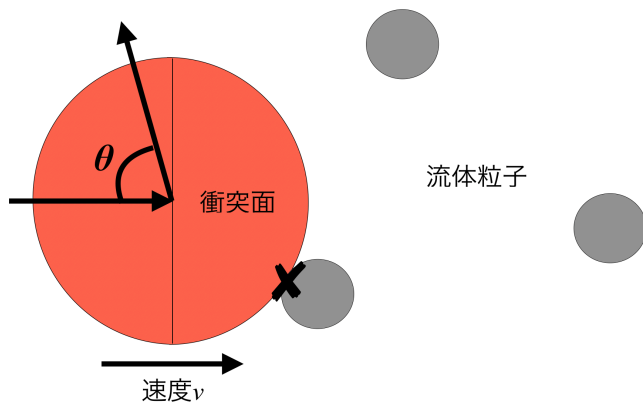
左図  
流体の数密度が  $N < 0.001$  のとき  
振動は起きない

右図  
流体の数密度  $N$  によって  $\omega_c$  に対する  $R, T, M$  の依存性が異なる  
流体の数密度が  $N \sim 0.1$  程度するとき  
 $\omega_c \propto R^2 T^{\frac{1}{2}} M^{-\frac{1}{2}}$   
流体の数密度が  $N > 1$  のとき  
 $\omega_c \propto R^1 T^{0 \sim 0.2} M^{-\frac{1}{2}}$

## 4. 考察：流体密度ごとに理論モデルを構築

### 無相関衝突モデル ( $N < 0.001$ )

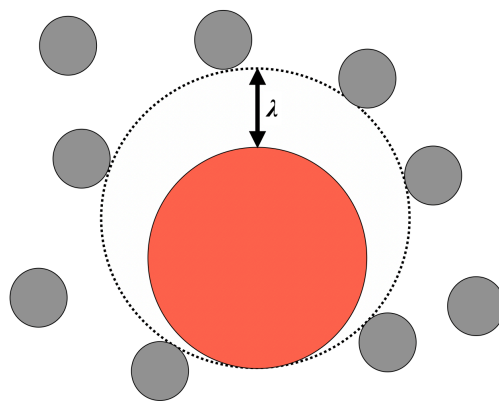
トレーサーの進行方向からのみ衝突  
しかし、散乱角の期待値  $\langle \cos\theta \rangle = 0$  であることを導出



速度の自己相関関数は  
指数関数型で単調減少し0に漸近  
振動は起きない

### ケージモデル ( $N \sim 0.1$ )

流体粒子による疑似的なケージ内を  
運動するモデル



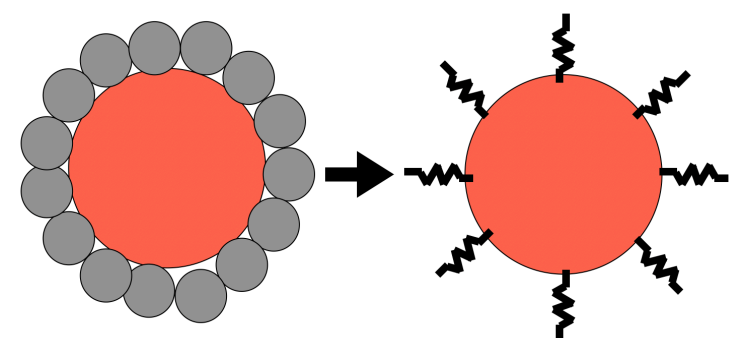
速さ  $V \propto T^{\frac{1}{2}} M^{-\frac{1}{2}}$       自由行程  $\lambda \propto R^{-2}$

$R, T, M$  の依存性

$$\omega_c \propto V/\lambda \propto R^2 T^{\frac{1}{2}} M^{-\frac{1}{2}}$$

### バネモデル ( $N > 1$ )

流体粒子による斥力ポテンシャル中を  
運動するモデル  
流体粒子を連続した線形バネとして近似



バネ定数  $k \propto R^2$

$R, T, M$  の依存性

$$\omega_c = \sqrt{k/M} \propto R^1 T^0 M^{-\frac{1}{2}}$$

[1] Langevin, Comptes Rendus Hebdomadaires Des Seances De L Academie Des Science, 530-533, 1908

[2] A. Rahman, Physical review, f36, 2A, 1964

[3] F. Nakai, IWEAYR, P23, 2018

# 衝突の確率過程に基づく流体中のトレーサーの速度相関関数の解析

名古屋大学大学院工学研究科物質科学専攻

仲井文明, 畝山多加志, 増淵雄一

Analysis of velocity autocorrelation function of tracer in fluids based on stochastic process of collisions

Dept. of Engineering, Nagoya Univ.

F. Nakai, T. Uneyama, M. Yuichi

## 緒言

高密度の流体中の分子の速度相関関数がある時間で負になる現象は広く報告されている<sup>[1]</sup>。しかし、その物理について十分な理解がなされていない。Barshteinらは流体中の特定の粒子（以降トレーサーと呼ぶ）に注目し、ダイナミクスを衝突の連続過程としてモデル化した。彼らは、衝突を瞬時に起こる速度のみが変化するイベントと仮定し、連続時間ランダムウォーク（CTRW）の枠組みを用いて速度の自己相関関数（VACF）を解析した<sup>[2]</sup>。CTRWの枠組みでVACFが負の値を示すには、①トレーサーと流体粒子の衝突の時間間隔が指数分布にならないこと、及び②トレーサーと流体粒子の衝突前後の速度相関が負になること、の2つが必要条件である。本研究では、流体中のトレーサーのVACFが負になる現象を上記の「衝突時間間隔の分布」と「衝突前後の速度相関」の2つの問題に分けて考える。分子シミュレーションを用いてこれらを解析する。

## 方法及び結果

LJ粒子により構成される流体中にトレーサーを一個導入し、トレーサーのダイナミクスを解析した。粒子間相互作用は、斥力でカットオフしたLJポテンシャルである。衝突時間間隔の分布 $P(\tau)$ と衝突前後の速度相関 $\gamma = \langle \mathbf{V} \cdot \mathbf{V}' \rangle$  ( $\mathbf{V}, \mathbf{V}'$ は1回の衝突前後の速度、 $\langle \dots \rangle$ は統計平均を表す) に対するトレーサーのサイズ $R$ 、質量 $M$ 、流体の数密度 $\rho$ の影響を調べた。トレーサーに加わる力の時間発展 $|\mathbf{f}(t)|$ が極大を示す点を衝突が起きた時刻と定義し、これらの間隔を調べた。得られた間隔の分布 $P(\tau)$ をFig1に示した。横軸は、平均値 $\bar{\tau}$ でリスケールした。 $P(\tau)$ は、 $\rho$ が小さいときは指数分布である。 $\rho$ が大きときは、ある時間で極大を示し、指数分布からずれる。衝突前後の速度は、トレーサーの速度のある方向の時間発展 $v_x(t)$ のプラトーから決めた。 $\gamma$ は、 $\rho$ が小さいとき正で、大きいとき負になる。また、VACFは、 $\rho$ が小さいときは指数関数的に減少するが、大きいときはある時間領域で負の値を示す。以上の結果はBarshteinらの主張をサポートする。トレーサーのサイズと質量もVACFが負になることに深く関係することが分かっている。講演では、これらを変えた場合の結果も併せて紹介する。

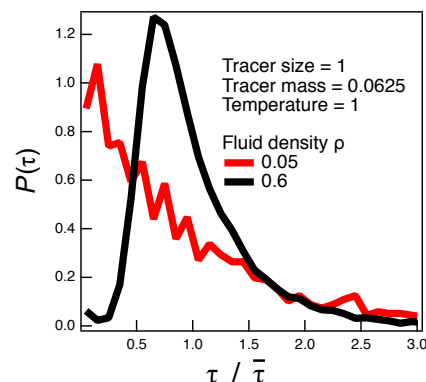


Fig1 Distribution function of the rescaled collision time interval

## 参考文献

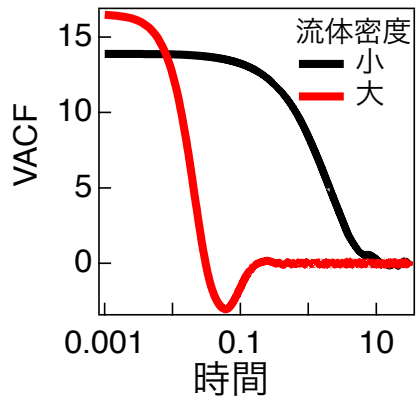
- [1] B. J. Alder, D. M. Gass, and T. E. Wainwright, Journal of Chemical Physics **53**, 3813 (1970).
- [2] A. I. Burshtein and M. V. Krongauz, Journal of Chemical Physics **102**, 2881 (1995).

# 衝突の確率過程に基づく流体中のトレーサーの速度相関関数の解析

○仲井文明, 畝山多加志, 増淵雄一(名大院工)

## 1. 背景

液体やガラスなど、中～高密度流体の分子の速度の自己相関関数(VACF)は短時間領域で負の相関を持つ[1]

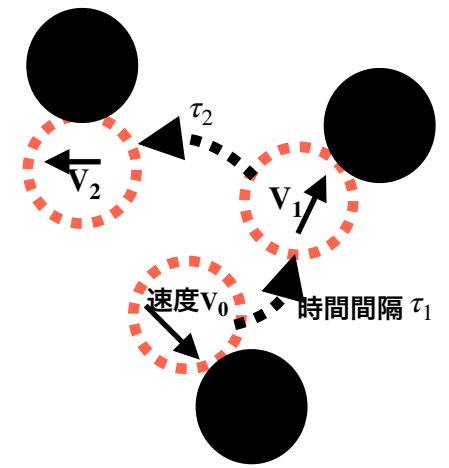


周囲粒子のケージ効果の影響とされているが理解が曖昧

## 2. 目的

Burshteinらは衝突を独立と仮定し連続時間ランダムウォークの枠組みでVACFが負になる2条件を提示した[2]

- 1 衝突時間間隔の分布 $P(\tau)$ が指数分布にならないこと
- 2 衝突前後の速度の相関 $\gamma(1) = \langle \mathbf{V}_p \cdot \mathbf{V}_{p+1} \rangle$ が負になること ( $\mathbf{V}_p$ はp回目の衝突直前の速度)



- ・衝突を独立とした仮定は妥当か?
- ・左記の2条件は実際に起きるのか?

## 3. シミュレーションの系

注目粒子: トレーサー

その他: 流体粒子 と呼ぶ

$M_r$ : 流体粒子に対するトレーサーの質量比 ( $M/m$ )

LJ系

- ・粒子同士の相互作用は斥力LJ
- ・ $M_r = 0.0625$ , サイズ比=1

剛体系

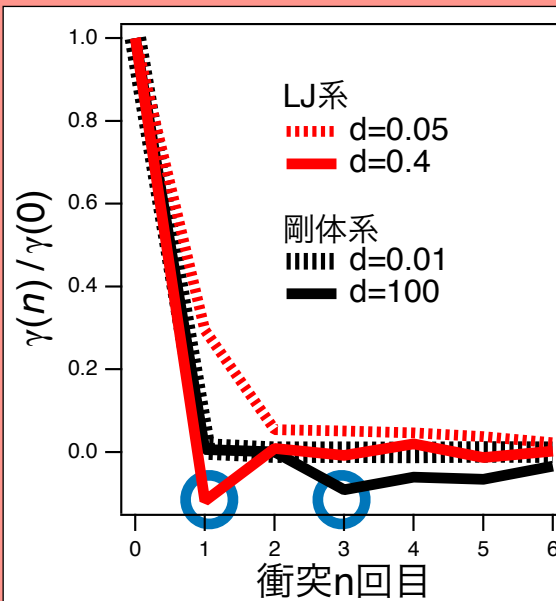
- ・流体粒子とトレーサーのみが衝突
- ・流体粒子同士は衝突しない
- ・ $M_r = 0.01$

$M_r$ が小さいとVACFが負の相関を持つ[3]

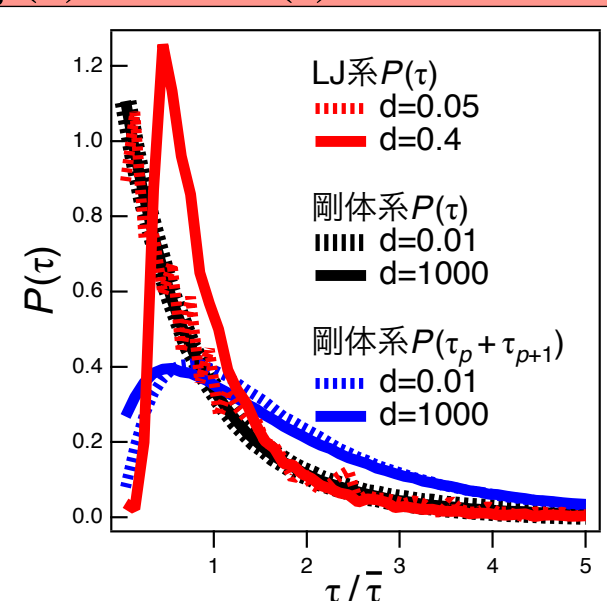
$M_r$ を小さく設定 流体粒子の数密度 $d$ を変える

$\gamma(n) = \langle \mathbf{V}_p \cdot \mathbf{V}_{p+n} \rangle$ ,  $P(\tau)$ および2回の衝突時間間隔 $P(\tau_p + \tau_{p+1})$ を解析

## 4. LJ系と剛体系の $\gamma(n)$ および $P(\tau)$ の解析結果

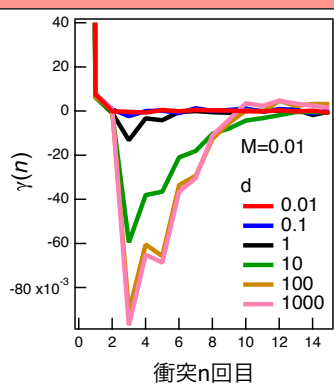


- 密度が大きいとき
- LJ系:  $n=1$ で負になる
- 剛体系:  $n=3$ から負となる



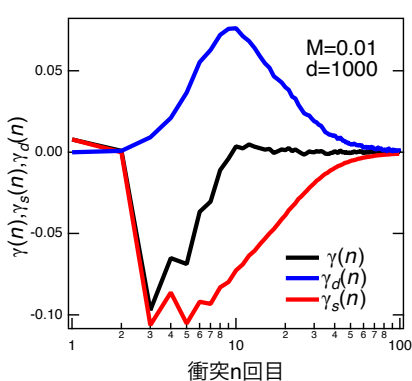
- LJ系: 密度が大きいと指数分布からずれる
- 剛体系: 密度によらず1回の衝突は指数分布
- 2回の衝突で指数分布からずれる

## 5. 剛体系を詳しく解析



$d$ を変えた時の $\gamma(n)$

- $d$ によらず  $n=3$ で $\gamma_n$ は最小
- $d$ が大きくなると $\gamma_n$ の負の値は大きくなる



1回目とn回目に同粒子と衝突した場合、異粒子と衝突した場合の条件付き $\gamma(n)$ を $\gamma_s(n)$ ,  $\gamma_d(n)$ と定義

- 1回目と $n(\geq 3)$ 回目の同粒子との衝突が $\gamma_n$ を負にしている ( $n=2$ で同粒子と衝突不可能)

## 6. 考察

LJ系の結果はBurshteinの解析結果をサポートする結果であるしかし、剛体系の結果をふまえると、LJ系の $d$ が大きい場合の解析は複数回の衝突を1回の衝突として検知している可能性がある

LJ系、剛体系の結果から、複数回の衝突を1回の素過程と置き直せばBurshteinらの理論を適用できるかもしれない

剛体系の結果よりVACFの負の相関には同粒子との衝突が影響している

## 7. 結論

- LJ系: Burshteinの主張をサポートする
- 剛体系: Burshteinの主張と以下のように異なる
- 1回の衝突では、 $P(\tau)$ は指数分布になり、 $\gamma(1)$ は負にならない
- 3回目以降の同粒子との衝突が重要で衝突は独立とみなせない

参考文献  
 [1] B. J. Alder, D. M. Gass, and T. E. Wainwright, Journal of Chemical Physics 53, 3813 (1970).  
 [2] A. I. Burshtein and M. V. Krongauz, Journal of Chemical Physics 102, 2881 (1995).  
 [3] F. Nakai, 日本レオロジー学会第46年会 ポスター発表P15,(2019)

(名大院工) ○仲井文明, 畝山多加志, 増淵雄一

E-Mail to Name: nakai.fumiaki@b.mbox.nagoya-u.ac.jp

キーワード: 理想気体, 速度相関関数, 衝突, ランジュバン方程式, 非ガウス性

【はじめに】 溶媒中の粒子 (トレーサー) のダイナミクスはガウシアンノイズを仮定した一般化ランジュバン方程式 (GLE) で記述される<sup>[1]</sup>。しかし、トレーサーと流体粒子の衝突が数回程度に限られる短時間においてはノイズ項がガウシアンにならないので、トレーサーのダイナミクスをガウシアンノイズを仮定したGLEで記述できない。現状、溶媒中のトレーサーの短時間ダイナミクスの理解は十分ではない。トレーサーの短時間ダイナミクスを理解するために、まずは理想化した簡単な系を理解する必要がある。多体相互作用が存在すると時間・空間的に相関が生じ、トレーサーのダイナミクスは複雑になる。本研究では、多体相互作用の影響をなくすために、トレーサーの周囲流体を理想気体として解析した。

【方法】理想気体中のトレーサーのダイナミクスを以下の方法でシミュレーションした。周期境界を課したシミュレーションボックスの中心にサイズ $\sigma$ のトレーサーを置き、トレーサーに重ならないようにサイズ0の粒子 (理想気体粒子) を10万個ランダムに導入した。各粒子の初期速度はマクスウェルボルツマン分布に従い生成した。粒子の座標および速度の時間発展は剛体シミュレーションの手法に従った<sup>[2]</sup>。トレーサーのサイズ $\sigma$ 、系の温度 $k_B T$ 、流体粒子の質量 $m$ で規格化を行った。本系はトレーサーと理想気体粒子のみが相互作用する。また、パラメータはトレーサーの質量 $M$ と理想気体の数密度 $\rho$ のみの単純な系である。

【結果】 $\rho$ が1より十分小さい場合、トレーサーと流体粒子の衝突は独立となり比較的簡単なダイナミクスになる。また、 $M$ が1より十分大きい場合、ノンガウシアンパラメータによる解析で変位はガウシアンになることがわかり、トレーサーのダイナミクスは近似的にガウシアンノイズを仮定したGLEで書ける。本研究は未知の領域である、 $M$ が1より小さく $\rho$ が1より大きい場合を対象とした。パラメータを $M = 1, 0.01, \rho = 1, 100$ の組み合わせで振った。 $M = 0.01, \rho = 100$ のとき、平均二乗変位 (MSD) はプラトーを示し、速度の自己相関関数 (VACF) は負の相関を示した。VACFの結果を図1に示した。比較のために縦軸を質量、横軸を衝突時間間隔の平均でリスケールした。周囲流体が理想気体である系で上記のような結果が生じたという報告例はない。Burshteinらは個々の衝突が独立な場合、VACFが負の相関を示すには次の2つが必要条件となることを示した<sup>[3]</sup>。すなわち「 $\gamma = \langle \mathbf{V}_p \cdot \mathbf{V}_{p+1} \rangle < 0$ であること」および「衝突の時間間隔の分布 $P(\tau_p)$ が指数分布からずれること」である。ここで $\mathbf{V}_p$ はトレーサーが $p$ 回目に理想気体粒子と衝突する直前の速度、 $\tau_p$ は $p-1$ 回目と $p$ 回目の衝突時間の間隔である。本系で上記の2つの条件を調べたところ、どのパラ

メータセットでも $\langle \mathbf{V}_p \cdot \mathbf{V}_{p+1} \rangle > 0$ となり、 $P(\tau_p)$ はおおよそ指数分布になった。よって、 $M = 0.01, \rho = 100$ のとき衝突は独立でないことがわかった。

【考察】理想気体中でトレーサーのVACFが負の相関を示す原因を考察する。結果より、衝突は独立ではなく、1回の衝突の相関を見るだけではその原因はわからない。ここで複数回の衝突の相関を解析するために、 $\gamma(n) = \langle \mathbf{V}_p \cdot \mathbf{V}_{p+n} \rangle$ を新たに導入した。解析結果を図2に示した。 $\gamma(n)$ は $M = 0.01, \rho = 100$ のとき、 $n \geq 3$ で負の値を示していることがわかる。これは、3回目以降の衝突で何かの相関が生じたことを意味する。本系の溶媒は理想気体なので、別個の理想気体粒子との衝突が相関を持つことはない。存在しうる相関は「同じ理想気体粒子と衝突する事象」のみだと考え、 $\gamma(n)$ を1回目に $n$ 回目に同粒子、異粒子に衝突した場合に分けて解析したところ、「同粒子と衝突する事象」が $\gamma(n)$ が負になる現象を引き起こすことがわかった。

【結論】理想気体中のトレーサーのダイナミクスをシミュレーションで解析した。トレーサーのダイナミクスは $M$ が1より十分大きいとガウシアンノイズを仮定したGLEで書け、 $\rho$ が1より十分小さいと衝突が独立な比較的簡単なダイナミクスになる。一方で、 $M$ が1より小さく $d$ が1より大きいと、MSDはプラトーを示し、VACFが負の相関を示すなど非自明なダイナミクスが生じる。この原因は「同じ理想気体粒子との衝突」である。

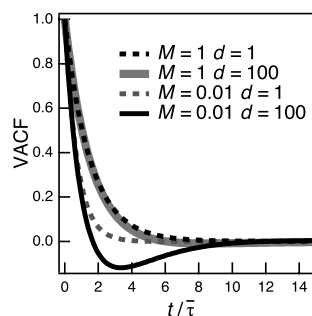


Fig.1 Velocity autocorrelation function of tracer in ideal gas. Tracer mass  $M$  and number density of ideal gas  $\rho$  were varied

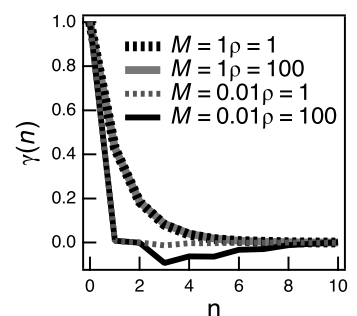


Fig.2  $\gamma(n) = \langle \mathbf{V}_p \cdot \mathbf{V}_{p+n} \rangle$  of tracer in ideal gas. Tracer mass  $M$  and number density of ideal gas  $\rho$  were varied

### 【引用文献】

- [1] H. Mori, Progress of Theoretical Physics 33, 423 (1965).
- [2] B. J. Alder, D. M. Gass, and T. E. Wainwright, Journal of Chemical Physics 53, 3813 (1970).
- [3] A. I. Burshtein and M. V. Krongauz, Journal of Chemical Physics 102, 2881 (1995).

# 理想気体中の粒子の短時間ダイナミクス

○仲井文明, 畝山多加志, 増淵雄一(名大院工)

## 1 短時間ダイナミクスを理想系で理解

流体中の粒子(トレーサー)の運動の記述に一般化ランジュバン方程式(GLE)が使われる

$$m \frac{d\mathbf{V}}{dt} = - \int_{-\infty}^t \Gamma(t-t')\mathbf{V}(t')dt' + \mathbf{W}(t)$$

$\mathbf{V}$ : トレーサー速度  
 $\Gamma$ : メモリカーネル  
 $\mathbf{W}$ : ガウシアンノイズ

流体分子との衝突が数回の短時間で $\mathbf{W}$ はノンガウシアン  
 →短時間ダイナミクスは記述できない

短時間ダイナミクスを理解したい

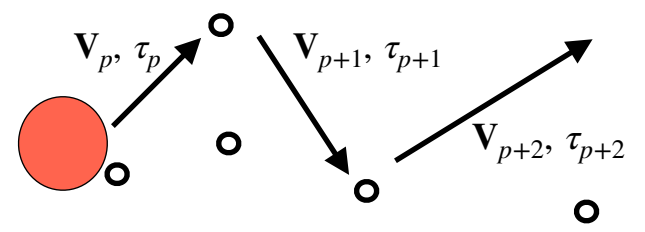
→まずは単純な理想気体中で理解する

## 2 三次元剛体シミュレーション[1]

- ・トレーサー1個  
質量 $M$  サイズ $\sigma$
- ・理想気体粒子10万個  
数密度 $\rho$  質量 $m$  サイズ $0$
- ・温度:  $k_B T$

$m, k_B T, \sigma$ で無次元化  
 パラメータは $M, \rho$ のみ

以下を取得  
 $p-1 \sim p$ 回目の衝突時間間隔 $\tau_p$   
 $p$ 回目の衝突直前のトレーサー速度 $\mathbf{V}_p$   
 $p$ 回目に衝突する理想気体粒子 $l_p$



$M \gg 1$ : GLEで記述可

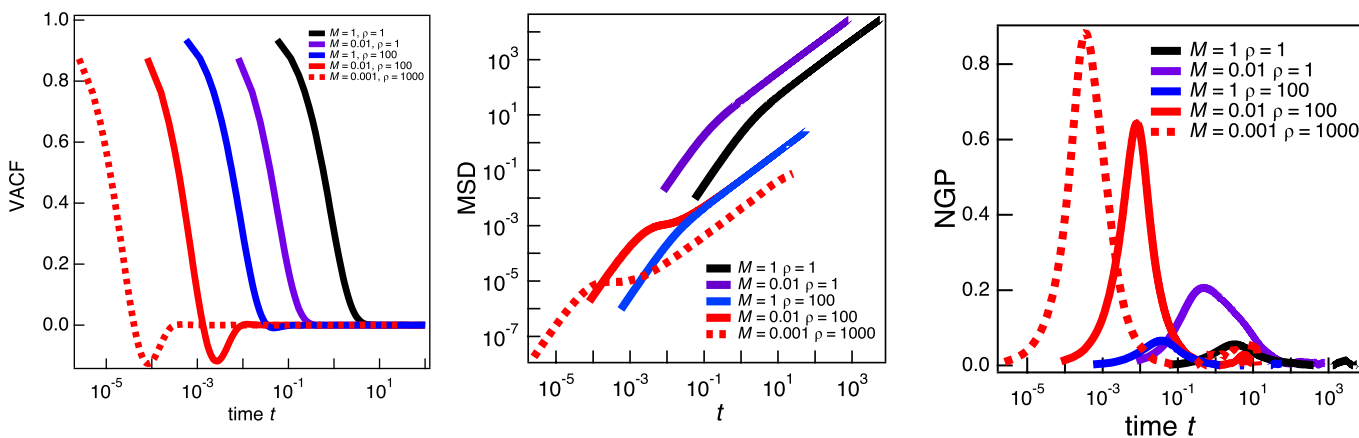
$\rho \ll 1$ : 希薄で単純

(本シミュレーションで確認済)

↓  
 $M < 1, \rho > 1$ を対象に

トレーサーのダイナミクスを解析

## 3 速度の自己相関関数(VACF = $\langle \mathbf{V}(t)\mathbf{V}(0) \rangle / \langle \mathbf{V}(0)^2 \rangle$ ) 平均二乗変位(MSD = $\langle \Delta \mathbf{r}(t)^2 \rangle$ ) ノンガウシアンパラメータ(NGP = $3\langle \Delta \mathbf{r}(t)^4 \rangle / 5\langle \Delta \mathbf{r}(t)^2 \rangle^2 - 1$ )



$M \leq 1, \rho \geq 1$ でVACFは負の相関 MSDは変曲点 NGPはピーク

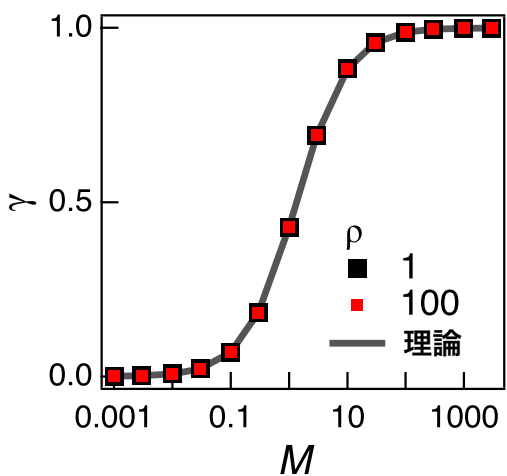
理想気体中で非自明なダイナミクス  
 初めての報告

現象は単純?  
 軽いから反対方向に散乱されやすい?  
 トレーサーと理想気体粒子の個々の  
 独立な衝突の連続で起きる現象?

以降「衝突」に注目

## 4 一回の衝突で生じる現象か?

衝突前後の速度相関[3]  $\gamma = \frac{\langle \mathbf{V}_p \cdot \mathbf{V}_{p+1} \rangle_p}{\langle \mathbf{V}_p^2 \rangle_p}$ をシミュレーションと理論で解析



理論  $\gamma = \frac{3M}{3M + 4m}$  (以下を考慮し導出)

- ・2体衝突における運動量&エネルギー保存
- ・トレーサー表面の衝突点の分布
- ・トレーサーの速度分布
- ・衝突する流体粒子の速度分布(相対速度考慮)

本質: 表面をかする衝突もあり $\gamma > 0$

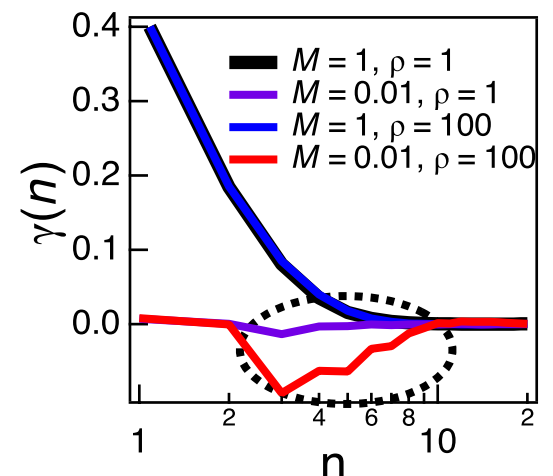
(かする衝突がない1次元では $\gamma = \frac{M-2m}{M+2m}$ となり負になりうる)

理論、シミュレーション共に常に $\gamma$ は正 → 1回の衝突では説明できない

## 5 複数回の衝突で相関発生

$n$ 回衝突後の相関を見たい

→  $\gamma(n) = \langle \mathbf{V}_p \cdot \mathbf{V}_{p+n} \rangle_p / \langle \mathbf{V}_p^2 \rangle_p$ を導入



3回以降の衝突で相関発生

## 6 何が相関を発生させている?

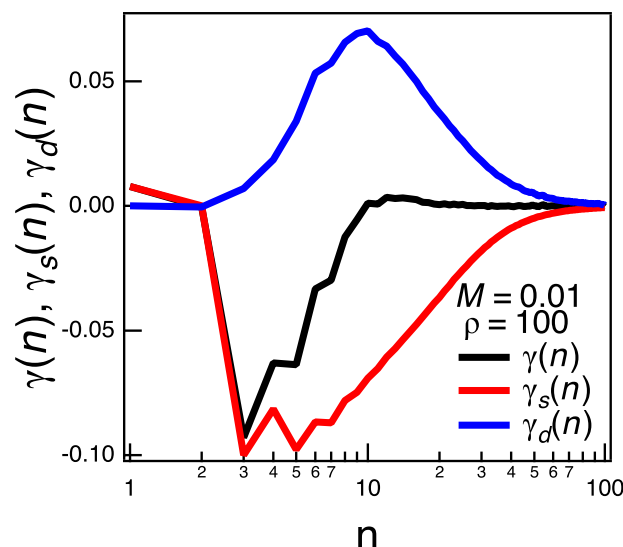
理想気体中で存在する相関は  
 同粒子との衝突?

同粒子との衝突には  
 最低3回の衝突が必要  
 → $\gamma(n)$ の結果と辻褃合う

$\gamma(n)$ を $n$ 回目に同粒子・異粒子と  
 衝突した場合に切り分け

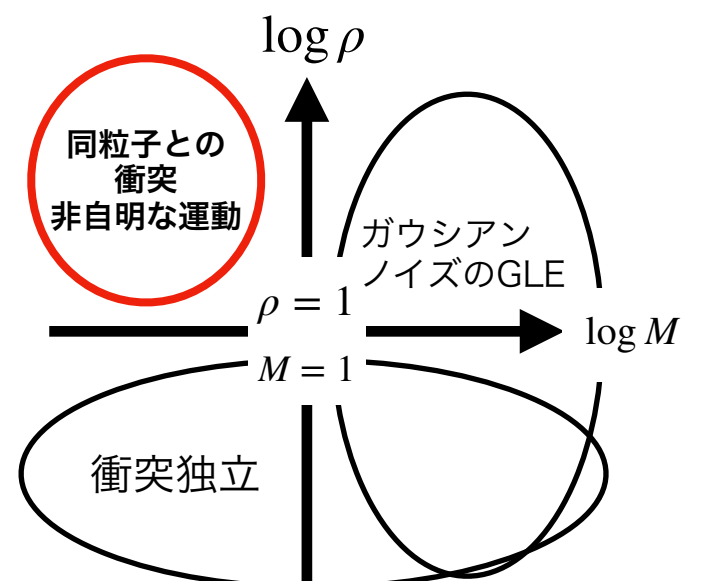
$$\gamma(n) = \gamma_{l_{p+1}=l_{p+n}}(n) + \gamma_{l_{p+1} \neq l_{p+n}}(n)$$

$$= \gamma_s(n) + \gamma_d(n)$$



同粒子との衝突が相関を生み出す

## 7 ダイナミクスの分類



# 理想気体中のトレーサーの短時間ダイナミクス 補助資料

○仲井文明, 畝山多加志, 増淵雄一(名大院工)

## $\gamma = \langle \mathbf{V}_p \cdot \mathbf{V}_{p+1} \rangle / \langle \mathbf{V}_p^2 \rangle$ の理論的導出の概要

運動量保存とエネルギー保存より  
1回の衝突で速度は次のように変化

$$\mathbf{V}_{p+1} = \mathbf{V}_p + \frac{2m}{m+M} \hat{\mathbf{r}} \cdot (\mathbf{v}_p - \mathbf{V}_p) \hat{\mathbf{r}}$$

$\mathbf{V}_p$ :  $p$ 回目衝突直前のトレーサー速度

$\mathbf{v}_p$ :  $p$ 回目衝突直前の理想気体粒子速度

$m$ : 理想気体粒子質量

$M$ : トレーサー質量

$\hat{\mathbf{r}}$ : トレーサーと衝突粒子の相対位置ベクトル

以下を考慮し $\gamma$ を計算

相対位置ベクトルの分布関数 $P_{\hat{\mathbf{r}}}(\hat{\mathbf{r}})$ : 立体角を考慮

トレーサー速度の分布関数 $P_{\mathbf{V}_p}(\mathbf{V}_p)$ : マクスウェルボルツマン分布 (MB分布)

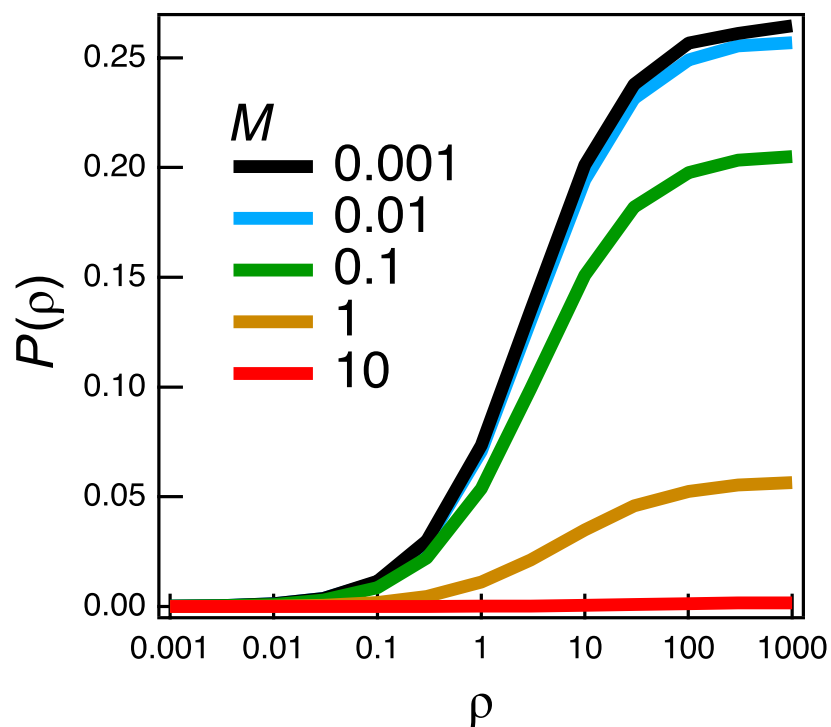
衝突する理想気体の速度の分布関数 $P_{\mathbf{v}_p}(\mathbf{v}_p)$ : MB分布に相対速度の重み付け

$$\gamma = \frac{\int d\hat{\mathbf{r}} \int d\mathbf{V}_p \int d\mathbf{v}_p (\mathbf{V}_{p+1} \cdot \mathbf{V}_p) P_{\hat{\mathbf{r}}}(\hat{\mathbf{r}}) P_{\mathbf{V}_p}(\mathbf{V}_p) P_{\mathbf{v}_p}(\mathbf{v}_p)}{\int d\hat{\mathbf{r}} \int d\mathbf{V}_p \int d\mathbf{v}_p (\mathbf{V}_p^2) P_{\hat{\mathbf{r}}}(\hat{\mathbf{r}}) P_{\mathbf{V}_p}(\mathbf{V}_p) P_{\mathbf{v}_p}(\mathbf{v}_p)} = \frac{3M}{3M + 4m}$$

ちなみに1次元だと $\gamma = \frac{M-2m}{M+2m}$  で負になりうる

$\gamma$  は次元に強く依存する

## 3回目に同粒子と衝突する確率 $P_3(\rho)$

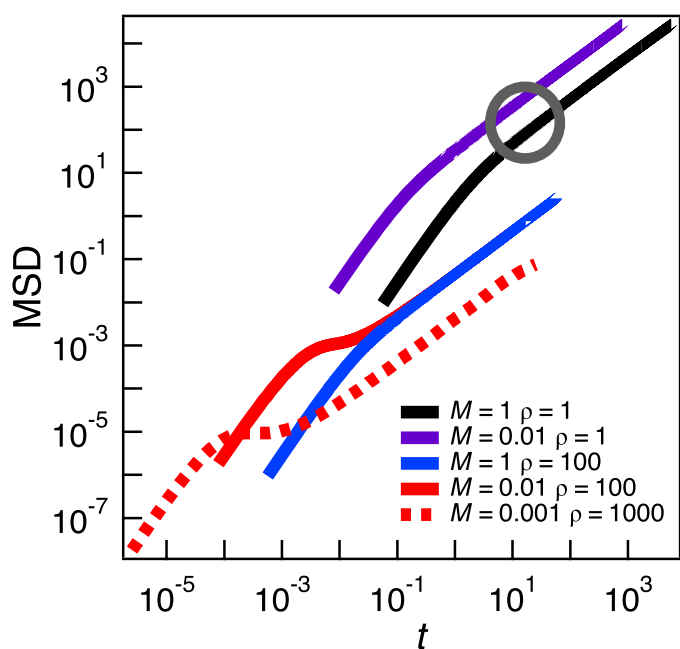


$M$ が小さいほど、 $\rho$ がおおきいほど $P_3(\rho)$ は大きい  
ただし、一定確率にさちる

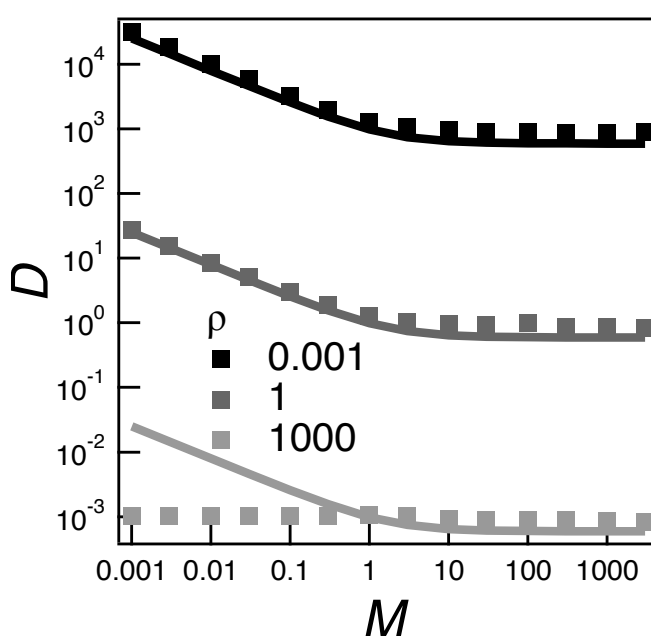
## 次の問題

- ・ 同粒子との衝突がなぜVACFやMSDやNGPの非自明な挙動を起こすのか
- ・ 3回目に同粒子と衝突するとバックリフレクションが起こる現象は分子衝突論から理解できそう
- ・ 同粒子との衝突がトレーサーの拡散係数にも影響を及ぼす (下図) が、なぜかは分かっていない
- ・ なぜ $P_3(\rho)$ がさちる (左図) のかは分かっていない (1次元系なら分子衝突論から理解できそう)

## (番外) 希薄気体中のトレーサーの自己拡散係数 $D$ の質量依存性の理論的導出の概要



希薄下でトレーサーの自己拡散係数 $D$ は  
 $M$ 依存性を示す



点: シミュレーション 線: 理論

理想気体が希薄なとき  
拡散係数は $M$ 依存性を持つ

$$M < 1 \text{ で } D \propto M^{-1/2}$$

$$M > 1 \text{ で } D \propto M^0$$

衝突が独立と仮定し理論構築  
(フィットパラメーター切なし)

$$D = \frac{1}{\rho \sigma^2} \sqrt{\frac{k_B T}{8\pi}} \frac{3M + 4m}{\sqrt{mM(m+M)}}$$

$\rho \leq 1$  (希薄下) で理論は  
シミュレーションとよく一致

# 理想気体中のトレーサーの短時間ダイナミクス

(名大院工) 仲井 文明, 畝山 多加志, 増淵 雄一

## 【はじめに】

溶媒中の粒子（以降トレーサー）の短時間のダイナミクスは、ガウシアンノイズを仮定した一般化ランジュバン方程式（GLE）<sup>[1]</sup>では記述できない。現状、トレーサーの短時間ダイナミクスの理解は十分ではない。トレーサーの短時間ダイナミクスを理解するために、まずは理想化した単純な系を理解する必要があると考え、本研究では周囲流体を理想気体とした。

## 【方法】

トレーサーのダイナミクスをシミュレーションで解析した。周期境界を課したボックス中にサイズ $\sigma$ のトレーサーを1個導入し、トレーサーと重ならないようにサイズ0の理想気体粒子を10万個ランダムに配置した。各粒子の初期速度はマクスウェルボルツマン分布に従うように生成した。粒子の座標と速度の時間発展は剛体シミュレーションの手法<sup>[2]</sup>に従った。トレーサーサイズ $\sigma$ 、系の温度 $k_B T$ 、理想気体粒子の質量 $m$ で規格化した。本系は、トレーサーの質量 $M$ と理想気体の数密度 $\rho$ のみがパラメータとなる。また、トレーサーと理想気体粒子のみが相互作用する。

## 【結果と考察】

$\rho$ が1より十分小さい場合、トレーサーと理想気体粒子の個々の衝突は独立になり、トレーサーのダイナミクスは比較的簡単になる。 $M$ が1より十分大きいとトレーサーの変位はガウシアンになり、トレーサーのダイナミクスはガウシアンノイズを仮定したGLEで近似的に記述できる。本研究では未知の領域である、 $M$ が1より小さい場合、 $\rho$ が1より大きい場合を対象とした。 $M$ が1より十分小さく $\rho$ が1より十分大きいと、平均二乗変位（MSD）はプラトーを示し速度の自己相関関数（VACF）は負の相関を示した。周囲流体が理想気体である系で上記の現象が生じたという報告例はない。個々の衝突が独立な場合、VACFに負の相関が生じるには次の2つが必要条件になる<sup>[3]</sup>。すなわち「 $\gamma = \langle \mathbf{V}_p \cdot \mathbf{V}_{p+1} \rangle < 0$ であること」および「衝突の時間間隔の分布 $P(\tau_p)$ が指数分布からずれること」である。ここで $\mathbf{V}_p$ はトレーサーが $p$ 回目に理想気体粒子と衝突する直前の速度、 $\tau_p$ は $p-1$ 回目と $p$ 回目の衝突時間の間隔である。本系ではパラメータによらず $\gamma$ は正になり、 $P(\tau_p)$ はおおよそ指数分布になった。よって、衝突は独立ではない。複数回の衝突の相関を見る必要があると考え、 $\gamma(n) = \langle \mathbf{V}_p \cdot \mathbf{V}_{p+n} \rangle$ という指標を新たに導入し解析した。 $M$ が1より十分小さく $\rho$ が1より十分大きいと $\gamma(n)$ は $n \geq 3$ から負になるという非自明な結果が得られた。これは、3回目以降の衝突で何かの相関が生じたことを意味する。理想気体粒子同士は相互作用しないので、存在しうる相関は「同じ理想気体粒子と衝突する事象」により生じると考えられる。 $\gamma(n)$ を1回目と $n$ 回目に同粒子、異粒子に衝突した場合に分けて解析したところ、「同粒子と衝突する事象」が $\gamma(n)$ が負になる現象を引き起こすことがわかった。

## 【結論】

理想気体中のトレーサーのダイナミクスをシミュレーションした。 $M$ が1より小さく $\rho$ が1より大きいとMSDやVACFに非自明な挙動が生じた。これは「トレーサーが同じ理想気体粒子と複数回衝突する事象」により引き起こされることがわかった。

## 【参考文献】

[1] H. Mori, Progress of Theoretical Physics 33, 423 (1965). [2] B. J. Alder, D. M. Gass, and T. E. Wainwright, Journal of Chemical Physics 53, 3813 (1970). [3] A. I. Burshtein and M. V. Krongauz, Journal of Chemical Physics 102, 2881 (1995).

# 理想気体中のトレーサーの短時間ダイナミクス

○仲井文明, 畝山多加志, 増淵雄一(名大院工)

## 1 短時間ダイナミクスを理想系で理解

流体中のトレーサーの運動は

一般化ランジュバン方程式 (GLE) で記述される

$$m \frac{d\mathbf{V}}{dt} = - \int_{-\infty}^t \Gamma(t-t') \mathbf{V}(t') dt' + \mathbf{W}(t)$$

$\mathbf{V}$ : トレーサー速度  
 $\Gamma$ : メモリカーネル  
 $\mathbf{W}$ : ガウシアンノイズ

流体分子との衝突が数回の短時間で  $\mathbf{W}$  はノンガウシアン  
 → 短時間ダイナミクスは記述できない

短時間ダイナミクスを理解したい

→ まずは単純な理想気体中で理解する

## 2 剛体シミュレーション[1]

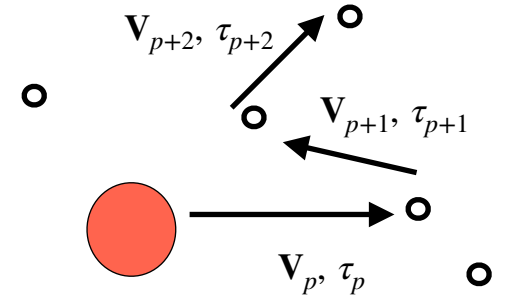
・ トレーサー 1 個  
 質量  $M$  サイズ  $\sigma$

・ 理想気体粒子 10 万個  
 数密度  $\rho$  質量  $m$  サイズ  $0$

・ 温度:  $k_B T$

$m, k_B T, \sigma$  で無次元化

パラメータは  $M, \rho$  のみ



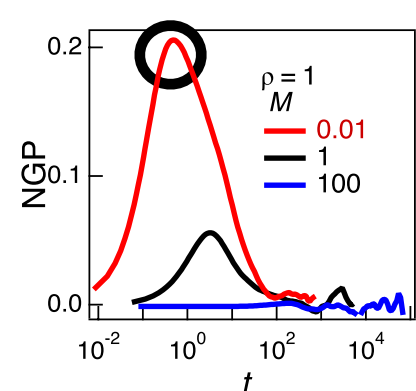
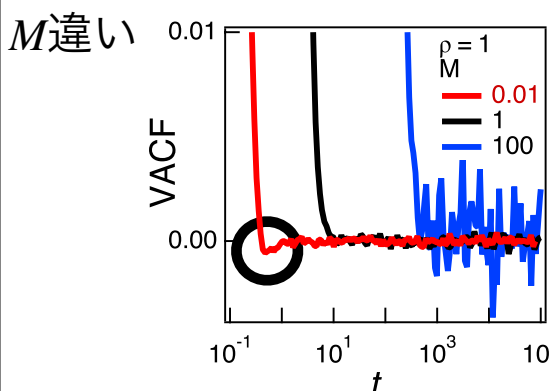
以下を取得

$p-1 \sim p$  回目の衝突時間間隔  $\tau_p$

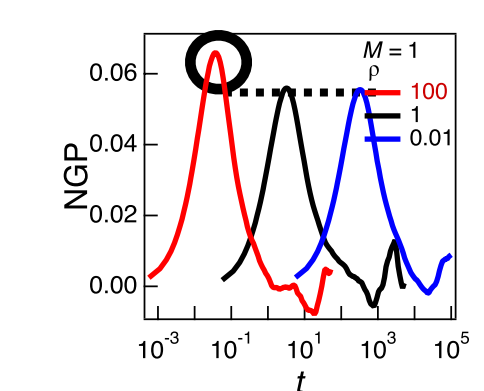
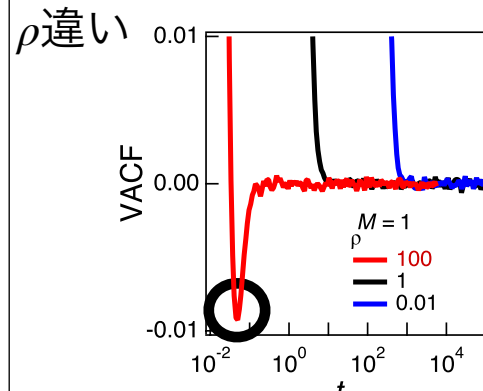
$p$  回目の衝突直前のトレーサー速度  $\mathbf{V}_p$

$p$  回目に衝突する理想気体粒子  $I_p$

## 3 速度の自己相関関数 (VACF = $\langle \mathbf{V}(t) \cdot \mathbf{V}(0) \rangle / \langle V^2(0) \rangle$ ) とノンガウシアンパラメータ (NGP = $\langle 3\Delta r^4 \rangle / \langle 5\Delta r^2 \rangle - 1$ ) [2]



$M < 1 \rightarrow$  VACF が負の相関 NGP が大きなピーク



$\rho > 1 \rightarrow$  VACF が負の相関 NGP が大きなピーク

理想気体中であるにも関わらず非自明なダイナミクスを観測

$M \leq 1, \rho \geq 1$  を調べる

## 4 トレーサーと理想気体粒子の個々の衝突は独立?

衝突が独立なとき

VACF が負の相関を持つための必要条件 [3]

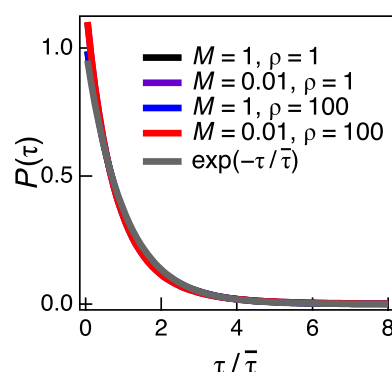
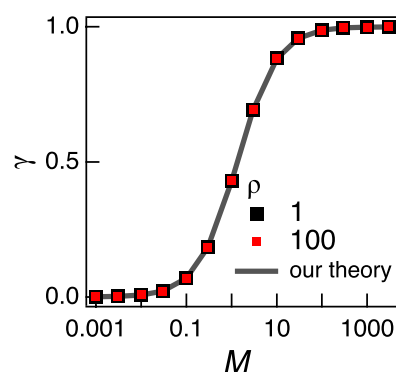
① 衝突前後の速度相関

$$\gamma = \frac{\langle \mathbf{V}_p \cdot \mathbf{V}_{p+1} \rangle_p}{\langle V_p^2 \rangle_p} \text{ が負}$$

かつ

② 衝突時間間隔分布

$P(\tau)$  が指数分布ではない



常に  $\gamma$  は正で  $P(\tau)$  は指数分布

しかし、VACF は負の相関

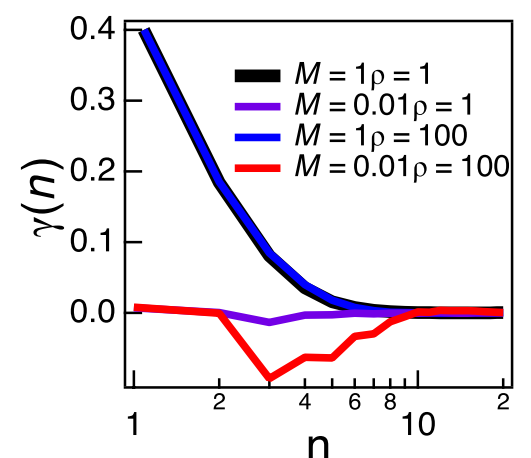
→ 理想気体中でも

個々の衝突は独立ではない

## 5 複数回の衝突で相関発生

$n$  回衝突後の相関を見たい

→  $\gamma(n) = \langle \mathbf{V}_p \cdot \mathbf{V}_{p+n} \rangle_p / \langle V_p^2 \rangle_p$  を新導入



$\gamma(n)$  は  $n \geq 3$  で負 (相関発生)

## 6 何が相関を発生させている?

理想気体中で存在しうる相関は同粒子との衝突?

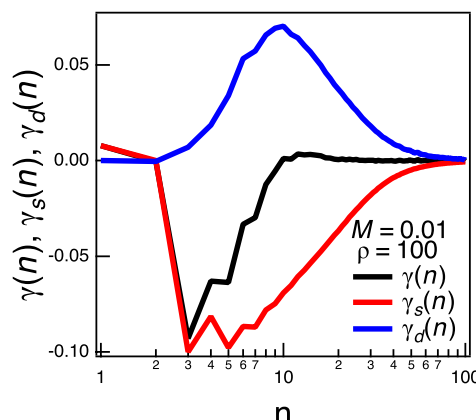
同粒子との衝突には最低 3 回の衝突が必要 →  $\gamma(n)$  の結果と辻褃合う

$\gamma(n)$  を  $n$  回目に同粒子・異粒子と衝突した場合で切り分ける

$\gamma(n)$

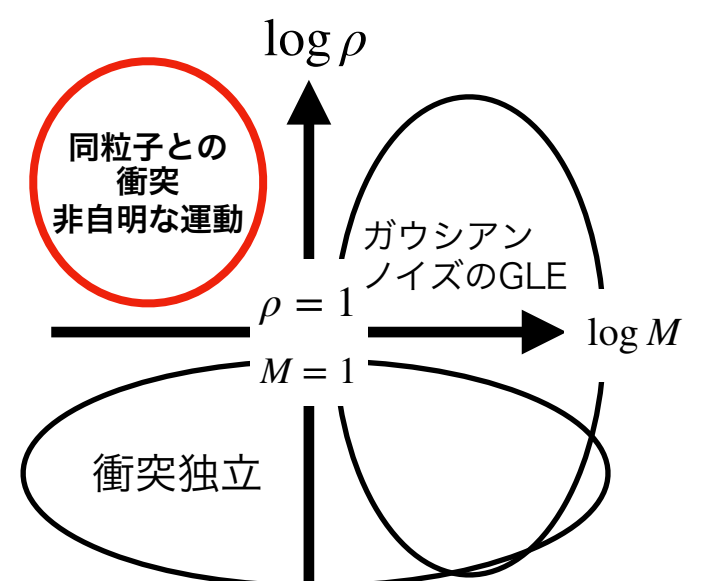
$$= \gamma_{I_{p+1}=I_{p+n}}(n) + \gamma_{I_{p+1} \neq I_{p+n}}(n)$$

$$= \gamma_s(n) + \gamma_d(n)$$



同粒子との衝突が負の相関を生み出す

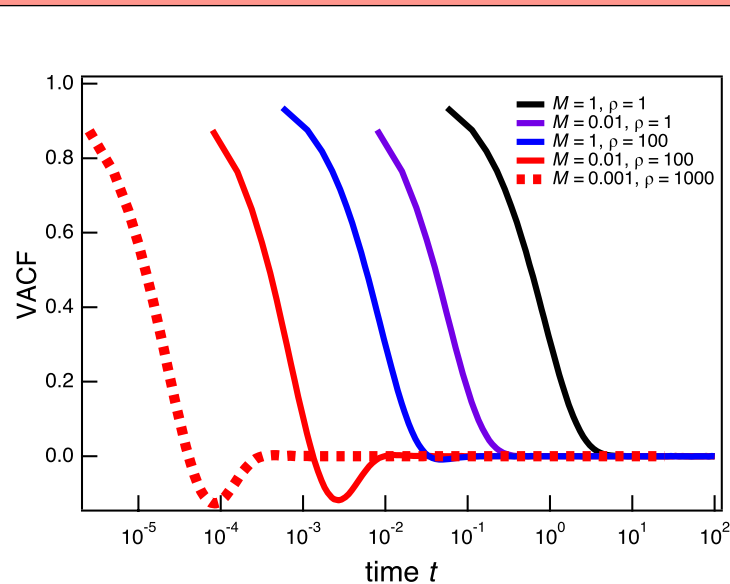
## 7 ダイナミクスの分類



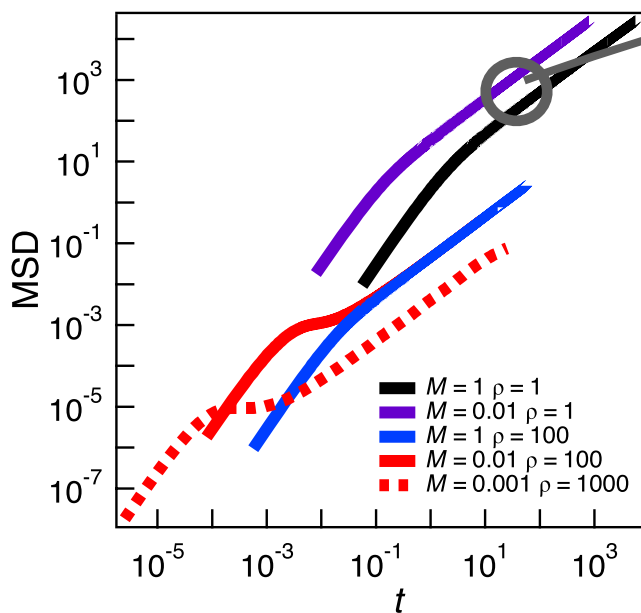
# 理想気体中のトレーサーの短時間ダイナミクス 補助資料

○仲井文明, 畝山多加志, 増淵雄一(名大院工)

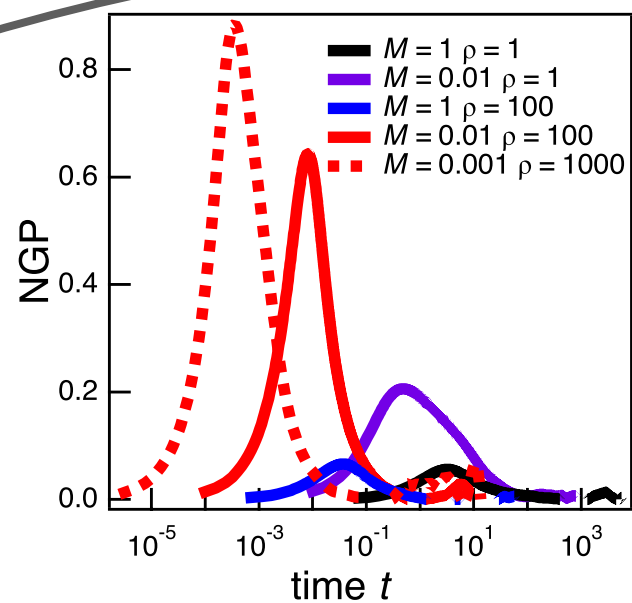
## 理想気体中のトレーサーのVACF、MSD、NGP



$M \ll 1, \rho \gg 1$ で  
負の相関



$M \ll 1, \rho \gg 1$ で  
プラトー



$M \ll 1, \rho \gg 1$ で  
大きなピーク

周囲流体が理想気体でも特定の状況下で

VACFは負の相関、MSDはプラトー、NGPは大きなピークを示す

### $\gamma = \langle \mathbf{V}_p \cdot \mathbf{V}_{p+1} \rangle / \langle V_p^2 \rangle$ の理論的導出の概要

運動量保存とエネルギー保存より  
1回の衝突で速度は次のように変化

$$\mathbf{V}_{p+1} = \mathbf{V}_p + \frac{2m}{m+M} \hat{\mathbf{r}} \cdot (\mathbf{v}_p - \mathbf{V}_p) \hat{\mathbf{r}}$$

$\mathbf{V}_p$ :  $p$ 回目衝突直前のトレーサー速度

$\mathbf{v}_p$ :  $p$ 回目衝突直前の理想気体粒子速度

$m$ : 理想気体粒子質量

$M$ : トレーサー質量

$\hat{\mathbf{r}}$ : トレーサーと衝突粒子の相対位置ベクトル

以下を考慮し $\gamma$ を計算

相対位置ベクトルの分布関数 $P_{\hat{\mathbf{r}}}(\hat{\mathbf{r}})$ : 立体角を考慮

トレーサー速度の分布関数 $P_{\mathbf{V}_p}(\mathbf{V}_p)$ : マクスウェルボルツマン分布 (MB分布)

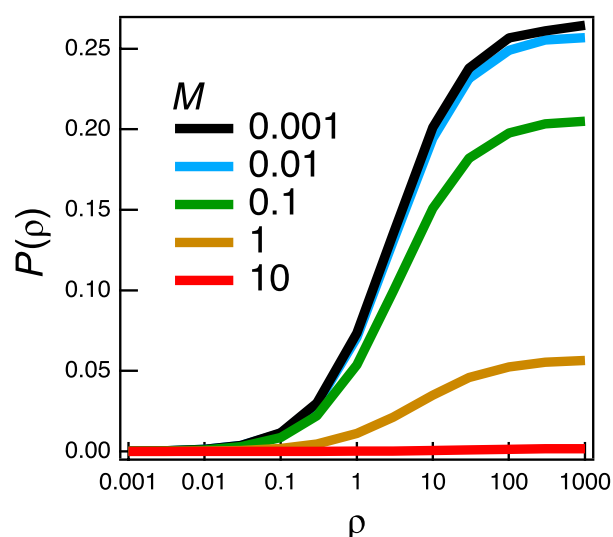
衝突する理想気体の速度の分布関数 $P_{\mathbf{v}_p}(\mathbf{v}_p)$ : MB分布に相対速度の重み付け

$$\gamma = \frac{\int d\hat{\mathbf{r}} \int d\mathbf{V}_p \int d\mathbf{v}_p (\mathbf{V}_{p+1} \cdot \mathbf{V}_p) P_{\hat{\mathbf{r}}}(\hat{\mathbf{r}}) P_{\mathbf{V}_p}(\mathbf{V}_p) P_{\mathbf{v}_p}(\mathbf{v}_p)}{\int d\hat{\mathbf{r}} \int d\mathbf{V}_p \int d\mathbf{v}_p (V_p^2) P_{\hat{\mathbf{r}}}(\hat{\mathbf{r}}) P_{\mathbf{V}_p}(\mathbf{V}_p) P_{\mathbf{v}_p}(\mathbf{v}_p)} = \frac{3M}{3M + 4m}$$

ちなみに1次元だと $\gamma = \frac{M-2m}{M+2m}$ で負になりうる

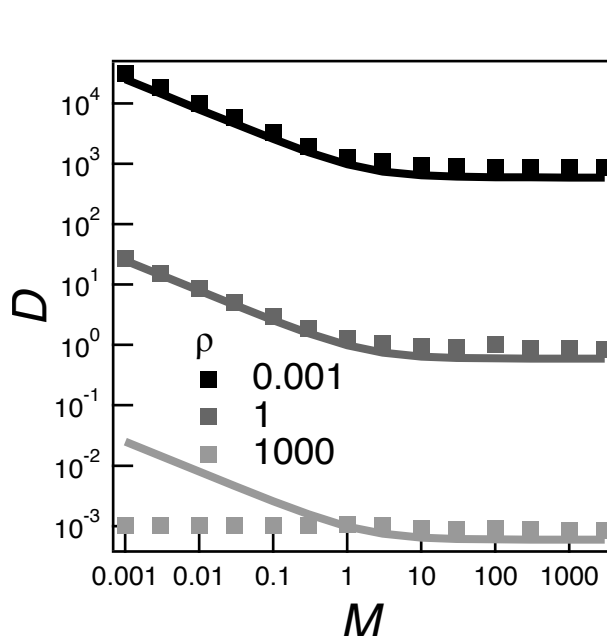
$\gamma$ は次元に強く依存する

### 同粒子との衝突確率 $P(\rho)$



$M$ が小さいほど、 $\rho$ がおおきいほど  
 $P(\rho)$ は大きい  
ただし、一定確率にさちる

### (番外) 自己拡散係数 $D$ の質量依存性



点: シミュレーション  
線: 理論

理想気体が希薄なとき  
拡散係数は $M$ 依存性を持つ

$M < 1$ で $D \propto M^{-1/2}$

$M > 1$ で $D \propto M^0$

衝突が独立と仮定し理論構築  
(フィットパラメーター切なし)

$$D = \frac{1}{\rho \sigma^2} \sqrt{\frac{k_B T}{8\pi}} \frac{3M + 4m}{\sqrt{mM(m+M)}}$$

$\rho \leq 1$  (希薄下) で理論は

シミュレーションとよく一致

# IN DILUTE FLUID, SELF DIFFUSION COEFFICIENT OF TRACER DEPENDS ON ITS MASS

Fumiaki Nakai, Takashi Uneyama and Yuichi Masubuchi  
 Graduate School of Engineering, Nagoya University, Nagoya 464-8603  
 nakai.fumiaki@b.mbox.nagoya-u.ac.jp

## Introduction

In general, the self diffusion coefficient  $D$  of the massive tracer immersed in a solvent obeys the Stokes-Einstein relation(SE)<sup>[1]</sup>. If  $D$  obeys the SE,  $D$  does not depend on the tracer mass  $M$ . However, when the tracer is not sufficiently larger than the solvent molecule, the SE can be violated. In such a case,  $D$  depends on  $M$ <sup>[2]</sup>. In the previous research<sup>[2]</sup>,  $M$  dependence of  $D$  of the tracer in a Lennard-Jones liquid was investigated. The multi-body correlation between the fluid particles induces a complex phenomenon. In our study, we consider a simple system without the multi-body correlation of the fluid particles, to reveal the tracer dynamics. We investigated the  $M$  dependence of  $D$  of the tracer in the ideal gas.

## Simulation

We employed the hard sphere simulation<sup>[3]</sup>. We put one tracer and  $10^5$  particles in the simulation box imposed periodic boundary conditions. We express the masses of the tracer and gas particles as  $M$  and  $m$ , the size of the tracer as  $\sigma$  (the ideal gas particle size is zero), the temperature of the system as  $T$ , and the number density of gas particles as  $\rho$ . Then,  $m$ ,  $k_B T$ ,  $\sigma$  are chosen as unity ( $k_B$  is the Boltzmann constant). With these dimensionless units, the system can be specified only by  $M$  and  $\rho$ . The  $M$  dependences of  $D$  of the tracer for several  $\rho$  obtained from our simulation are shown in Fig.1. For  $\rho \leq 1$ ,  $M$  dependence of  $D$  is  $D \propto M^{-1/2}$  when  $M < 1$ , whereas  $D \propto M^0$  when  $M > 1$ . Such results have not been reported in the literature. On the other hand, for  $\rho = 1000$ ,  $D$  is almost independent of  $M$ .

## Theory

To understand the nontrivial  $M$  dependence of  $D$ , we constructed a theoretical model. Burshtein analyzed the velocity autocorrelation function  $C(t)$  focusing on the collisional dynamics theoretically<sup>[4]</sup>. Following Burshtein, we assumed the successive collision events are statistically independent. The time interval distribution between successive collisions  $P(\tau)$  is given by exponential. Also, the velocity correlation before and after a collision is independent of the time interval. We express the velocity after the  $p$ -th collision as  $\mathbf{V}_p$ . We introduced  $\gamma = \langle \mathbf{V}_p \cdot \mathbf{V}_{p+1} \rangle / \langle \mathbf{V}_p^2 \rangle$  as a constant which characterizes the velocity change by a collision. From  $C(t)$ , we can calculate  $D$  by the following equation.

$$D = \frac{k_B T}{M} \int_0^\infty C(t) dt = \frac{k_B T \bar{\tau}}{M(1-\gamma)}$$

Where  $\bar{\tau}$  is the average interval between collisions. To determine the  $M$  dependence of  $D$ , we must calculate  $\bar{\tau}$  and  $\gamma$ . We theoretically calculated  $\gamma$  and  $\bar{\tau}$  by calculating statistical averages of a collision process, in which the momentum and the kinetic energy are conserved. Finally, we have following expressions for  $\gamma$ ,  $\bar{\tau}$  and  $D$ .

$$\gamma = \frac{3M}{3M+4m}, \quad \bar{\tau} = \frac{1}{\rho \sigma^2} \sqrt{\frac{2mM}{\pi k_B T (m+M)}}, \quad D = \frac{1}{\rho \sigma^2} \sqrt{\frac{k_B T}{8\pi}} \frac{3M+4m}{\sqrt{mM(m+M)}}$$

In dimensionless units,  $D$  becomes  $(3M+4)/\sqrt{8\pi\rho^2 M(1+M)}$ . The result is shown in

Fig.1 by solid curves. For  $\rho \leq 1$ , theoretical results agree almost perfectly with the simulation results. However, for  $\rho > 1$  the theoretical value does not agree with the simulation results. This inconsistency would be due to the fact that the several collisions between the tracer and the ideal gas particles are not statistically independent for  $\rho > 1$ .<sup>[5]</sup>

## Conclusion

We investigated the  $M$  dependence of  $D$  of the tracer in the ideal gas by numerical simulations and theoretical analysis. From the simulation results, we found the nontrivial  $M$  dependence of  $D$  for  $\rho < 1$ . We developed theory which can explain the nontrivial  $M$  dependence of  $D$  for  $\rho \leq 1$  obtained by the simulation.

## References:

1. J.-P. Hansen and I. R. McDonald, Theory of Simple Liquids, (Academic, London, 1986).
2. F. Ould-Kaddour and D. Levesque, Physical Review E **63**, 9, 011205 (2001).
3. B. J. Alder, D. M. Gass, and T. E. Wainwright, Journal of Chemical Physics **53**, 3813 (1970).
4. A. I. Burshtein and M. V. Krongauz, Journal of Chemical Physics **102**, 2881 (1995).
5. F. Nakai, T. Uneyama and Y. Masubuchi, Soft matter kenkyukai, poster, P10 (2019)

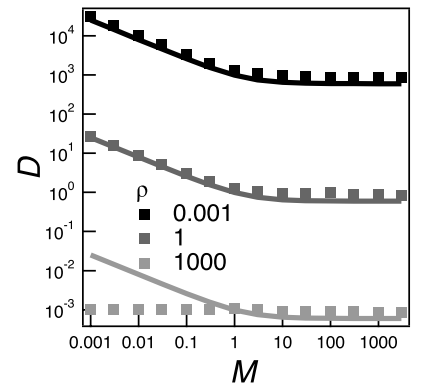
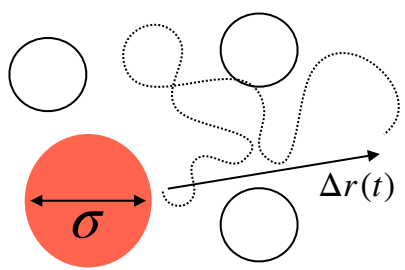


Fig.1  $M$  dependence of  $D$  of tracer in ideal gas for several  $\rho$ . Dots and Lines show the simulation and theoretical results.

# IN DILUTE GAS, THE DIFFUSION COEFFICIENT OF TRACER DEPENDS ON ITS MASS

○ F. Nakai, T. Uneyama and Y. Masubuchi (Nagoya university)

## 1 Mass depends on diffusion constant $D$



Stokes-Einstein relation(SE)

$$\langle \Delta \mathbf{r}^2(t) \rangle = 6Dt$$

$$D = \frac{k_B T}{3\pi\eta\sigma}$$

When tracer is not sufficiently large,

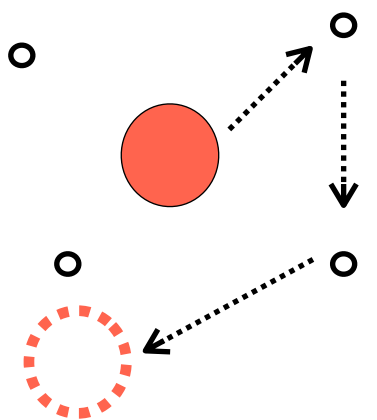
$D$  depends on tracer mass  $M$  nontrivially<sup>[1]</sup>

We want to know nontrivial  $M$  dependence of  $D$

Consider simple system

Tackle by simulation and theory

## 2 Target: Tracer diffusion in ideal gas



Ideal gas mass	$m$	Unit
Tracer size	$\sigma$	
Temperature	$T$	Only 2 Parameters
Tracer mass	$M$	
Number density	$\rho$	
Ideal gas size	$0$	

Investigate  $M$  dependence of  $D$  by changing  $\rho$

## 3 Hard sphere simulation<sup>[2]</sup>

$D$  is calculated from  $\langle \Delta r^2(t) \rangle$

Points

- For  $\rho \leq 1$ ,  $D$  depends on  $M$
- For  $\rho > 1$ ,  $D$  do not depends on  $M$

## 4 Theory based on stochastic collision dynamics

Tracer velocity autocorrelation function derived by Burshtein

$$\langle \mathbf{V}(t) \cdot \mathbf{V}(0) \rangle = \frac{3k_B T}{M} \exp\left(-\frac{1-\gamma}{\bar{\tau}} t\right) \quad \gamma, \bar{\tau} : \text{constant}$$

Assumption

1 Velocity after collision depend only on one before collision

$$\int d\mathbf{V}_{p+1} \mathbf{V}_{p+1} P(\mathbf{V}_{p+1} | \mathbf{V}_p) = \gamma \mathbf{V}_p \quad \mathbf{V}_p : \text{Velocity just before } p\text{-th collision}$$

2 Distribution of collision time interval is exponential

$$P(\tau) = \bar{\tau} \exp(-\tau/\bar{\tau}) \quad \tau : \text{Collision time interval}$$

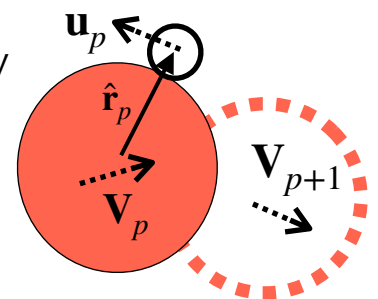
$D$  derived from Green-Kubo formula

$$D = \frac{1}{3} \int_0^\infty \langle \mathbf{V}(t) \cdot \mathbf{V}(0) \rangle dt = \frac{\bar{\tau} k_B T}{M(1-\gamma)} \quad \dots(1)$$

Analyze  $\gamma$  and  $\bar{\tau}$  by considering distribution of  $\mathbf{V}_p$ ,  $\mathbf{u}_p$  and  $\hat{\mathbf{r}}_p$

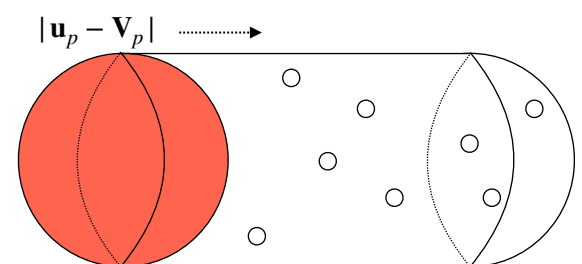
From conservation of momentum and energy

$$\gamma = \langle \mathbf{V}_p \cdot \mathbf{V}_{p+1} \rangle / \langle \mathbf{V}_p^2 \rangle = \frac{3M}{3M+4m} \quad \dots(2)$$



Consider collision frequency

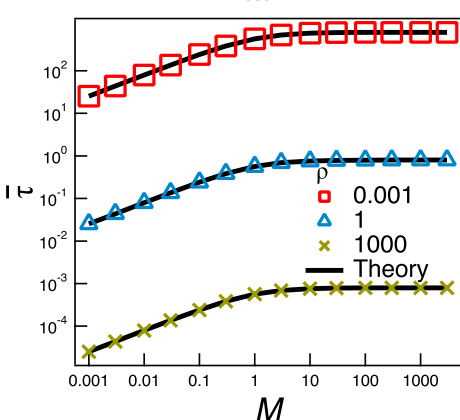
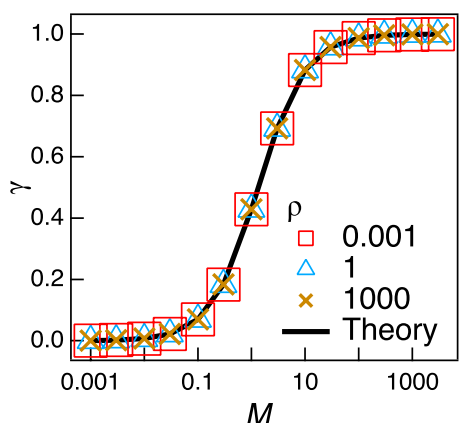
$$\frac{1}{\bar{\tau}} = \rho \sigma^2 \sqrt{\frac{\pi k_B T (m+M)}{2mM}} \quad \dots(3)$$



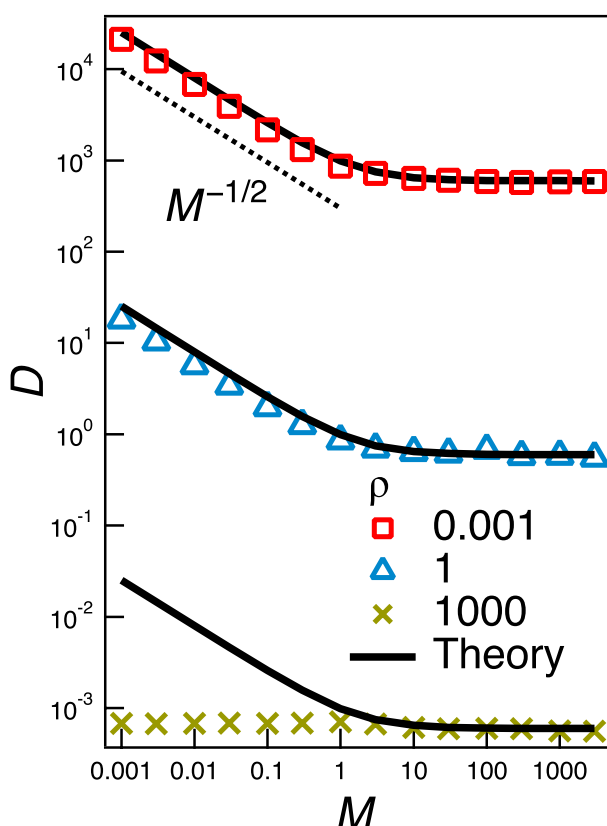
From equations (1),(2),(3)

$$D = \frac{1}{\rho \sigma^2} \sqrt{\frac{k_B T}{8\pi}} \frac{3M+4m}{\sqrt{mM(m+M)}}$$

## 5 Compare our theory with simulation results



Theory perfectly reproduces  $\gamma$  and  $\bar{\tau}$  from simulation



For  $M \leq 1$  and  $\rho \leq 1$ ,  $D$  depends on  $M$ . We clarified this mechanism

For  $\rho \leq 1$

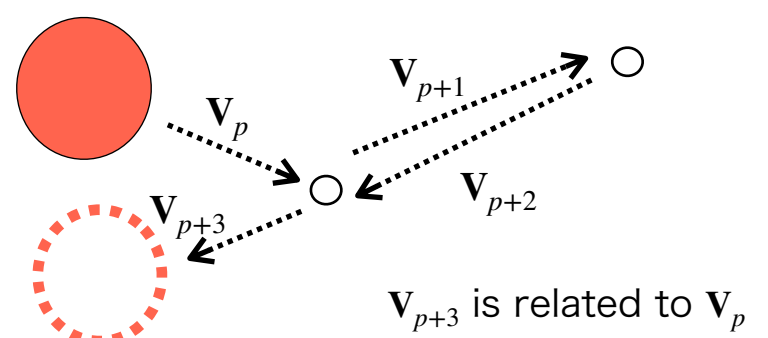
Theory reproduces  $D$  from simulation

For  $\rho > 1$

Theory does not reproduce  $D$  from simulation

Several collisions have correlation attributed to collisions with same ideal gas particles<sup>[4]</sup>

→ Assumption 1 is not correct for  $\rho > 1$



[1] J. Ould-Kaddour and D. Levesque, Physical Review E **63**, 9, 011205 (2001). [2] B. J. Alder, D. M. Gass, and T. E. Wainwright, Journal of Chemical Physics **53**, 3813 (1970).

[3] A. I. Burshtein and M. V. Krongauz, Journal of Chemical Physics **102**, 2881 (1995). [4] F. Nakai, T. Uneyama and Y. Masubuchi, Bunshi simulation gakkai, Oral 304S and Poster 114P

# 任意次元における理想気体中の粒子の衝突による速度変化

(名大院工) ○仲井 文明, 土肥侑也, 畝山多加志, 増淵 雄一

## Velocity change due to collision of tracer in ideal gas in arbitrary dimension

F. Nakai, Y. Doi, T. Uneyama, and Y. Masubuchi

Graduate School of Engineering, Nagoya University

### ABSTRACT

We studied the velocity change of a tracer particle due to the single collision with an ideal gas particle by using the kinetic theory in arbitrary dimensions. We calculated the correlation of the tracer velocity before and after a collision event,  $\gamma_1$ . We analytically calculated  $\gamma_1$  and obtained the explicit expression in terms of the mass and the dimensions. Our analytical expression shows that  $\gamma_1$  depends on the dimensions rather strongly.

### 1. 緒言

流体中に粒子 (以降トレーサーと呼ぶ) を浮かべると, トレーサーは流体分子の衝突に駆動されてランダムに運動する (ブラウン運動). このようなランダムな運動はランジュバン方程式という形で確率微分方程式を用いて記述されることが多い. ランジュバン方程式はさまざまな系に広く適用されているが, その適用範囲には限界がある. ランジュバン方程式では周囲の流体分子の多数回の衝突を粗視化して扱っているため, 衝突が数えられる程度の回数しか生じないような短時間領域の運動に対しては使えない. 例えば, Yamaguchi と Kimura は [1] は希薄気体中のトレーサーの運動をシミュレーションで解析しており, 短時間領域でトレーサーの変位分布が非ガウスのになり, トレーサーの運動がランジュバン方程式で書けないことを示している.

流体中の粒子の短時間の運動を記述するには, 運動の素過程である「トレーサーと流体分子の衝突」に立ち返る必要がある. 以降, 簡単化のために, トレーサーと流体分子の衝突を厳密に定義できる剛体球モデルを考える. 剛体球流体中のトレーサーの運動は, 衝突時間間隔と流体分子との衝突による速度変化で完全に決まる. 剛体球流体中のトレーサーの運動を理論的に解析したものとして, Burshtein と

Krongauz の研究 [2] がある. 彼らは, トレーサーに対する衝突時間間隔と速度変化に単純な確率分布を仮定し, さらにこれらが独立であるとしてトレーサーの速度の時間相関関数を導き, 速度相関が負になりうることを示している. しかし, 彼らのモデルでは使用している衝突パラメータと個々の剛体球同士の衝突の関係に関しては言及されていない. 本研究では, 任意の空間次元におけるトレーサーの速度相関関数を衝突の統計に基づいて詳細に調べる.

### 2. 衝突の統計

我々は最近, 流体中のトレーサー粒子の衝突の統計を理解するために, 理想気体に浮かべたトレーサーの運動を 3 次元の剛体シミュレーションで解析した [3]. この系は, 理想気体分子の質量  $m$  とトレーサーのサイズ  $\sigma$  と各自由度の運動エネルギーの平均  $k_B T$  で無次元化すると, トレーサーの質量  $M^*$  と理想気体の数密度  $\rho^*$  だけで特徴付けられる簡単な系である.

トレーサーと流体分子の衝突を解析するため, 我々は複数回の衝突が生じた後の速度相関の指標

$$\gamma_n = \langle \mathbf{V}_0 \cdot \mathbf{V}_n \rangle_{\text{coll}} / \langle \mathbf{V}_0^2 \rangle_{\text{coll}} \quad (1)$$

を導入して解析を行った. ここで,  $\mathbf{V}_0, \mathbf{V}_n$  は衝突前と  $n$  回衝突後のトレーサーの速度を,  $\langle \dots \rangle_{\text{coll}}$  は, 衝突における統計平均を表している. シミュレーションの結果,  $M^*$  が十分小さく  $\rho^*$  が十分大きいときに,  $\gamma_1$  は指数関数的に減少しないことから, 衝突が相関することが分かった. 一方で,  $\gamma_1$  (1 回の衝突前後の速度相関) は  $\rho$  に依存せず,  $M^*$  が十分小さい場合は 0 に漸近し,  $M^*$  が十分大きい場合は 1 に漸近することが分かった. また,  $\gamma_1$  のシミュレーション結果は気体分子運動論に基づく解析とも整合した.

しかし, この  $\gamma_1$  の結果は直感的予測とは必ずしも合致しない. トレーサーの質量  $M^*$  が小さいと, トレーサーの平均速度はマクスウェル・ボルツマン分布に従い大きくなるために, 流体分子と正面衝突す

る確率が大きくなる．また， $M^*$  が小さいと1回の衝突でトレーサーの速度ベクトルは容易に異なる方向へと変化する．その結果として，トレーサーの速度は流体分子との1回の衝突で逆向きになる（すなわち  $\gamma_1 < 0$  となる）ように思われる．これは先ほど述べたシミュレーションと理論の結果と一致しない．

このようなことが起こる原因として，速度相関が空間次元に依存していることが考えられる．本研究では  $\gamma_1$  の理論解析を任意の次元で実施することで，3次元で  $\gamma_1$  が負にならない原因を突き止める．任意の次元における衝突の統計の理論解析は，衝突時間間隔の分布についてはなされている [4] が， $\gamma_1$  のような速度変化の指標については実施されていない．

### 3. 気体分子運動論による解析

物理を明確にするため，ここでは無次元化を行わずに解析を実行する．平衡状態において，質量  $m$  でサイズが0の質点により構成される  $N$  次元空間の理想気体粒子中に，質量  $M$  でサイズが  $\sigma$  のトレーサーを導入した系を考える．トレーサーが速度  $\mathbf{V}_0$  で運動しているときに，理想気体分子が速度  $\mathbf{v}_0$  で衝突すると， $N$  次元においてトレーサーの速度は次のように変化する．

$$\mathbf{V}_1 = \mathbf{V}_0 + \frac{2m}{m+M} (\mathbf{v}_0 - \mathbf{V}_0) \cdot \hat{\mathbf{r}} \hat{\mathbf{r}} \quad (2)$$

ここで， $\hat{\mathbf{r}}$  は，衝突時におけるトレーサー粒子と理想気体分子の中心間を結ぶベクトルである．両辺から  $\mathbf{V}_0$  を内積して衝突に関する統計平均を考えると次式を得る．

$$\begin{aligned} \langle \mathbf{V}_1 \cdot \mathbf{V}_0 \rangle_{\text{coll}} &= \mathcal{N}^{-1} \int d\mathbf{V}_0 \int d\mathbf{v}_0 \int d\hat{\mathbf{r}} |\mathbf{v}_0 - \mathbf{V}_0| \\ &\times P_{MB}(M, \mathbf{V}_0) P_{MB}(m, \mathbf{v}_0) P_{\hat{\mathbf{r}}}(\hat{\mathbf{r}}) \\ &\times \left( \mathbf{V}_0 + \frac{2m}{m+M} (\mathbf{v}_0 - \mathbf{V}_0) \cdot \hat{\mathbf{r}} \hat{\mathbf{r}} \right) \cdot \mathbf{V}_0 \quad (3) \end{aligned}$$

ここで， $\mathcal{N}$  は確率の規格化因子， $P_{MB}(M, \mathbf{V}_0)$ ， $P_{MB}(m, \mathbf{v}_0)$  はマクスウェル・ボルツマンの速度分布， $P_{\hat{\mathbf{r}}}(\hat{\mathbf{r}})$  は  $\hat{\mathbf{r}}$  の分布を表す．両辺を  $\langle \mathbf{V}_0^2 \rangle_{\text{coll}}$  で割って計算を進めると，次の  $\gamma_1$  を得る．

$$\gamma_1 = \frac{NM + (N-3)m}{NM + (N+1)m} = \frac{NM^* + (N-3)}{NM^* + (N+1)} \quad (4)$$

$\gamma_1$  は無次元化したトレーサーの質量  $M^*$  と次元  $N$  に依存していることが分かる． $N=3$  のとき，式 (4) は我々の以前の解析結果 [3] と一致する．

### 4. 結果及び考察

各次元  $N$  における  $\gamma_1$  の  $M$  依存性を図1に示す．次元によらずに， $M$  の増大に伴い  $\gamma_1$  は単調に増大し

1に漸近することが分かる．これは，トレーサーの質量  $M$  が大きいときは，1回の理想気体分子との衝突で速度が殆ど変化しないことを表している．一方で， $M$  が1より小さい領域においては  $\gamma_1$  は次元によって異なる振る舞いを示している．すなわち， $N=1$  のときは  $\gamma_1$  は  $-1$  に漸近し，次元の増大に伴い  $\gamma_1$  は増大し， $N$  が十分大きい場合には1に近づくことが分かる．このような次元依存性は，式 (3) において  $M \rightarrow 0$  とすることで解析できる．次元依存性は衝突時のトレーサーと流体分子の中心間を結ぶ単位ベクトルの分布  $\hat{\mathbf{r}}$  の影響に依るものであることを示すことができる．すなわち， $M \rightarrow 0$  における  $N$  の増加に伴う  $\gamma_1$  の増加は， $N$  の増大に伴いトレーサーが理想気体分子と擦るように衝突する確率が大きくなり，その結果として衝突時に跳ね返される確率が減少するために生じると解釈できる．

### 5. 結論

任意の次元でトレーサー粒子の  $\gamma_1$  を理論的に導出した．3次元で  $\gamma_1$  が負にならない要因は，次元の増大に伴いトレーサーと気体粒子が擦るような形での衝突の寄与が増えることであると明らかとなった．

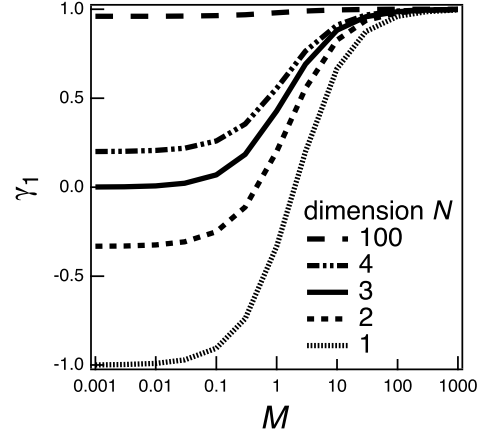


Fig.1 Mass  $M$  dependence of velocity correlation before and after collision,  $\gamma_1$ , for various dimensions  $N$ .

### 参考文献

- [1] T Yamaguchi and Y Kimura. *The Journal of Chemical Physics*, 114(7):3029–3034, 2001.
- [2] AI Burshtein and MV Krongauz. *The Journal of Chemical Physics*, 102(7):2881–2887, 1995.
- [3] F Nakai, Y Masubuchi, and T Uneyama. *Physical Review E (to appear)*, 2020.
- [4] L Lue. *The Journal of Chemical Physics*, 122(4):044513, 2005.

# 任意次元における理想気体中の粒子の衝突による速度変化

○仲井文明, 土肥侑也, 畝山多加志, 増淵雄一(名大院工)

## 1 背景：流体中のトレーサー粒子の短時間運動の複雑さ

ランジュバン方程式によるブラウン運動の記述

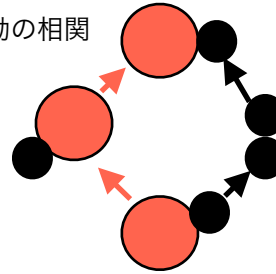
流体分子同士の相互作用で難解な相関が生じる[2]

$$m\dot{\mathbf{V}}(t) = -\eta\mathbf{V}(t) + \mathbf{W}(t)$$

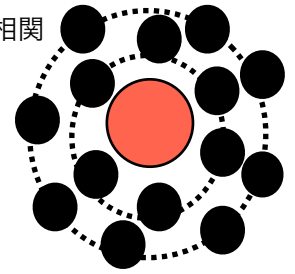
$m$  : トレーサー質量  $\mathbf{V}$  : 速度  
 $\eta$  : 粘性抵抗  $\mathbf{W}$  : ガウシアンノイズ

$\mathbf{W}$ は分子衝突が数回程度の時間領域でノンガウシアン  
 →ランジュバン方程式は短時間領域で使えない[1]

運動の相関



構造の相関



→まず簡単な系でトレーサーの短時間運動を理解する

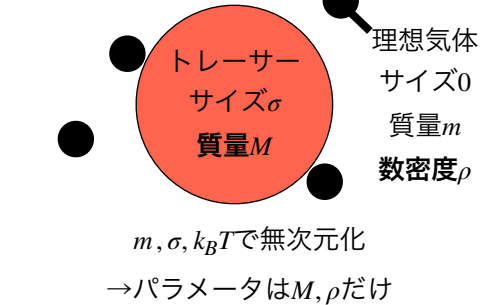
## 2 これまでの研究：理想気体中のトレーサーの短時間運動の衝突に着目した解析[3]

対象：理想気体中のトレーサー

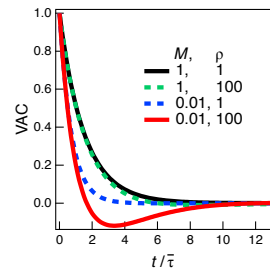
速度の時間相関関数(VAC)

速度相関の衝突回数依存性

運動エネルギー平均 $k_B T$



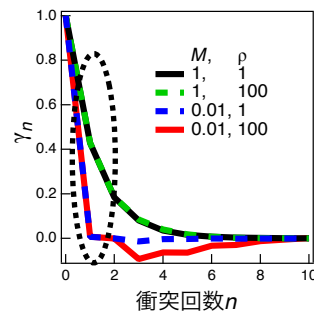
$$\langle \mathbf{V}(t/\bar{\tau}) \cdot \mathbf{V}(0) \rangle / \langle \mathbf{V}^2 \rangle$$



$M \ll 1, \rho \gg 1$ で負相関

衝突に着目

$$\gamma_n = \langle \mathbf{V}_n \cdot \mathbf{V}_0 \rangle_{coll} / \langle \mathbf{V}^2 \rangle_{coll}$$



3回以上の衝突を経て負相関

1回の衝突で負相関は出ない

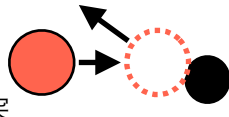
## 3 目的：1回の衝突 $\gamma_1$ の理解

3次元で $\gamma_1$ は常に正だが直感的には奇妙

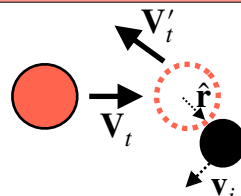
質量が小さいと

- ・速さが大きいので正面衝突
- ・1回の衝突で運動量が容易に変化
- 1回の衝突で速度の負相関が起きそう

しかし実際は1回の衝突で負相関は生じない  
 なぜ？



## 4 理論解析：N次元で $\gamma_1$ を計算



$$\begin{aligned} \gamma_1 &= \int \text{衝突頻度} \times \text{衝突前後の速度の内積} / \text{規格化因子} \\ &= \frac{\int d\hat{\mathbf{r}} \int d\mathbf{V}_t \int d\mathbf{v}_g P_d(\hat{\mathbf{r}}) P_t(\mathbf{V}_t) P_g(\mathbf{v}_g) |\mathbf{V}_t - \mathbf{v}_g| (\mathbf{V}_t \cdot \mathbf{V}_t')}{\int d\hat{\mathbf{r}} \int d\mathbf{V}_t \int d\mathbf{v}_g P_d(\hat{\mathbf{r}}) P_t(\mathbf{V}_t) P_g(\mathbf{v}_g) (\mathbf{V}_t^2)} \\ &= \frac{NM + N - 3}{NM + N + 1} \end{aligned}$$

$P_t(\mathbf{V}_t), P_g(\mathbf{v}_g)$  : マクスウェル分布  
 $P_d(\hat{\mathbf{r}})$  : 衝突角度分布

$\gamma_1$ の質量 $M$ と次元 $N$ の依存性を解析できた

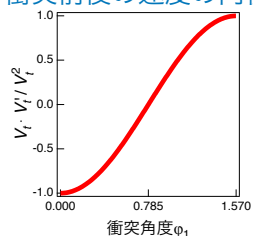
$M \rightarrow 0$ のとき $\gamma_1$ は1、2次元では負、3次元以上で正となる

## 5 考察： $M \ll 1$ 領域の衝突角度 $\phi_1$ に着目した解析

$$\gamma_1 = \lim_{M \rightarrow 0} \gamma_1 = \lim_{M \rightarrow 0} \frac{\int d\hat{\mathbf{r}} \int d\mathbf{V}_t \int d\mathbf{v}_g P_d(\hat{\mathbf{r}}) P_t(\mathbf{V}_t) P_g(\mathbf{v}_g) |\mathbf{V}_t - \mathbf{v}_g| \mathbf{V}_t \cdot \mathbf{V}_t'}{\int d\hat{\mathbf{r}} \int d\mathbf{V}_t \int d\mathbf{v}_g P_d(\hat{\mathbf{r}}) P_t(\mathbf{V}_t) P_g(\mathbf{v}_g) |\mathbf{V}_t - \mathbf{v}_g| \mathbf{V}_t^2}$$

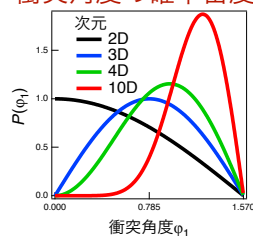
$$= \int P_t(\hat{\mathbf{r}}) d\hat{\mathbf{r}} (1 - 2 \cos^2 \phi_1) = \int (N-1) \cos \phi_1 \sin^{N-2} \phi_1 d\phi_1 (1 - 2 \cos^2 \phi_1)$$

衝突前後の速度の内積



次元によらず $\phi_1 > \pi/2$ で正  
 高角側で掠る

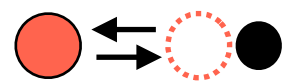
衝突角度の確率密度



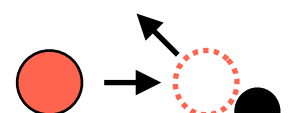
次元の増大に伴い高角側の  
 掠り衝突が増加

## 6 結論：問題の原因は掠る衝突

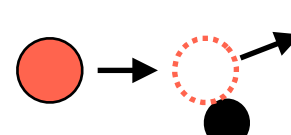
1次元



2次元



3次元



次元の増大に伴い掠る衝突増加  
 →次元が3以上で $\gamma_1$ は非負

**1.1 はじめに** 流体中の小さな粒子(以降トレーサーとする)はブラウン運動する。ブラウン運動はランジュバン方程式で記述されることが多いが適用範囲に限界がある。例えば, トレーサーと流体分子の衝突が十分な回数生じない短い時間スケールでは, ランジュバン方程式は使えない [1, 2]. そのような短い時間スケールの運動を議論するには, トレーサーと流体分子の衝突をあらわに考える必要がある。以降, 簡単化のために剛体球系を考える。流体が希薄であれば, トレーサーの運動は Enskog 理論 [3] でよく記述できる。一方で, 流体が希薄でない場合には, 流体分子同士の相互作用の影響で複雑な動的相関が生じるため Enskog 理論は使えない。

**1.2 衝突の統計** そのような複雑なトレーサーの運動を理解するために, まずは流体分子同士の相互作用がない簡単な系を理解する必要があると考えて, 我々は最近, 理想気体中のトレーサーの短時間運動を解析した [4]. トレーサーの速度の時間相関関数は, トレーサーの質量が小さく理想気体の数密度が大きい場合に短時間領域で負値を示すことが分かった。速度の衝突回数に対する相関を解析する以下の指標を導入した。

$$\gamma(n) = \langle \mathbf{V}_0 \cdot \mathbf{V}_n \rangle_{coll} / \langle \mathbf{V}_0^2 \rangle_{coll} \quad (1)$$

$\mathbf{V}_i$  は  $i$  回衝突後のトレーサーの速度,  $\langle \dots \rangle_{coll}$  は衝突頻度を考慮した統計平均である。  $\gamma(n)$  の解析により, トレーサーの速度の負相関は, 1 回の衝突ではなく, 3 回以上の衝突を経て同一の理想気体粒子と衝突することに起因することを見出した。

**1.3 一回の衝突** 3次元系において, 一回の衝突で軽いトレーサーの速度に負相関が生じない結果は直感とずれている。平衡状態では粒子の平均の速さは質量の  $1/2$  乗に反比例するために, 軽いトレーサーは高速で運動して理想気体粒子と進行方向から衝突する頻度が増加する。また, 軽いトレーサーは一回の衝突で容易に進行方向が変わる。結果として, 一回の衝突でトレーサーの速度の負相関が生じると安直には期待できるが, シミュレーション結果とは食い違う。本発表では,  $\gamma(1)$  が3次元で負にならない原因を任意次元の解析を以て示す。

**2.1 シミュレーションの方法** 周期境界を課した  $N$  次元のボックス中に, 質量  $M \cdot$  サイズ  $\sigma$  のトレーサーを1つと質量  $m \cdot$  サイズ  $0$  の理想気体分子 10 万個を導入し, 剛体シミュレーションを実施した。理想気体の数密度は  $\rho$  で各自由度ごとの平均エネルギーは  $k_B T$  である。ここで,  $\sigma, m, k_B T$  によって無次元化するとパラメータは  $N, M^*, \rho^*$  の3つになる。トレーサーと理想気体の相互作用は剛体的で, 衝突時に速度が瞬時に入れ替わる。一方で, 理想気体同士は相互作用しない。

**2.2 シミュレーションの結果** 1, 2, 3, 4 次元における  $\gamma(1)$  の  $M^*$  依存性を図 1 にシンボルで示した。  $\rho^* = 0.01$  としたが,  $\gamma(1)$  は  $\rho^*$  に依存しないことを確認している。  $M^* \gg 1$  の場合に,  $\gamma(1)$  は  $N$  によらずに 1 に漸近することが分かる。また,  $M^* \ll 1$  の場合には,  $\gamma(1)$  は 1 次元で  $-1$  になり, 次元の増大とともに増加し 3 次元を境に負から正に切り替わることが分かる。

**3.1  $\gamma(1)$  の理論解析** 理想気体粒子と一回衝突するとトレーサー

の速度は次のように変化する。

$$\mathbf{V}_1 = \mathbf{V}_0 + \frac{2}{1 + M^*} (\mathbf{v}_0 - \mathbf{V}_0) \cdot \hat{\mathbf{r}} \hat{\mathbf{r}} \quad (2)$$

$\mathbf{v}_0$  は衝突する理想気体粒子の速度,  $\hat{\mathbf{r}}$  は衝突時のトレーサーと理想気体粒子の中心間の単位ベクトルである。  $\mathbf{V}_0, \mathbf{v}_0, \hat{\mathbf{r}}$  で衝突する確率密度  $P(\mathbf{V}_0, \mathbf{v}_0, \hat{\mathbf{r}})$  は衝突頻度を考慮して次式で表される。

$$P(\mathbf{V}_0, \mathbf{v}_0, \hat{\mathbf{r}}) = \mathcal{N} |\mathbf{V}_0 - \mathbf{v}_0| P_B(M, \mathbf{V}_0) P_B(m, \mathbf{v}_0) P_d(\hat{\mathbf{r}}) \quad (3)$$

$P_B(M, \mathbf{V}_0)$  はボルツマン分布,  $P_d(\hat{\mathbf{r}})$  は  $\hat{\mathbf{r}}$  の確率密度,  $\mathcal{N}$  は規格化因子である。  $\gamma(1)$  は,  $\mathbf{V}_1$  と  $\mathbf{V}_0$  の内積に  $P(\mathbf{V}_0, \mathbf{v}_0, \hat{\mathbf{r}})$  を乗じて統計平均をとることで次のように得られた。

$$\begin{aligned} \gamma(1) &= \frac{\int d\mathbf{V}_0 \int d\mathbf{v}_0 \int d\hat{\mathbf{r}} P(\mathbf{V}_0, \mathbf{v}_0, \hat{\mathbf{r}}) \mathbf{V}_1 \cdot \mathbf{V}_0}{\int d\mathbf{V}_0 \int d\mathbf{v}_0 \int d\hat{\mathbf{r}} P(\mathbf{V}_0, \mathbf{v}_0, \hat{\mathbf{r}}) \mathbf{V}_0^2} \\ &= \frac{NM^* + (N - 3)}{NM^* + (N + 1)} \end{aligned} \quad (4)$$

得られた  $\gamma(1)$  の  $M$  依存性を 1, 2, 3, 4, 10 次元に対して図 1 に実線でプロットした。理論はシミュレーションを良好に再現した。

**3.2  $M^* \ll 1$  の場合の考察** さらに,  $M^* \ll 1$  の場合,  $\gamma(1)$  の次元依存性は  $\hat{\mathbf{r}}$  の次元依存性のみを反映していることが分かった。すなわち, 次元の増大に伴い, 掠めるような衝突の頻度が増加することにより一回の衝突で速度の負相関が生じにくくなる。3次元では, 掠めて進行方向に散乱する割合と逆方向に散乱する割合が等しくなるために  $\gamma(1) \simeq 0$  になる。

**4 結論** 3次元で  $\gamma(1)$  が負にならない要因は掠める衝突の寄与に依る。

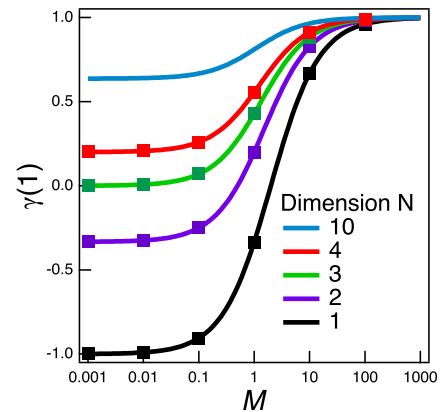


Fig.1  $M$  dependences of  $\gamma(1)$  in various spatial dimensions. Symbols and curves represent simulation and theoretical results.

- [1] A Rahman. *Phys. Rev.*, 136(2A):405–411, 1964.
- [2] T Yamaguchi and Y Kimura. *The Journal of Chemical Physics*, 114(7):3029–3034, 2001.
- [3] S Chapman, T G Cowling, and D Burnett. Cambridge university press, 1990.
- [4] F Nakai, Y Masubuchi, and T Uneyama. *Phys. Rev. E*, 102:032104, Sep 2020.

## 1 背景：流体中の粒子（トレーサー）の短時間運動の複雑さ

ランジュバン方程式による粒子運動の記述

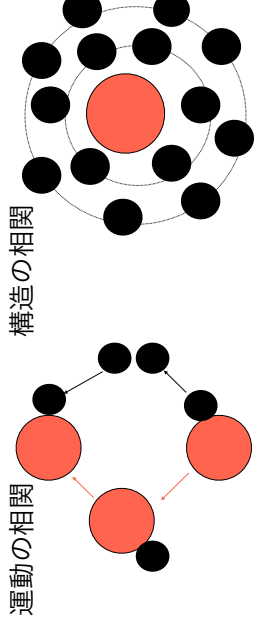
$$m\dot{\mathbf{V}}(t) = -\eta\mathbf{V}(t) + \mathbf{W}(t)$$

$m$ : トレーサー質量  $\mathbf{V}$ : 速度

$\eta$ : 粘性抵抗  $\mathbf{W}$ : ガウシアンノイズ

$\mathbf{W}$ は分子衝突が数回程度の時間領域で非ガウシアン  
→ランジュバン方程式は短時間領域で使えない[1-2]

流体分子同士の相互作用が複雑に影響[3]

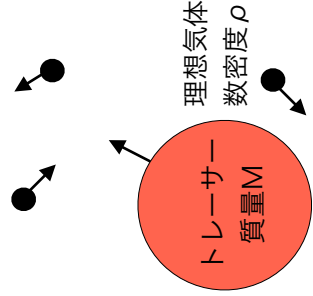


まず簡単な系でトレーサーの短時間運動を理解する

## 2 これまでの研究：理想気体中のトレーサーの運動の解析[4]

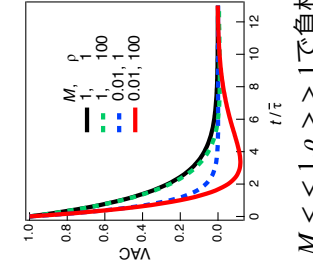
対象

理想気体中のトレーサー



速度の時間相関関数(VAC)

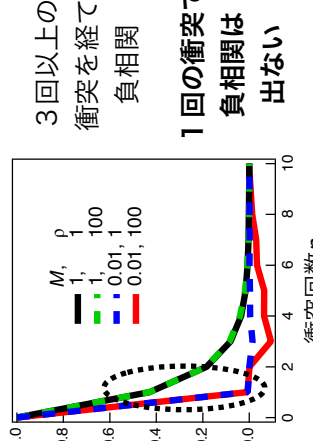
$$\langle \mathbf{V}(t/\tau) \cdot \mathbf{V}(0) \rangle / \langle V^2 \rangle$$



$M < 1, \rho > 1$  で負相関

速度相関の衝突回数依存性

$$\gamma_n = \langle \mathbf{V}_n \cdot \mathbf{V}_0 \rangle_{coll} / \langle V^2 \rangle_{coll}$$



衝突に着目



3回以上の衝突を経て負相関  
1回の衝突は負相関は出ない

## 5 理論解析：N次元で $\gamma_1$ を計算

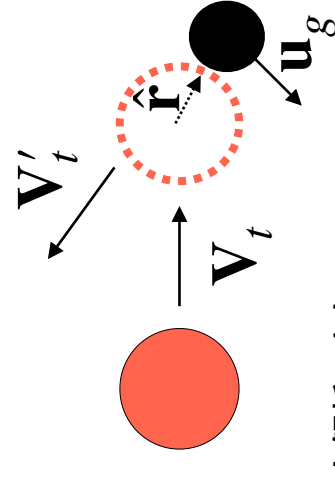
$\gamma_1 = \int$  衝突頻度×衝突前後の速度の内積/規格化因子

$$= \frac{\int d\hat{\mathbf{r}} \int d\mathbf{V}_t \int d\mathbf{u}_g P_d(\hat{\mathbf{r}}) P_t(\mathbf{V}_t) P_g(\mathbf{u}_g) |\mathbf{V}_t - \mathbf{u}_g| (\mathbf{V}_t \cdot \mathbf{V}_t')}{\int d\hat{\mathbf{r}} \int d\mathbf{V}_t \int d\mathbf{u}_g P_d(\hat{\mathbf{r}}) P_t(\mathbf{V}_t) P_g(\mathbf{u}_g) (V_t^2)}$$

$= \frac{NM + N - 3}{NM + N + 1}$

$P_t(\mathbf{V}_t), P_g(\mathbf{u}_g)$ : マクスウェル分布

$P_d(\hat{\mathbf{r}})$ : 衝突角度分布



フィットパラメータなしで $\gamma_1$ の質量Mと次元Nの依存性を解析できた

## 6 結果：理論とシミュレーションで得た $\gamma_1$ をプロット

■: シミュレーション —: 理論

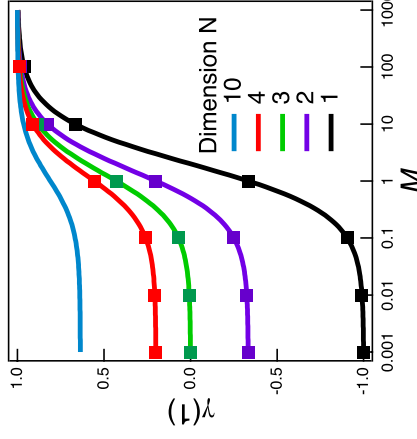
理論はシミュレーションの $\gamma_1$ を良好に再現

$M \gg 1$ : 次元に依存せず $\gamma_1 \rightarrow 1$ となる

$M \ll 1$ : 次元が増大すると $\gamma_1$ も増大し

1、2次元では負で3次元以上で正

$M \ll 1$ でなぜ $\gamma_1$ に次元依存性は生じる?



## 3 目的：トレーサーの1回の衝突前後の速度相関 $\gamma_1$ の理解

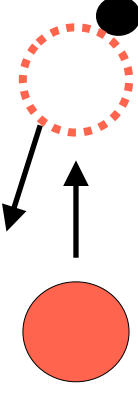
3次元で $\gamma_1$ は常に正だが直感的には奇妙

質量が小さいと

・速さが大きいので正面衝突

・1回の衝突で運動量が容易に変化

→1回の衝突で速度の負相関が起きそう



3次元では1回の衝突で負相関は生じない なぜ? 次元が関係する?

## 4 シミュレーション方法：剛体シミュレーション

パラメータ

● 理想気体

● トレーサー

● サイズ $\sigma$

● 質量 $m$

● 数密度 $\rho$

● 質量 $M$

● 運動エネルギー平均 $k_B T$

$m, \sigma, k_B T$ で無次元化→パラメータは $M, \rho$ だけ

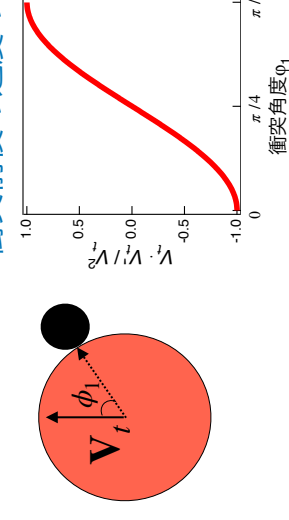
イベントドリブン型なので衝突を厳密に定義可能

衝突前後の速度相関 $\gamma_1 = \langle \mathbf{V}_0 \cdot \mathbf{V}_1 \rangle_{coll} / \langle V_0^2 \rangle_{coll}$ を次元Nを変えて解析

## 7 考察： $M < 1 < 1$ 領域の衝突角度 $\phi_1$ に着目した理論解析

$$\lim_{M \rightarrow 0} \gamma_1 = \lim_{M \rightarrow 0} \frac{\int d\hat{\mathbf{r}} \int d\mathbf{V}_t \int d\mathbf{u}_g P_d(\hat{\mathbf{r}}) P_t(\mathbf{V}_t) P_g(\mathbf{u}_g) |\mathbf{V}_t - \mathbf{u}_g| (\mathbf{V}_t \cdot \mathbf{V}_t')}{\int d\hat{\mathbf{r}} \int d\mathbf{V}_t \int d\mathbf{u}_g P_d(\hat{\mathbf{r}}) P_t(\mathbf{V}_t) P_g(\mathbf{u}_g) (V_t^2)} = \int P_d(\hat{\mathbf{r}}) d\hat{\mathbf{r}} (1 - 2 \cos^2 \phi_1) = \int (N-1) \cos \phi_1 \sin^{N-2} \phi_1 d\phi_1 (1 - 2 \cos^2 \phi_1)$$

衝突前後の速度の内積

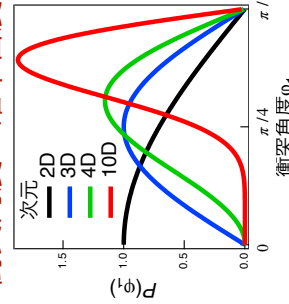


次元によらず

$\phi_1 > \pi/4$ で正

高角側で掠る

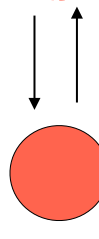
衝突角度の確率密度



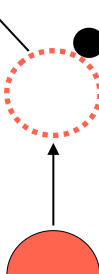
次元の増大に伴い高角側の衝突が増加

## 8 結論：掠る衝突の寄与で3次元以上で $\gamma_1$ は正になる

1次元



3次元以上



次元の増大に伴い掠る衝突の割合が増加

→3次元以上で $\gamma_1$ は正

[1] A Rahman. Phys. Rev., 136, A405, 1964. [2] T Yamaguchi and Y Kimura. J. Chem. Phys. 114, 3029, 2001.

[3] Hansen, Jean-Pierre, and Ian Randal McDonald. Theory of simple liquids. Academic Press, 2013. [4] F Nakai, Y Masubuchi, and T Uneyama. Physical Review E 102, 032104, 2020.